Studies on high power ultrasonic microembossing and organic light emitting diodes (OLEDs) for the creation of lab-on-CD devices for sensor related applications

by

Srikanth G. Vengasandra

A dissertation submitted to the graduate faculty

in partial fulfillment of the requirements for the degree of

DOCTOR OF PHILOSOPHY

Major: Industrial and Agricultural Technology

Program of Study Committee:
David Grewell, Major Professor
Joseph Shinar
Michael Kessler
Steve Mickelson
Chenxu Yu

Iowa State University

Ames, Iowa

2009

DEDICATION

I would like to dedicate my PhD work to all the teachers that I have had in my entire life.

This work was accomplished keeping always in mind the words of encouragement from my well wishers and the blessings from my mother - Smt. Ramamani, father – Sri. Gopinatha Rao and my late grandfather – V. R. Nagesh Rao. Hence, this is due to them and for them.

Of course, this is also dedicated to my beautiful wife – Shruthi for her unwavering belief and love in me.

TABLE OF CONTENTS

LIST OF TABLES

LIST OF FIGURES

LIST OF SYMBOLS

μ Micro (10^{-6})

ρ density (kg/m^3)

ω angular velocity

Δr radial length

γ_{al} surface energy per unit area of the liquid-air interface

θ_c equilibrium contact angle

$\bar{r}$ average distance from the liquid element to the center of the CD

D_h hydraulic diameter

ε_o applied strain

E'' loss modulus

ρ_1, ρ_2, ρ_3 density of the unembossed microcellular foam, foamed substrate after embossing, microchannel region

V_1, V_2, V_3 volume of the unembossed microcellular foam, volume of the foamed substrate after embossing, microchannel region

$m_1 mass$

h^+ hole

e^- electron

ϕ workfunction

Ω Ohms

I_o luminescence intensity in the absence of a quencher

I intensity in the presence of a quencher

Q quencher concentration

k_q rate of collisional quenching

τ luminescence lifetime

F fluorophore concentration

ϕ_F quantum yield

k_r radiative rate constant

k_i non-radiative rate constant

k_{isc} intersystem crossing rate constant

k_{SV} stern-volmer constant

τ_o mean PL lifetime of the fluorophore in the absence of quencher

P Pressure

T Temperature (°C)

N Newtons

γ_w Surface energy of water

γ_g Surface energy of Polyehtylene glycol (PEG)

γ_l^d, γ_s^d Dispersive components of the liquid and solids respectively

γ_l^p, γ_s^p Polar components of liquid and solids respectively

γ^d_{peg} Dispersive component value for PEG

γ^{p}_{peg} Polar component value for PEG

γ^{d}_{H20} Dispersive component value for Water

γ^{p}_{H20} Polar component value for Water

$[DO]_{final}$ final dissolved oxygen

$[DO]_{0}$ initial dissolved oxygen

$[analyte]_{0}$ initial analyte concentration

ACKNOWLEDGEMENTS

A majority of my PhD work was supported by Dr. David Grewell and the department of Agricultural and Biosystems Engineering (ABE) at Iowa State University (ISU). I would like to sincerely thank Dr. Grewell and the department for this support. It is a dream of any PhD seeking graduate student to be offered an interesting project that would retain interest and enthusiasm until the very end and this project on developing a functional biomedical device was indeed a challenging one at its every stage. The success of this project needed thorough insight, creativity, collaboration and guidance. I would like to express my sincere gratitude to Dr. Grewell for considering me for this project and also for his guidance. It was due to Dr. Grewell that I was able to participate in several conferences nationwide and was also able to take advantage of an important scholarship award from within ISU. I thank him for providing me with all these opportunities.

I would also like to thank Dr. Michael Kessler (Assistant Professor, Department of Materials Science and Engineering, ISU) for forwarding my resume to Dr. Grewell in 2005 and putting in kind words on my behalf, which in turn led me to pursue this PhD opportunity.

My special thanks to Dr. Ruth Shinar (Senior Scientist and Adjunct Professor at the Microelectronics Research Centre and Electrical Engineering Department, ISU, respectively) for providing me helpful suggestions throughout this research. Her advice helped me achieve major breakthroughs in the research especially during times when I needed some inputs to be able to think from ‘outside the box’.

I would also like to express my immense gratitude towards Dr. Joseph Shinar (Professor and Chair, Department of Physics and Astronomy, ISU and a Senior Physicist at Ames Laboratory - USDOE) for allowing me to be a part of his research group in Ames Lab. His keen interest in my research work led towards financial support during critical times of my PhD study. My big take away from working with him is his 'humility'. Dr. Shinar's patience and diligence towards the students was uncompromising and with this I have observed him bring out the best from a wide category of students – just like he did in my case along with Dr. Grewell. He is another exceptional individual to know and work with. Again, big thanks to Dr. Grewell - as this was another opportunity that was made possible to me by him.

It was a pleasure to collaborate and learn from my colleagues especially, Yuankun Cai, Rui Liu and Zhengqing Gan (Photonics and Condensed Matter Physics students in Dr. Shinar's group). They were always there whenever I needed help in understanding the Physics behind the working of Organic Light Emitting Diodes (OLEDs) and I would like to thank all of them for guiding me towards learning all I know about OLEDs and their fabrication. I would like to recognize Yuankun Cai for being part of my research that won the 'Best Technical Paper Award' from the Society of Plastic Engineers in May of 2008.

During the summer semesters of 2008 and 2009 I also had the privilege to work for ISU Foundation as a Student Fundraiser. The Foundation provided me a unique opportunity to give back to ISU even while I was a student. I thank ISU Foundation for hiring me to personally raise more than $40,000 towards various departments and facilities on campus.

I would also like to express my sincere appreciation towards my entire program of study committee members for their kind cooperation.

It has been a very interesting learning experience, here at ISU, both on the personal and professional front. For this, I thank God, Almighty, and my parents, in parallel, for providing me with all that I required to be where I am today.

ABSTRACT

This study demonstrates the application of High Power Ultrasonic Microembossing Technology (HPUMT) in producing microfeatures on polymer substrates. The work reviews a novel method of obtaining flash free and precise microfeatures by manipulating the material density through microcellular foaming. The microfeatures created on the polymer substrates were further characterized by analyzing the feature depth with respect to the critical ultrasonic embossing operating parameters such as embossing heating times (s), embossing amplitude (μm) at a constant embossing trigger force (N). An experiment design was constructed and performed to characterize the parameters on foamed and unfoamed (or regular) versions of polystyrene (PS) and polypropylene (PP) sample materials. Results indicated feature depth was proportional to heating times, amplitude and force. It was also seen the maximum depth was achieved in the shortest cycle times with higher amplitudes and forces of operation.

HPUMT was further studied to create functional network of microchannels functioned as reservoirs, reaction chamber and burst or gate valves to form a centrifugal biosensing platform that is also referred to as a lab-on-CD or a bio-CD device. The surface energy of the polymer substrates was increased to enable fluid flow by using a surfactant based organic coating to facilitate hydrophilicity. Using an organic light emitting diode (OLEDs) as an electroluminescence source provided luminescence decay results in good agreement with stern-volmer relationship. The functionality of the OLED-coupled lab-on-CD device was further tested in measuring unknown concentrations of a particular analyte in

corn slurry sample which contained numerous contaminants. Combinatorial multianalyte sensing was also made possible on a single bio-CD using a four photodetector (PD) quad preamp disk sensor.

CHAPTER 1: INTRODUCTION

The primary motivation of this research project was to develop a polymer embossing microfabrication technique to create precise, flash-free microfeatures. The ultimate goal was to produce functional lab-on-CD device for bio-chemical sensing applications. This work required the development of microfabrication techniques, surface engineering and characterization techniques, microfluidics and microstructure characterization and analysis techniques, and thin film technology. The final lab-on-CD (LOC) was coupled with photoluminescence (PL) based biosensors such as organic light emitting diodes (OLED).

This research studied the use of high power ultrasonic microembossing technology (HPUMT) for the manufacturing of polypropylene (PP) and polystyrene (PS) LOC devices. Because polymer bio-microelectromechanicalsystem (bioMEMS) devices require precise and flash-free microfeatures, the end goal was to produce features with such quality. In addition, bioMEMS devices require functionality in terms of being able to perform biosensing of various analytes. For this reason, the initial tasks of the project involved testing, selection, and characterization of various polymer materials that would be suitable for the manufacturing of the LOC device. The results are detailed in the subsequent Chapter 2 (accepted in Polymer Engineering and Science journal). Assuming Chapter 2 represented the first of the three tasks, the balance of the project was further divided into two additional tasks. Task two involved identifying an appropriate and proven biochemical test or assay that could be based on OLEDs as a PL excitation source in conjunction with the developed LOC device. OLEDs were selected as excitation sources because they are easy to fabricate, and

relatively inexpensive. Task three involved a feasibility study of the technology, using corn slurry sample with unknown sugar concentrations and also monitoring of multianalyte concentrations on a single LOC. Chapters 3 and 4, respectively detail these tasks.

Polymer substrates were selected for the bio-MEMS devices as opposed to the other commonly used substrates such as silicon and glass, because of their low cost, disposability and recyclability, feasibility of high volume manufacturing and biocompatibility.

In order to fully gain insight of the work presented in this thesis, five technologies must be reviewed; namely 1) Polymer bioMEMS, 2) Lab-on-Chip, 3) Lab-on-CD (LOC) 4) Polymer Microfabrication Methodologies, 5) High power Ultrasonic Micro-embossing and 6) OLEDs based biosensing platform. Each of these will be reviewed in the following section.

1.0 Polymer bioMEMS: Research on bioMEMS has lead to their continuous development and growth of application base. Researchers are continuously developing novel applications for these devices in a wide range of technologies. For example, bioMEMS devices that incorporate microfluidic components and micromixers have effectively found applications in the areas of drug discovery and delivery, cell culture, proteomics, disease diagnostics [1, 2] and environmental studies [3]. One of the major advantages to bioMEMS devices is that they can control and optimize the flow of micro to pico liter volumes of fluid samples without experiencing cross contamination or undesired intermixing. It is important to note that the bioMEMS is a broad terminology for devices that may include lab-on-Chip or LOC based assay platforms.

2.0 Lab-on-Chip: Lab-on-Chip devices are a subset of MEMS devices and are also referred to as micro-total analysis systems (micro-TAS or μ-TAS). They are typically manufactured on polymers or glass substrates. While the overall size of these devices range from a few millimeters to a few square centimeters, the novelty of these devices arises from the intricacy and preciseness of the functional microfeatures that are built onto them using various microfabrication techniques. These microfeatures differ from those found on silicon based microchips by their functional capabilities, as they primarily rely on fluid flow. Commonly known applications for lab-on-chip devices are studies of living cells in liquid flow or static conditions, nucleic acid and protein analysis studies [4]. The applications are typically limited by the type of detection method, which are generally optical, electrochemical or mass spectrometry based. However, with the invention of the atomic force microscopy (AFM) in 1986 by IBM researchers [5], it has also been possible to use morphological detection of pathogens [6] on a lab-on-chip platform.

Table 1 details selected companies that manufacture lab-on-chip devices for various applications.

Table 1: List of selected companies making lab-on-chip products and their applications

COMPANY	LAB-ON-CHIP PRODUCT NAME	APPLICATION
Agilent www.agilent.com/chem/chip	Glass and polymer lab-on-a-Chip	On-chip electrophoresis, proteomics
STMicroelectronics http://www.st.com/	In-Check lab-on-chip platform	Rapid bacterial diagnosis
Dolomite http://www.dolomite-microfluidics.com	Microreactor Chips, Mitos T-Junction Chips	Compound synthesis and reaction kinetics studies
ThinXXS Microtechnology http://www.thinxxs.com	Lab-on-Chip systems	Blood diagnostics
Bioident Technology Inc. http://www.bioident.com	ControlR^{TM}, CheckR^{TM}	Biosensing applications
Micronit Microfluidics http://www.micronit.com/	Microreactor chip, micromixer chips, cross channel chips made of glass and polymer substrates	Invitro diagnostics
Fluigence http://www.fluigence.com/	Microfluidic chip made of plastic substrates	On-chip chromatography
Cellix http://www.cellixltd.com	Vena8^{TM} Biochip, VenaEC^{TM} Biochip made of glass and polymer	Cell based analysis for therapeutics

3.0 Lab-on-CD (LOC): LOCs are a subset of MEMS devices but typically have dimensions of the standard CDs. Their advantage is the capability of supporting centrifugal fluid propulsion. This driving force can be augmented by other fluid propulsion mechanisms, such as a differential pressure [7], acoustics [8], electrokinetics [9, 10], electroosmotic flow [11], capillary [12], magnetohydrodynamic pumping [13] and pneumatic control [14] type of fluid propulsion mechanisms [15, 16].

Some of the critical design issues of LOC include:

- The sub-components of a LOC device determine the effectiveness, efficiency, consistency and versatility of a particular device. Those sub-components include: - the chambers or reservoirs for performing biochemical reactions and allowing effective feedback signals for assay analysis; reservoirs for storage of buffers and waste solution; and burst valves (or gate). Figure 1 (A) shows the schematic of the LOC design with four similar segments of the subcomponents that involve the reaction chamber (RC – the largest chamber of all), reagent chamber 1 (RB1 – the second largest chamber), reagent chamber 2 (RB2 – the third largest chamber), two burst valves at each side of both of the reagent chambers, and the microchannel that inter-connects all the chambers. Figure 1 (B) and (C) are the photographs of the sub-components.

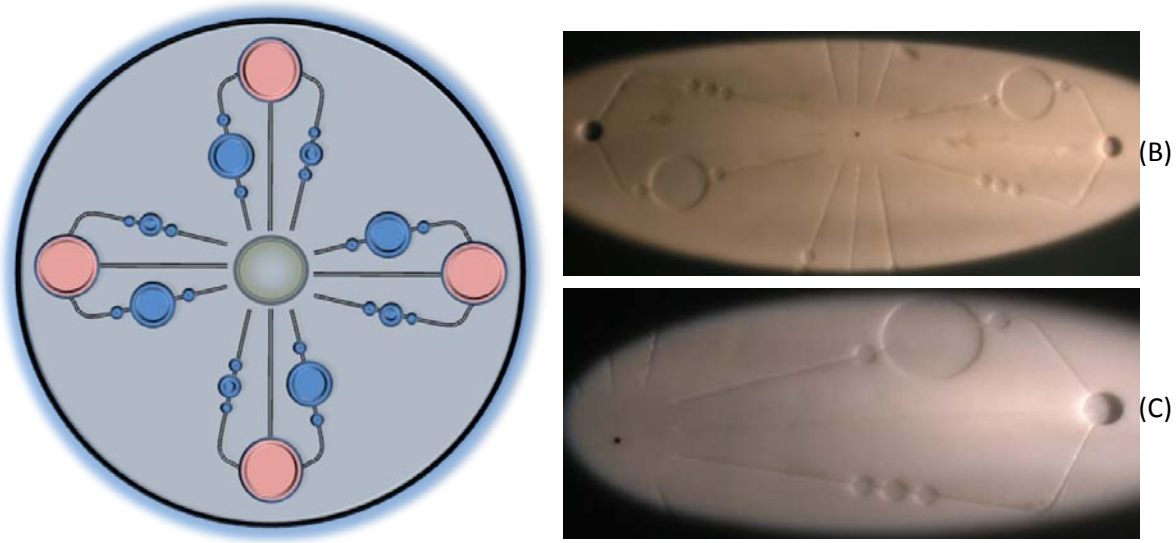

Figure 1 (A). Schematic of the LOC design that was considered for this study and (B) and (C) are close-up photographic images of the sub-components

$$\rho\omega^2 \bar{r}\,\Delta r < 4\gamma_{al}\sin\theta_c / (D_h)^n \qquad (1)$$

- Burst valves open and allow fluid at a designated rotational speed, as detailed in equation 1 [17, 18], where ρ is the density of the liquid, ω is the angular velocity, Δr is the radial length of the liquid sample, γ_{al} is the surface energy per unit area of the liquid-air interface, θ_c is the equilibrium contact angle, $\bar{r}$ is the average distance from the liquid element to the center of the CD and D_h is the hydraulic diameter. This equation is based on two competing forces, surface tension, and centrifugal force. Once the later exceeds the former, flow through the chamber occurs ("bursting"). Figure 2 (A) and (B) shows a scanning electron microscopy (SEM) image of the cross section and a top view respectively, of the burst valve that was used as a sub-component in this LOC study.

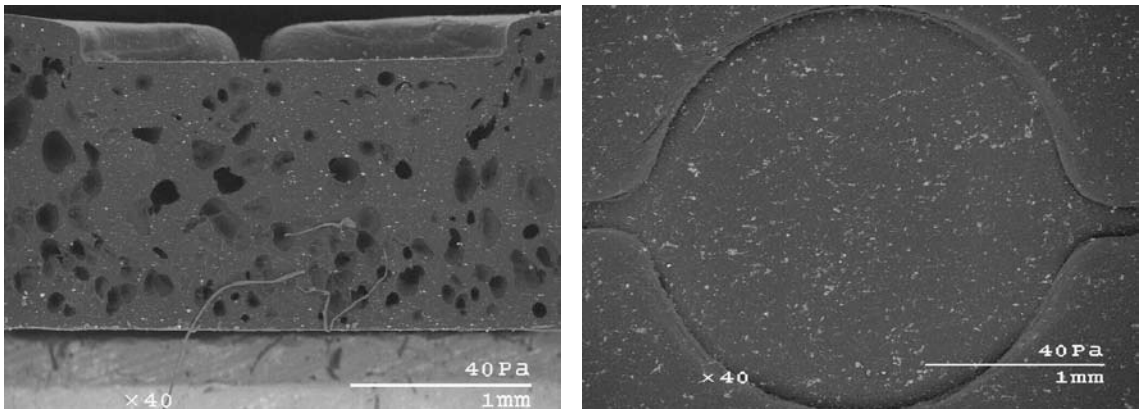

(A) (B)

Figure 2 (A). SEM image of the cross sectional view of the burst valve and (B). shows another SEM image of the top view of the same burst valve

- LOC technology offers complete automation of the entire assay process and promotes high throughput screening (HTS). However, to allow detection methods based on fluorescence or optical measurement, the technology relies on substrates that are transparent, such as Polycarbonate (PC), Polydimethoxysiloxane (PDMS), Polymethylmethacrylate (PMMA) and cyclic olefin copolymer (COC).
- Polymer substrate based LOC technology offers flexibility in terms of the wide range of microfabrication techniques that could be used in its manufacture. In this work, HPUMT was used to create the sub-components on microcellular (µcell) foamed polypropylene (PP) and polystyrene (PS) substrates to eliminate the generation of flash.

Several companies such as Tecan Boston and Burnstein offer LOC based products for several biomedical applications. Recent development in LOC manufacturing methodology and application area is also published by the Samsung Advanced Institute of Technology [19]. Table 2 details selected companies currently manufacturing LOC devices.

Table 2: List of companies making lab-on-CD products and their applications

COMPANY	LAB-ON-CD Product Name	APPLICATION
Abaxis http://www.abaxis.com	Piccolo Express panels or Reagent discs	Blood, serum or plasma analysis
Gyros AB http://www.gyros.com	Gyrolab Bioaffy 1000, 200, HC	Immuno assays
Alliance Protein Laboratories http://www.ap-lab.com	Circular dichroism spectroscopy	Protein Characterization

4.0 Polymer Microfabrication Methodologies: Novel methods to create high quality and precise micro-features on polymer substrates with high aspect ratio are continuously being explored. Some of the common microfabrication techniques include: UV lithography of ultra thick SU-8 [20]; lithographie galvanoformung abformung (LIGA) process [21]; nanoimprinting [22]; hot embossing [23], ablation, and micromachining [24]. There are also various net shape forming techniques that can be employed to create microfeatures on polymer substrates, such as injection molding [25], casting, wire imprinting, compression molding, photopolymerization and other methods that may be a combination of different techniques [26]. However, the most commonly used microfabrication techniques widely used to manufacture LOC devices include computer numerically controlled (CNC) micromachining [27], hot embossing technique [28, 29] and microinjection molding [30].

However, both CNC micromachining and microinjection molding are expensive for mass production. In addition, molding results in relatively high residual stresses. To address these issues, this research study evaluates the use of HPUMT. Also to resolve the problem of flash generation this work studies microcellular foamed polymer substrates.

5.0 High Power Ultrasonic Microembossing Technology (HPUMT): HPUMT is similar to the high power ultrasonic welding technology (HPUWT), which is a widely used fusion bonding technology for thermoplastics and thermoplastic composites. HPUMT is accomplished by applying low amplitude (in the range of 10 µm – 180 µm) and high frequency mechanical vibrations (in the range of 10 kHz – 70 kHz) to the sonotrode or horn that makes contact at the desired location of a substrate to produce an embossed feature. HPUMT has similar advantages to HPUWT, namely, high speed with cycle times often less than 1 second, ease of automation, amenability to a wide range of thermoplastics and relatively low capital costs compared to injection molding and CNC micromachining technologies (Table 3). Figure 3 shows a typical 3D image of a microchannel on the µcell foamed PP that was created with HPUMT, the image being captured via an optical profiler (Microphotonics, Irvine, CA).

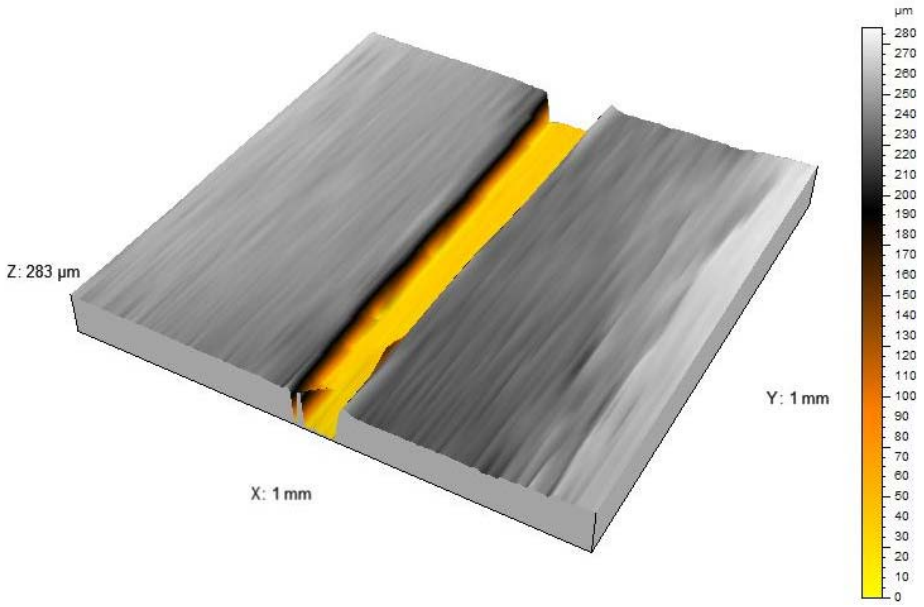

Figure 3. 3D image of the microfeature on the Polypropylene substrate created by HPUMT

There are seven main components of HPUMT: power module, control system, actuator, converter, booster, horn (sonotrode) and fixture as shown in Figure 4. The part of the HPUMT that holds the converter, booster and horn is considered the stack assembly (Figure 4 B). All components in the stack are tuned to resonate at a particular frequency in order to operate/vibrate at high energy efficiencies. The converter, which is considered to be the heart of the system typically contains a piezo-electric material and performs the function of converting electrical energy to mechanical vibrations. Ultrasonic systems are offered in a wide range of frequencies from 10 to 40 kHz. Although the selection of frequencies is application dependent, for the purpose of embossing LOC features, 20 kHz offers the optimal size of the converter, which determines the maximum power capacity of a particular ultrasonic system. In more detail, the converter size is inversely proportional to frequency

and maximum available power is inversely proportional to size. Thus, higher frequency systems tend to have limited power capacities. Therefore, the system used for this research had an operational frequency of 20 kHz that produces maximum amplitude of 20 µm at the converter with a maximum power of 2kW.

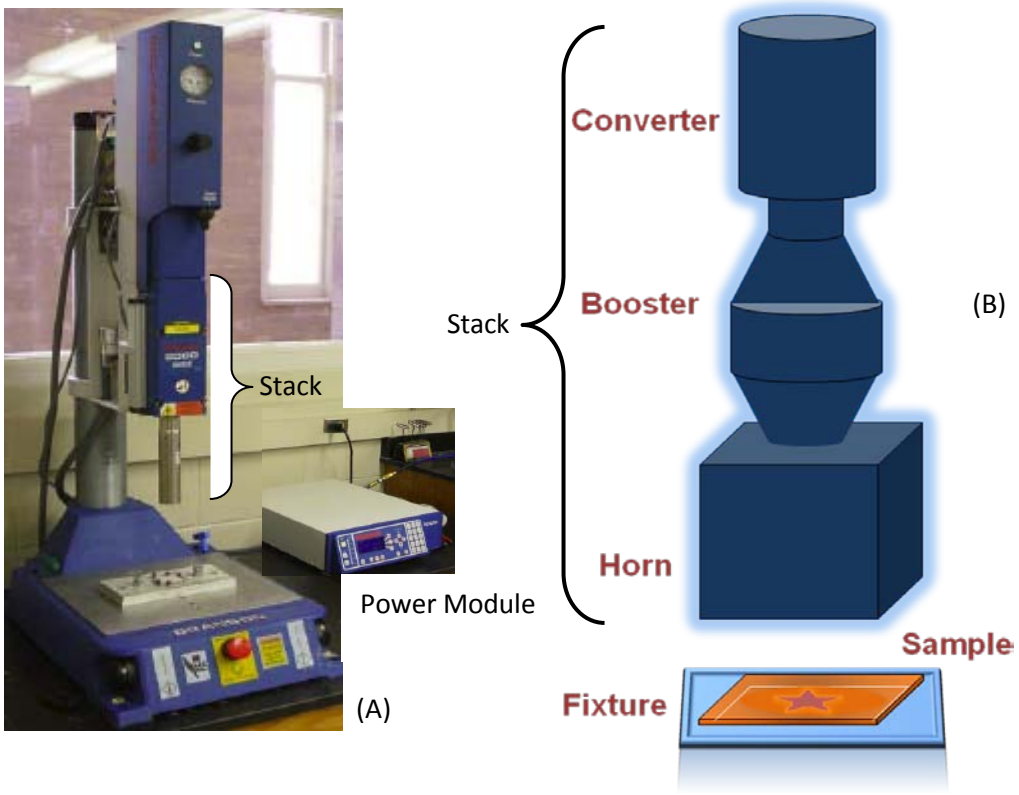

Figure 4. Branson 2000 series Ultrasonic system and its seven main components

Unlike the closely related ultrasonic plastic welding technology, HPUMT works by localized heating via the designed features at specified locations on the face of the horn surface. This is

more favorable because the entire part is not heated unlike hot embossing technology. The average heating observed with HPUMT can be expressed by the following equation:

$$Q = \frac{E^{"}\omega\varepsilon_o^2}{2} \tag{2}$$

Where ω is the angular frequency, ε_o is the applied strain and $E^{"}$ is the loss modulus of the substrate.

5.1 Microinjection Molding:

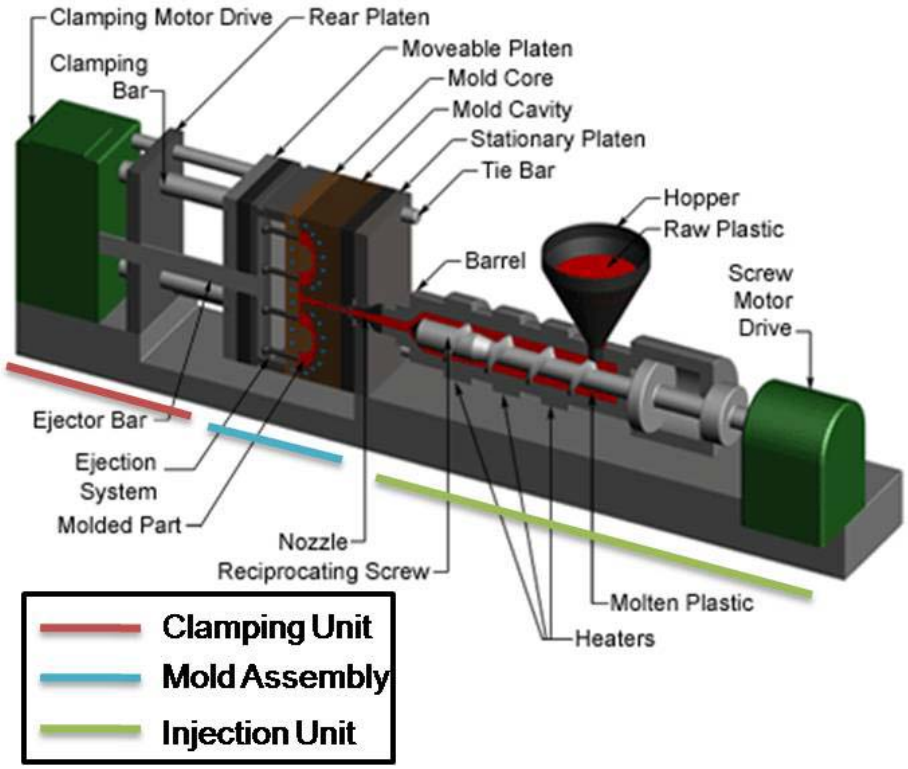

Figure 5. Conventional Injection molding machine from CustomPartNet

In general, injection molding machines are widely used in plastics processing industries. Figure 5 shows the major components of an injection molding machine. Micro injection can

be achieved with additional enhancements of standard machines, such as precise control of pressure. High precision injection is achieved using electric drives operated in a closed loop control system, which also assists in optimal injection control.

5.2 CNC micromachining: CNC is a computer 'controller' that interprets a dedicated programmable coding that in turn, drives a machine tool used to fabricate components by selective material removal.

Table 3 details comparison of the HPUMT with respect to injection molding and CNC micromachining:

Table 3: Table comparing the features of HPUMT, injection molding and CNC micromachining technologies

Technology / **Features**	**High Power Ultrasonic Microembossing Technology (HPUMT)**	**Injection Molding**	**Computer Numerically Controlled (CNC) Micromachining**
Residual Stresses	Low	High	High
Speed	High	High	Slower
Localized Heating	Yes	No	No
Capital Cost	Lower	High	High
Ease of automation	Yes	Yes	Yes
Continuous Manufacturability	Yes	Yes	No
Mass Production	Yes	Yes	No

Table 3: Continued

Cycles/second	High	Low	Low
Maintenance Cost	Low	High	High
Operating Cost	Low	High	High
Level of Expertise	Low	Low	High
Space requirement	Low	High	High
Versatility	High	Low	High

5.3 Microcellular (µcell) Foamed materials:

Properties offered by plastics make them highly suitable for biological applications. However, during embossing with localized heating, so-called ‘flash’ or ‘squeeze flow’ is generated [31]. This mechanism is detailed in Chapter 2. However, in general terms, when a polymer surface is heated (with localized heating) for embossing, the melt is squeezed out of the embossed feature. This results in an undesired deformation in the vicinity of the embossed region and often requires costly secondary operations to remove these deformations. For this purpose, µcell foamed materials were used as the substrates for the LOC applications due to their ability to absorb ‘flash’ generation during embossing.

Figure 6 (A) and (B) compares embossed features on a standard thermoplastic (PP) substrate and a foamed substrate respectively. The arrows highlight the flash that is generated on standard (unfoamed) PP substrate. It is seen that with the foamed substrate (B) there is no evidence of flash as the material absorbed it.

The micro-embossed features can be made suitable for various biotechnological applications by rendering the surface feasible for chemical functionalization via a thin film metal coating. Figure 7 shows an SEM image of a 100 nm silver (Ag) coated microembossed feature.

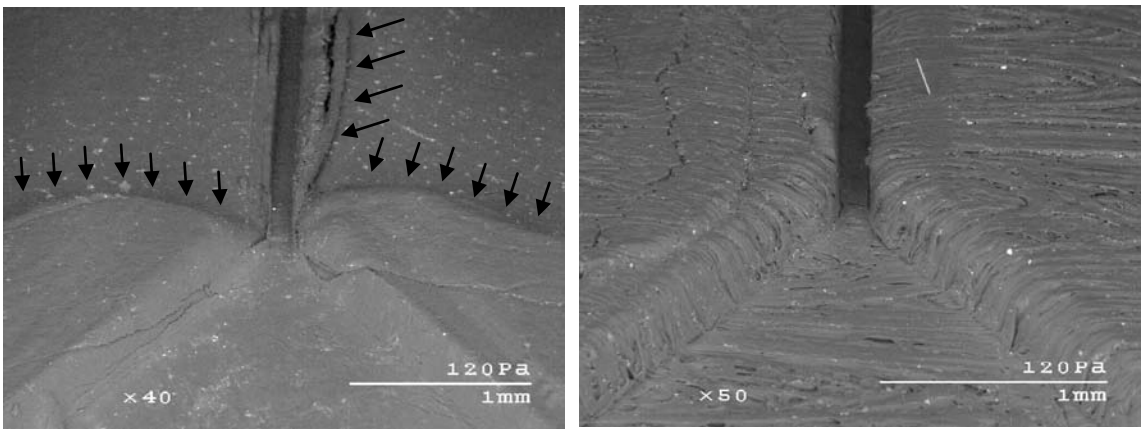

(A) (B)

Figure 6. SEM images of the microfeature that was created by HPUMT on a regular polymer substrate (A) and microcellular foamed polymer substrate (B).

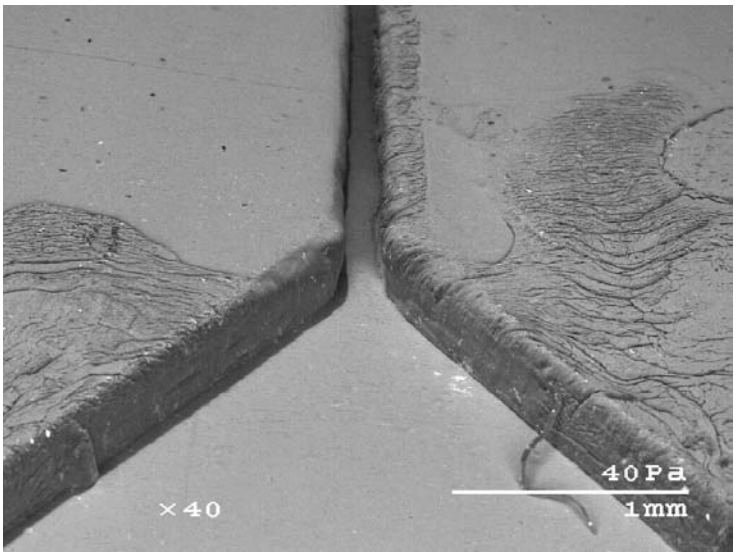

Figure 7. SEM image of the thin film of gold (Au) coated microfeature embossed on microcellular foamed PP substrate by HPUMT

A typical cross section image of a foamed substrate is seen in the SEM image shown in Figure 8 (A). Figure 8 (B) details an embossed feature image at the same cross section, where it is seen that the bubble (free volume) absorbed the displaced material.

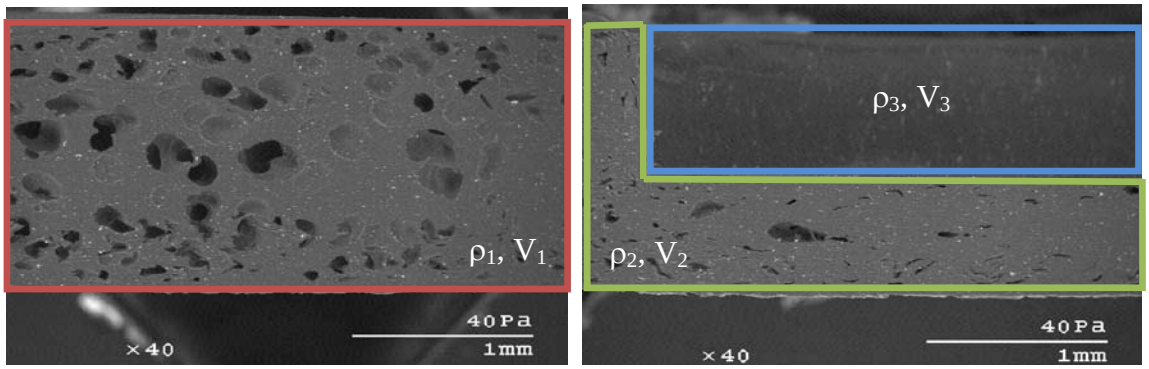

(A) (B)

Figure 8. SEM image of a cross-section of a microcellular foamed PP substrate before (A) and after (B) performing the microembossing using HPUMT.

Consider the density and volume of the non-embossed microcellular foam to be ρ_1 and V_1 respectively (region enclosed in red – Figure 8 (A). Similarly ρ_2 and V_2 correspond to the density and volume of the foamed substrate after embossing (region enclosed in green – Figure 8 (B). and ρ_3 and V_3 that of the microchannel region (region enclosed in blue – Figure 8 (B). that is air).

By evaluating the various volumes and assuming (1) law of conservation of mass and that the (2) density of air is negligible compared to the plastic of mass, m_1, the following can be derived;

$$\rho_1 V_1 = \rho_2 V_2 + \rho_3 V_3 \quad (3)$$

$$V_1 = V_2 + V_3 \quad (4)$$

We Know,

$$\text{mass, } m_1 = V_1 \rho_1 \quad (5)$$

$$\text{i.e } m = (V_2 + V_3)\, \rho_1 \quad \text{(from substituting 4 in 5)} \quad (6)$$

$$\text{i.e } m = \rho_1 V_2 + \rho_1 V_3 = \rho_1 (V_2 + V_3) \quad (7)$$

$$\text{i.e } \rho_1 (V_2 + V_3) = \rho_2 V_2 + \rho_3 V_3 \quad \text{(from 3)} \quad (8)$$

Therefore,

$$\rho_1/\rho_2 = V_2/(V_2 + V_3) \quad [\text{as } \rho_3 V_3 \text{ in air is negligible}]. \quad (9)$$

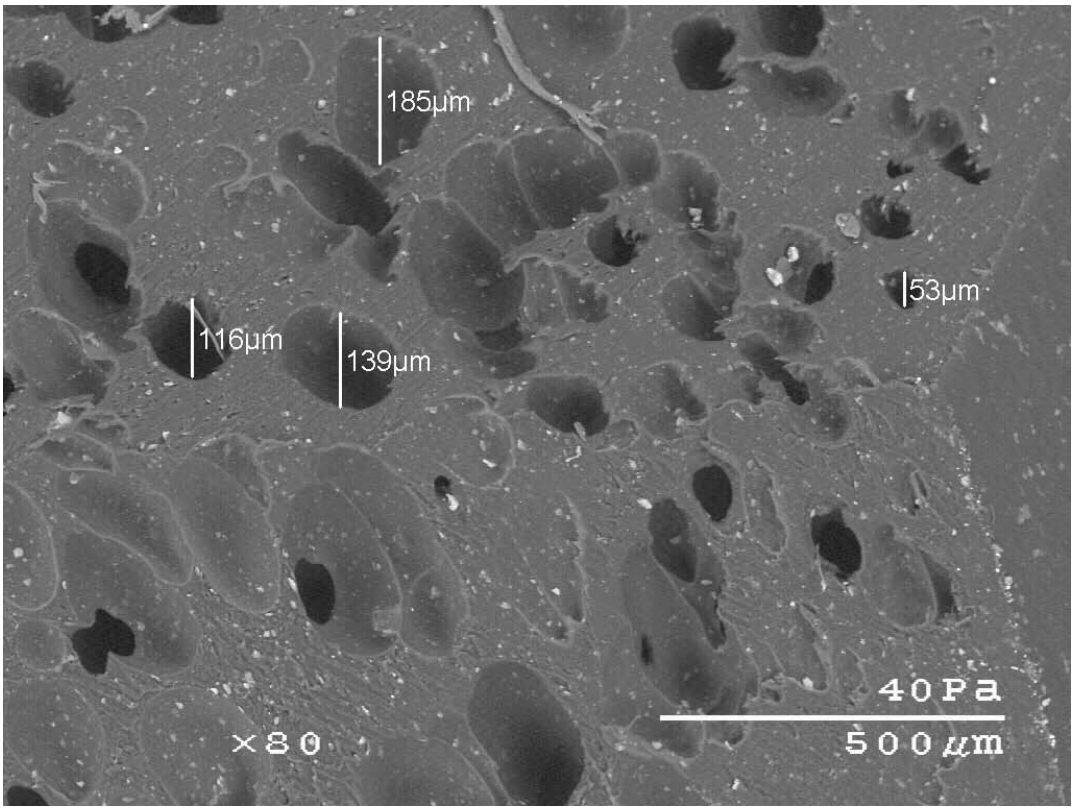

Figure 9. SEM image of the cross-section of the microcellular foamed PP material that was chosen as the LOC substrate shows the typical mucell size

Microcellular foamed materials reduce material usage and increase manufacturing efficiency for many applications. The process that enables these materials was invented in 1984 at the Mechanical Engineering lab by Dr. Nam Suh at MIT. In more detail, Dr. Suh received a request from Eastman Kodak to develop a material that would help them reduce plastics usage, maintain physical properties and at the same time, maintain and improve manufacturing efficiency. The enabling technology relies on dissolving foaming gasses under super-critical condition within a polymer melt. Once exposed to atmospheric conditions, the supersaturated solution becomes unstable resulting in a phase change that forms a foamed

material. Microcell's or µcell's results in bubbles that range between 5 to 50 microns in diameter [32], hence the name "Microcellular foamed Plastic". Figure 9 shows an SEM image of the cross sectional view of the µcell foamed PP substrate that was considered for this study. This view shows that the bubbles were found to be as large as 185 µm.

The feasibility studies of microembossing on such µcell substrates were tested by embossing a dog bone pattern on polystyrene (PS) and polypropylene (PP) substrates as shown in Figure 10.

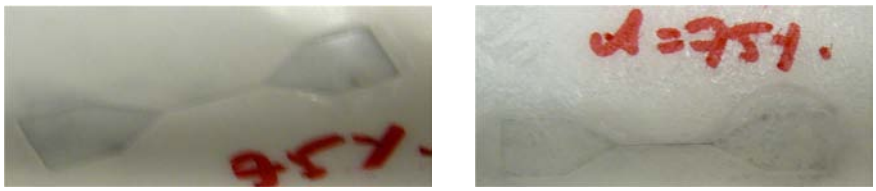

(A) (B)

Figure 10. Photographic images of the dog bone design embossed by HPUMT at an amplitude of 30µm (i.e 75%) on microcellular foamed PP (A) and microcellular foamed Polystyrene (PS) material (B)

6.0 Organic Light Emitting Diodes (OLEDs):

6.1 Basic Structure and operation:

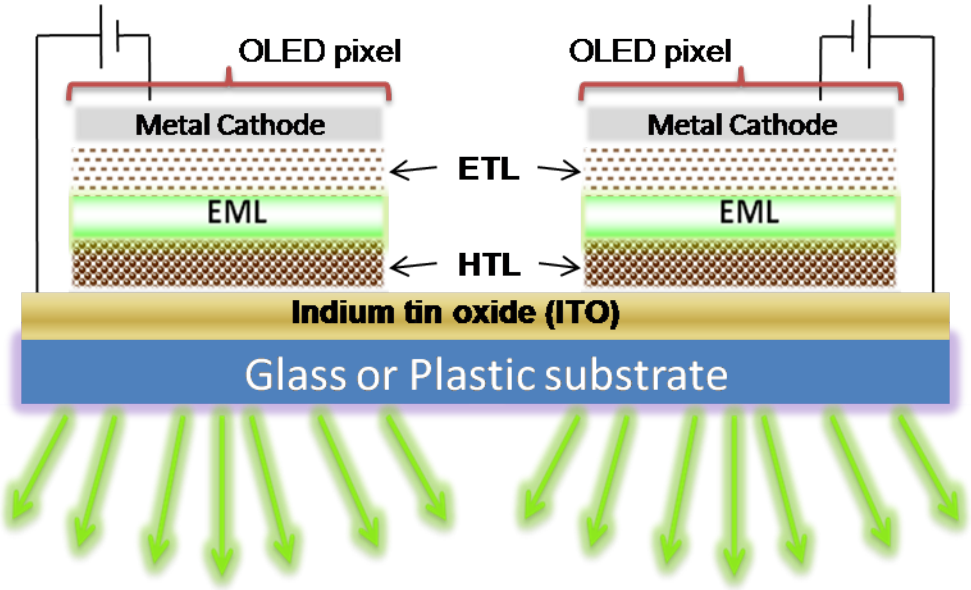

Figure 11. Basic structure of a bilayer OLED

Figure 11 shows the basic structure of an OLED, an electroluminescent device comprising of organic semiconducting layers sandwiched between electrodes. OLEDs are typically fabricated on transparent electrically conducting indium tin oxide (ITO)-coated glass, where the ITO is the anode (-). The organic layers include hole transport layers (HTLs), the emitting layer, the electron transport layers (ETLs) and an inorganic metal cathode. The organic, small or large (polymeric) molecular layers are deposited by thermal vacuum evaporation or spin coating, respectively. Electron transport layer (ETL) helps in transporting the electrons from the metal cathode (+) to the emitting layer (EML). Hole transport layer (HTL) transports the holes from the metal anode to the EML. The metal anode above the substrate is typically a transparent conducting layer of indium tin oxide (ITO). It

should be noted that the mobility of electrons and holes is different in organic compounds. Flexible OLEDs, in which the anode is made of a transparent conducting organic compound, deposited on a suitable plastic (e.g. transparency plastic) have also been demonstrated [33, 34].

The basic operation of an OLED can be understood from Figure. 12. Application of a positive potential to the anode relative to the cathode results in hole injection from the anode, and electron injection from the cathode; electrons and holes then drift towards the emitting layer, where they recombine. A fraction of the recombination events result in the electroluminescence. As shown in Figure 12, there is typically a triangular barrier for both hole (h^+) and electron (e^-) injection. The key point in operating OLEDs is to control the excitons (bound electron and hole pairs), so that holes and electrons meet in the emissive layer in equal quantities [35]. Thus appropriate thin layers (few nanometers – single or multilayer) of small organic molecular or polymeric materials are deposited on the transparent anode to assist in lowering the barrier for hole injection from the anode. The cathode is typically prepared by depositing several hundred nanometer thick layer of a low-to-medium workfunction (ϕ) metal such as Ca (ϕ = 2.87 eV), Al (ϕ = 4.3 eV) or $Mg_{0.9}Ag_{0.1}$ (for Mg, ϕ = 3.66 eV) by either thermal or e-beam evaporation [36].

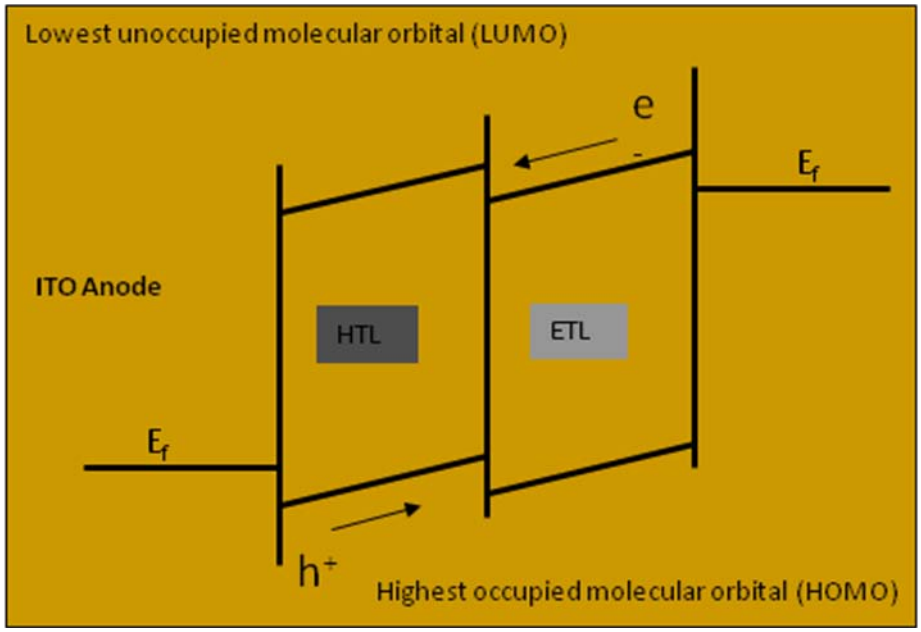

Figure 12. Basic operation of an OLED

6.2 OLED Fabrication process:

Figure 13 shows the schematic of an OLED pixel. In this work all the organic films, including the Al cathode metal electrode, were deposited using a thermal evaporator in a vacuum chamber at a pressure of 10^{-6} mbar. The thin film thermal evaporation system was set up in a glove box, in which oxygen and water levels are typically below 1 ppm. Approximately 200 nm thick indium tin oxide (ITO) -coated glass substrates with a resistance of 20Ω/square were purchased from Applied Films Corporation (Longmont, CO).

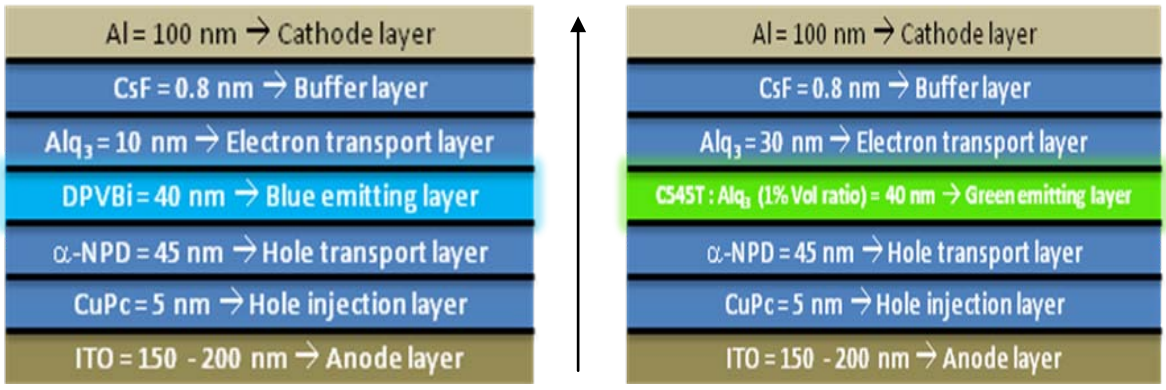

(A) Blue emitting (~ 460 – 470 nm) DPVBi OLED (B) Green emitting (~ 535 nm) Alq_3 OLED

Figure 13. Sequence of the thermal evaporation based thin film deposition of the organic materials and the metal electrode in the two OLED types used

Prior to deposition of organic materials, the ITO coated glass substrates were cleaned with a solution of surfactant, acetone, and isopropanol in an ultrasonic bath, and were subsequently exposed to UV-ozone (UVOCS INC. Model T16X16/OES) to remove organic residues. The substrates were then etched to obtain 2 mm-wide ITO strips. Following etching, the first organic layer deposited above the ITO was a 5 nm hole injection copper phthalocyanine (CuPc) layer. Subsequently, a 45 nm thick HTL of N, N'-diphenyl-n, n'-bis(2,2'-diphenyl1-4, 4'-diamine (α-NPD) was deposited. Then, as shown in Figure 13 (A) and (B), a blue light emitting 4,4'-bis(2,2'-diphenylvinyl)-1,1'-biphenyl (DPVBi) layer or a green light emitting layer of 1% volume C545T dopant (10-(2-benzothiazolyl)-1,1,7,7-tetramethyl-2,3,6,7-tetrahydro-1H,5H,11H-[1]benzopyrano [6,7,8-ij]-quinolizin-11-one) in tris (8-hydroxyquinoline) Al (Alq_3) was deposited, respectively, depending on the sensor application (described in detail in Chapter 3). Following this layer, a 10 to 30 nm thick Alq_3 ETL was deposited. A 0.8 nm thick layer of CsF was then deposited on the organic films, as

a buffer layer just before the deposition of the ~100-150 nm Al cathode. The Al cathode was deposited using a mask containing 2 mm-wide slits aligned perpendicular to the ITO strips. The deposition rate of the organic materials and the cathode were 2 and 4 $Å s^{-1}$, respectively. Individual OLED pixels, being defined by the overlap between ITO and Al strips, were 2x2 mm^2, with a 2 mm gap between the pixels. The array of 12x2 OLED pixels was encapsulated by adhesive bonding of a glass cover to the substrate with high vacuum epoxy [37].

6.3 Collisional quenching of photoluminescence (PL) and the Stern-Volmer relation:

Quenching refers to the process that causes a reduction in the quantum yield of a given luminescence process, and can be categorized as either collisional or static quenching. Collisional quenching occurs when the fluorophore and another molecule diffuse and collide without forming a complex. In contrast, static quenching is observed when two molecules bind to form a complex. Collisional quenching can be described by the Stern-Volmer equation:

$$\frac{I_o}{I} = 1 + k_q[Q]\tau \qquad (10)$$

Where I_o is the luminescence intensity in the absence of a quencher, I is the intensity in the presence of a quencher at concentration $[Q]$, k_q is the rate of collisional quenching and τ is the luminescence lifetime [38].

The PL lifetime is the time the fluorophore remains at the excited state. Collisional quenching is a process that depopulates the excited state in parallel to the other processes such as photon absorption, fluorescence, intersystem crossing, internal conversion and phosphorescence. Therefore, the PL lifetime of the excited state will be shorter in the presence of a collisional quencher than in its absence.

The rate of the deactivation by a quencher can be written as:

$$v = k_q[F][Q] \tag{11}$$

Where k_q is the bimolecular quenching rate constant expressed in $M^{-1}s^{-1}$, [F] is the fluorophore concentration, and $[Q]$ is the quencher concentration. If $[Q]$ is significantly higher than $[F]$, the deactivation can be considered as a pseudo-first order with a rate constant equal to $k_q . [Q]$.

$$v = k'[F] = k_q[Q][F] \tag{12}$$

The quantum yield (ϕ_F) in the absence of a quencher is equal to:

$$\phi_F = \frac{k_r}{k_r + k_i + k_{isc}} \tag{13}$$

Where k_r is the radiative rate constant, k_i is the non-radiative rate constant and k_{isc} is the intersystem crossing rate constant.

In the presence of a quencher the quantum yield will be equal to:

$$\phi_{F(Q)} = \frac{k_r}{k_r + k_i + k_{isc} + k_q[Q]} \tag{14}$$

$$\frac{\phi_F}{\phi_{F(Q)}} = \frac{k_r + k_i + k_{isc} + k_q[Q]}{k_r + k_i + k_{isc}} = \frac{k_r + k_i + k_{isc}}{k_r + k_i + k_{isc}} + \frac{k_q[Q]}{k_r + k_i + k_{isc}} =$$

$$1 + k_q[Q]\frac{1}{k_r + k_i + k_{isc}} = 1 + k_q\tau_o[Q] = 1 + k_{SV}[Q] \tag{15}$$

Where k_{SV} is the stern-volmer constant and τ_o is the mean PL lifetime of the fluorophore in the absence of quencher. Equation 11 is the Stern-Volmer equation.

Because the PL intensity is proportional to the quantum yield, the Stern-Volmer equation can be written as:

$$\frac{I_o}{I} = 1 + k_{SV}[Q] = 1 + k_q\tau_o[Q] \tag{16}$$

Where I_o and I are respectively the PL intensities in the absence and presence of quencher [39].

6.4 Oxygen Sensors:

An oxygen molecule (O_2) is an efficient quencher of both fluorescence and phosphorescence. The phosphorescence quenching is especially efficient due to the triplet ground state of O_2, enabling efficient energy transfer from an excited phosphorescent triplet state. The value of k_q is proportional to the probability of collisions between fluorophore and quencher. Therefore, the bimolecular diffusion constant k_q observed for oxygen in solution is the most important variable among all the cited quenchers [37].

The quenching of PL by oxygen is a phenomenon that is frequently observed in many luminescent materials. In general terms, photoluminescence occurs when a material absorbs a photon of sufficient energy for self-illumination. The entity that absorbs the photon may be a discrete molecule, or a defect in a solid-state material, and is often referred to a "carrier". When the photon has been absorbed, the carrier is elevated into a higher energy, "excited" state. The carrier will then relax back to its ground state after a certain length of time. This "lifetime" of the excited state is usually on the order of nanoseconds to microseconds. The mechanism by which the carrier relaxes determines whether the photoluminescence is termed "fluorescence" or "photoluminescence (PL)." If an oxygen molecule collides with a carrier while it is in its excited state, the oxygen molecule will absorb the excess energy of the carrier and quench the photoluminescence. The oxygen molecule absorbs the energy and undergoes a triplet-to-singlet transition, while the carrier undergoes a non-radiative relaxation. The efficiency of the photoluminescence quenching is, therefore, determined by the number of collisions between the material containing the carrier, and the oxygen

molecules. The collision frequency of gases is determined by the pressure (P), temperature (T), and the number of molecules present. At a certain P and T, the quenching efficiency and, consequently, the photoluminescence intensity, will be determined by the concentration of oxygen in the atmosphere surrounding the material.

Oxygen sensors based on this principle have been extensively studied. Typically, an oxygen-sensitive dye, such as Pt octaethylporphyrin (PtOEP), is embedded in a thin polymeric matrix. Collisions of oxygen molecules with the dye result in quenching of *I* and shortening of τ ; ideally, the inverse of both is linear with O_2 concentration [O_2] (see Eqn. 1). Coupling the oxygen sensing film with specific enzymes results in biosensors e.g., glucose, alcohol, and lactate, enabling fabrication of a multianalyte sensor array, in particular when using an OLED pixel array as the excitation source [40].

Glucose sensing methods often rely on the enzymatic oxidation of glucose in the presence of glucose oxidase (GOx). The glucose concentration can be determined by analyzing the reaction products, or by measuring the PL intensity *I* or PL decay time or lifetime τ of an oxygen-sensitive dye, co-embedded with GOx in a thin film or dissolved in solution. In the presence of glucose, the PL quenching of the oxygen-sensitive dye molecules is reduced (i.e., their PL intensity and lifetime increase) due to the enzymatic glucose-oxidation-induced reduction in the local O_2 level [41].

Summary of the Detection principle:

In summary, for this novel biosensing mechanism an efficient and conducive excitation source, and an appropriate oxygen sensitive dye acts as crucial components. The experimental set up, as shown in Figure 14, involved placing the final reaction chamber (RC) of the LOC device, immediately after sealing its microembossed features and rotating the device, directly above the OLED pixels and the light sensitive photodetector.

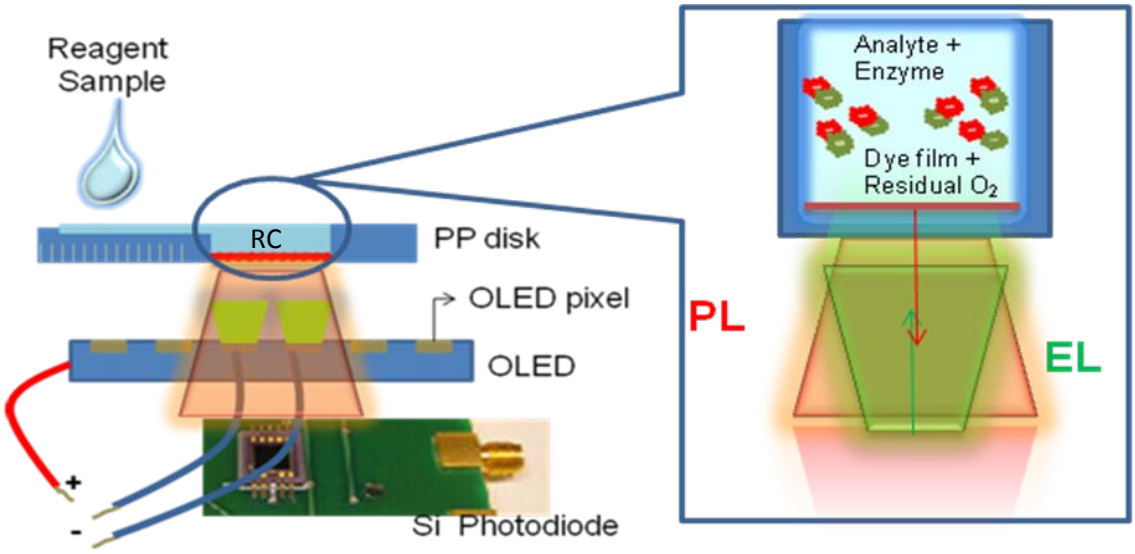

Figure 14. Experimental set up for the proposed detection mechanism

The structure of the oxygen sensitive dyes (tris(4,7-diphenyl-1,10-phenanthroline) Ru chloride (Rudpp) and Pt octaethyporphyrin (PtOEP) that were used in this study are detailed in Figure 15 (A) and (B). Rudpp is a blue light absorbing dye. For studies that involved

Rudpp, the blue light emitting DPVBi based OLED was used; PtOEP is a green light absorbing dye, and for studies that involved PtOEP, green light emitting Alq_3-based OLED was used.

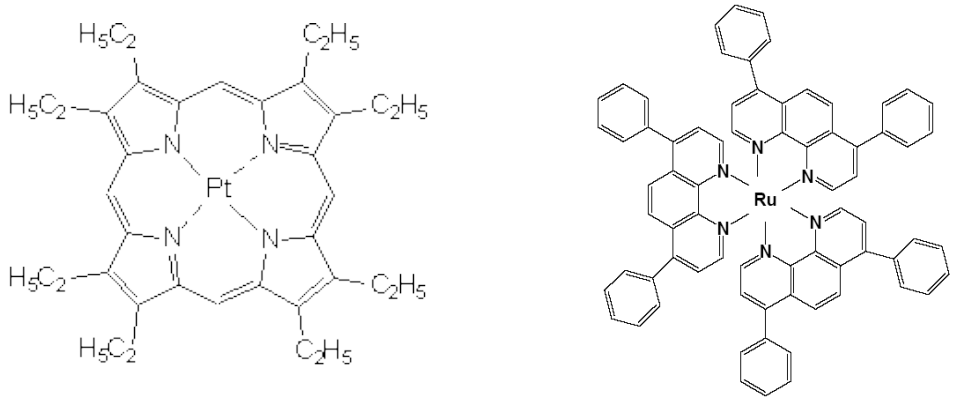

(A) Red emitting (635 nm) PtOEP dye (B) Red emitting (650 nm) Rudpp dye structure

Figure 15. Chemical structures [41] of the two oxygen sensitive dyes used for the study

The different analytes that were studied with the proposed LOC platform were glucose, lactate and ethanol. In general, when an analyte molecule (often in water) comes in contact with its enzyme, which is an oxidase (often also in water) in our case, the analyte molecule will react with the ambient oxygen. This will lead to a decrease in the local oxygen level around the dye molecule, this amount of oxygen content determines the extent of quenching. The level of quenching determines the brightness of the *I* signal and also the duration of the luminance (τ) signal. In other words, when the concentration of the analyte molecule in its buffer is high, more oxygen will be consumed and therefore less quenching will take place. This leads to a longer τ of the excited state of the dye molecules and higher intensity of the

emission. Thus, by measuring the τ or the I of the particular dye sample, it is possible to determine accurately the concentration of a given analyte sample in solution.

A.

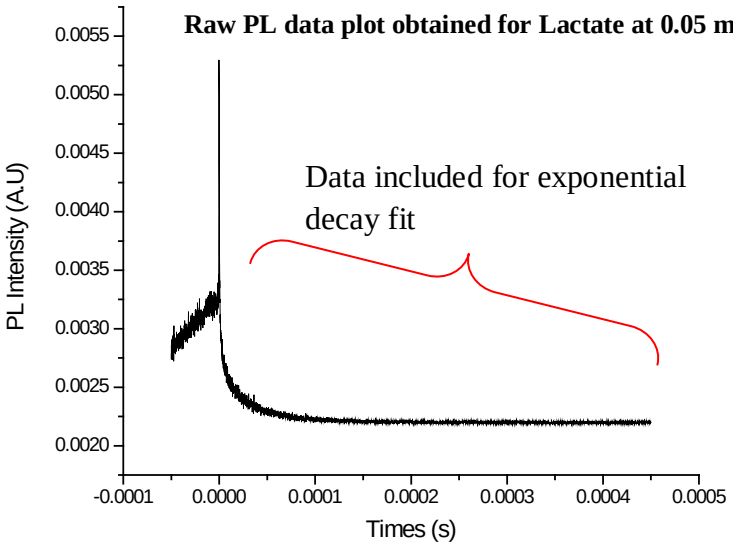

B.

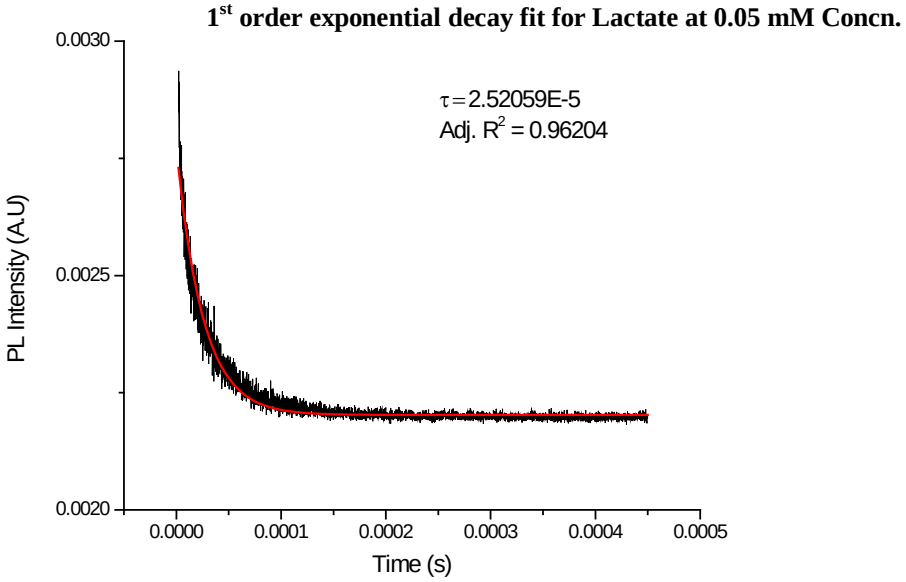

Figure 16 (A). PL intensity plot obtained with Lactate at an initial concentration of 0.05mM and (B). first order exponential decay fit of the selected portion of the raw data.

A.

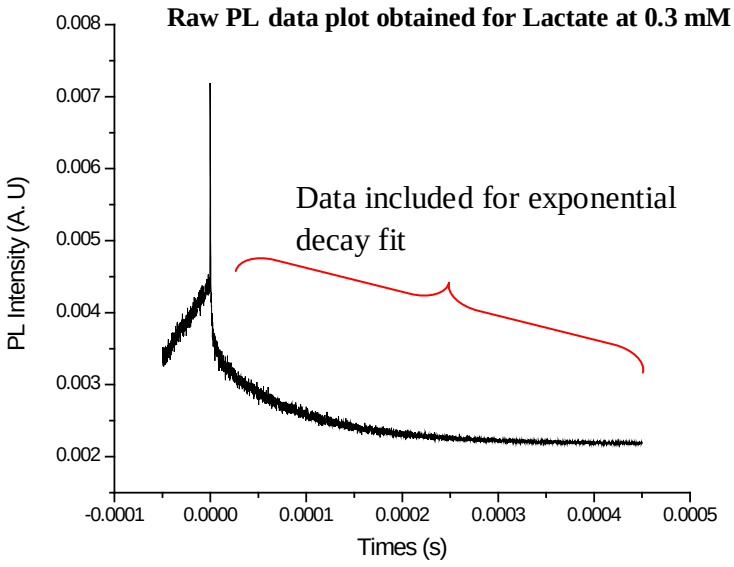

B.

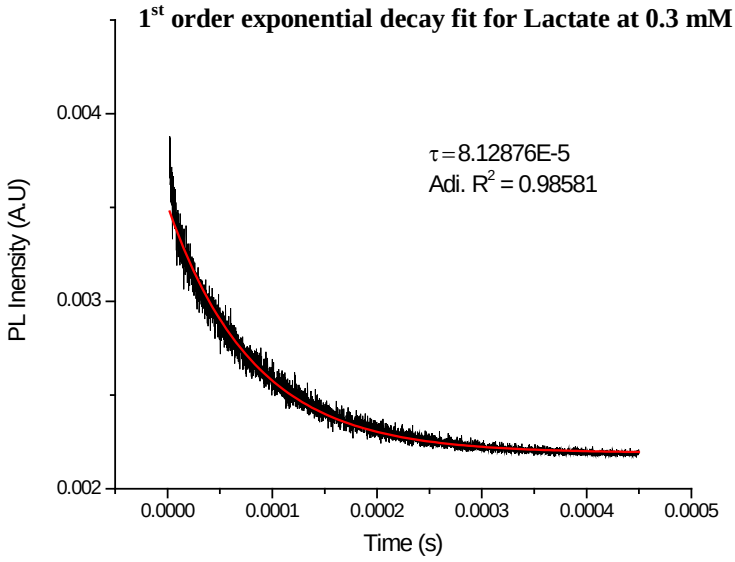

Figure 17 (A). PL intensity plot obtained with Lactate at an initial concentration of 0.3mM and (B). first order exponential decay fit of the selected portion of the raw data.

For example, in this work, typical raw PL intensity data obtained via Labview software and plotted as *I* (in arbitrary units) as a function of time (s) with OriginPro graphical software at low and high concentrations of Lactate are shown in Figures 16 (A) and 17 (B) respectively. Figures 16 (B) and 17 (B). show the plots with τ values after exponentially fitting the raw data in first order at respective lactate concentrations. This procedure of determining the τ values from a preselected range of raw data, at different concentrations, of all analytes (glucose, lactate and ethanol) was adopted throughout this study.

Research Questions

Research questions in this lab-on-CD platform based biosensing project:

Research Question 1

Can the flash formation during polymer microfabrication process be eliminated using microcellular foamed polymer substrates?

Research Question 2

Will the lab-on-CD platform prove to be an efficient biosensing device?

Research Question 3

What degree of versatility can be expected in terms of being able to adopt this biosensing platform for combinatorial studies and real world sample detections?

FUTURE WORK

As future work, I propose:

- using an organic photovoltaic cell (OPV) to power the OLED
- using thin film silicon (Si) photodiodes instead of photomultiplier tube (PMT)

Dissertation Organization

This dissertation begins with an introductory – Chapter 1 is an effort to provide a thorough background of this research project. Most importantly, the outcome of this study will result in three journal publications. While chapter 2 is accepted to be published in the journal of Polymer Engineering and Science (PES), chapters 3 and 4 will be submitted as journal paper manuscripts. Chapter 5 is a brief summary of general conclusions and the proposal for future work.

Chapter 2, titled "Zero Flash Ultrasonic Micro Embossing on Foamed Polymer Substrates A Proof of Concept" details the design of experiment for embossing characterization and also describes the advantages of using microcellular foamed polymer substrates.

Chapter 3, titled "Ultrasonic micro embossed foamed polypropylene bio-CD: A photoluminescence-based estimation of glucose and lactate concentrations " explains the experimental set up, results and discussions.

Chapter 4, titled "OLED-Polypropylene Bio-CD for combinatorial sensor study" provides details on the feasibility studies on detection of unknown concentrations of sugar in corn slurry samples. In addition, results on photoluminescence-based estimation of ethanol concentrations and monitoring concentrations of multianalytes simultaneously on a single bio-CD are also explained in this chapter.

REFERENCES

1. Bashir, R., "BioMEMS: State-of-the-art in detection, opportunities and prospects", *Advanced Drug Delivery Reviews*, Vol. 56, 2004, 1565 – 1586.

2. La Van, D. A., Lynn, M. D., and Langer, R., "Moving smaller in drug discovery and delivery", *Nature*, Vol. 1, 2002, 77 – 84.

3. Yoo S. K., Lee J. H., Yun S., Gu M B, Lee J H., " Fabrication of a bioMEMS based cell-chip for toxicity monitoring", *Biosensors and bioelectronics*, Vol 22, 2007, 1586 – 1592.

4. Wanjun Wang., Steven A. Soper., *Bio-MEMS Technologies and Applications*, 2006

5. Bennig, G., Quate, C. F., and Gerber, C., Atomic Force Microscope, Phys. Rev. Letters, Vol. 56, No. 9. P930, 1986.

6. Nettikadan, S. R., Johnson, J. C., Vengasandra, S. G., Muys, J., Henderson, E., *Virchip: a solid phase assay for detection and identification of viruses by atomic force microscopy*, Nanotechnology, Vol. 15, 2004, pp. 383-389

7. Kuczenski, B., LeDuc, P. R., Messner, W. C., *Pressure-driven spatiotemporal control laminar flow interface in a microfluidic network*, Lab Chip, Vol. 7, 2007, pp. 647-649

8. Jagannathan, H., Yaralioglu, G. G., Ergun, A. S., Khuri-Yakub, B. T., *An implementation of a microfluidic mixer and switch using micromachined acoustic transducers*, IEEE, 2003, pp. 105-107

9. Cabrera, C. R., Yager, P., *Continuous concentration of bacteria in a microfluidic flow cell using electrokinetic techniques*, Electrophoresis, 2001, Vol. 22, pp. 355-362

10. Razunguzwa, T. T., Lenke, J., Timperman, A. T., *An electrokinetic/hydrodynamic flow microfluidic CE-ESI-MS interface utilizing a hydrodynamic flow restrictor for delivery of samples under low EOF conditions*, Lab Chp, Vol. 5, 2005, pp. 851-855

11. Gaudioso, J., Craighead, H. G., *Characterizing electroosmotic flow in microfluidic devices*, Journal of Chromatography A, Vol. 971, 2002, pp. 249-253

12. Natarajan, S., Katsamba, P. S., Miles, A., Eckman, J., Papalia, G. A., Rich, R. L., Gale, B. K., Myszka, D. G., *Continuous-flow microfluidic printing of proteins for array-based applications including surface Plasmon resonance imaging*, Analytical Biochemistry, Vol. 373, 2008, pp. 141-146

13. US Patent 6241480 - Micro-magnetohydrodynamic pump and method for operation of the same (http://www.patentstorm.us/patents/6241480/fulltext.html)

14. Chen-Fu, L., Gwo-Bin, Lee., Chih-Hao, W., Huei-Huang, Lee., Wei-Yin, Liao., Tse-Chuan, Chou., *Microfluidic pH-sensing chips integrated with pneumatic fluid-control devices, Biosensors and Bioelectronics*, Vol. 21, 2006, pp. 1468-1475

15. Paul C. H. Li., *Microfluidic Lab-on-a-Chip for Chemical and Biological Analysis and Discovery*, Chromatographic Science Series, Vol. 94. 2006

16. Madou, M., Zoval, J., Jia, G., Kido, H., Kim, J., Kim, N., *Lab on a CD*, Annual Review of Biomedical Engineering, Vol. 8, 2006, pp. 601-628

17. Zoval, J. V., Madou, M, J., Centrifuge-Based Fluidic Platforms, Proceedings of the IEEE, Vol. 92., 2004, pp. 140-153

18. Duffy, D. C., Gillis, H. L., Lin, J., Sheppard, N. F. Jr., Kellogg, G. J., Microfabcricated Centrifugal Microfluidic Systems: Characterization and Multiple Enzymatic Assays, *Analytical Chemistry*, Vol. 71., 1999, pp. 4669-4678.

19. Lee, B. S., Lee, J. G., Lee, J. N., Parl, J. M., Cho, Y. K., Kim, S., Ko, C., One-step Target Protein Detection from Whole Bllod in a Lab-on-a-Disc, NSTI-Nanotech, Vol. 3., 2008, pp. 241-244

20. Yang, R., Mullen, C., Schaline, M., Reithmaier, K., Sheets, R., High throughput projection UV lithography of high-aspect-ratio thick SU-8 microsturcture, *Microsystems Technology*, Vol. 14., 2008, pp. 1233-1243

21. Alonso-Amigo, M. G., *Polymer Microfabrication for Microarrays, Microreactors and Microfluidics*, Journal of the Association for Laboratory Automation, Vol. 5., No. 6., 2000, pp. 96-101

22. Kuo-Shen, C., I-Kuan, L., Fu-Hsang, Ko., *Fabrication of 3D polymer microstructures using electron beam lithography and nanoimprinting technologies*, Journal Micromechanics and Microengineering, Vol. 15., 2005, pp. 1894-1903

23. Juang, Y., Lee, L, J., Koelling, K. W., *Hot Embossing in Microfabrication. Part I: Experimental*, Polymer Engineering and Science, Vol. 42., No. 3., 2002, pp. 539-550

24. Nguyen, N. T., Chan, S. H., *Micromachined polymer electrolyte membrane and direct methanol fuel cells- a review*, Journal of Micromechanics and Microengineering, Vol. 16, 2006, pp. R1-R12

25. Woo-Chul, J., Young-Moo, H., Gil-Sang, Y., Kwang-Ho, S., Sung-Ho, C., Gun-Hee, K., Myeong-Woo, C., *Micro Machining of Injection Mold Inserts for Fluidic Channel of Polymeric Biochips*, Sensors, Vol. 7., 2007, 1643-1654

26. Paul C. H. Li., *Microfluidic Lab-on-a-Chip for Chemical and Biological Analysis and Discovery*, Chromatographic Science Series, Vol. 94. 2006

27. Lai, S., W, S., Luo, J., Lee, J., Y, S, T., Madou, M, J., *Design of a Compact Disk-like Microfluidic Platform for Enzyme-Linked Immunosorbent Assay*, Analytical Chemistry, Vol. 76., 2004, pp. 1832-1837

28. Tzong-Shyng, L., Pei-Yu, C., *Pressure barrier of capillary stop valves in micro samples separators*, Sensors and Actuators A, Vol. 115., 2004, pp. 508-515

29. Madou, M. J., Lee, L. J., Koelling, K. W., Daunert, S. , Lai, S., Koh, C.G., Juang, Y.J., Yu, L., *Design and Fabrication of Polymer Microfluidic Platforms for Biomedical Applications*, ANTEC-SPE 59th, Vol. 3, 2001, pp. 2534–2538

30. Xu, G., Yu, L., Lee, L. J., Koelling, K. W., Experimental and Numerical Studies of Injection Molding With Microfeatures, Polymer Engineering and Science, 2005, pp. 866-875

31. H. Chih-Mingand Yu-Ching Tai, *Annu. Rev. Fluid Mech.*, 30, 579–612, (1998).

32. Okamoto, K. T., Microcellular Processing, 1st Ed., 2003, ISBN 1-56990-344-1

33. Ortiz, S. Jr., "New Monitor Technologies are on display" *Computer*, 36 (2), 13 – 16, 2003

34. Sugimoto. A, Ochi H, Fujimura S, Yoshida A, Miyadera T, Tsuchida M, "Flexible OLED displays using plastics substrates", 10 (1), 107 – 114, 2004.

35. Scott, J. C.; Malliaras, G. G.; Salem, J.R.; Brock, P. J.; Bozano, L.; Carter, S. A. *SPIE Proc.* **1998**, *3476*, 111-122.

36. Shinar, J. *Organic light emitting devices*; AIP press: New York, 2005.

37. Zhou, Z., Shinar, R., Allison, A. J., Shinar, J., *Enhanced Photoluminescence of Oxygen Sensing Films through Doping with High Dielectric Constant Particles*, Vol. 17., 2007, pp. 3530-3537

38. Ewing's Analytical Instrumentation Handbook, 3rd Edition., 2004, ISBN 0824753488

39. Albani, J. R., Structure and Dynamics of Macromolecules: Absorption and Fluorescence Studies 2004 Published by Elsevier ISBN 044451449X

40. Shinar, J., Shinar, R., Organic light-emitting devices (OLEDs) and OLED-based chemical and biological sensors: an overview, Vol. 41, 2008, pp. 1-26

41. Choudhury, B., Shinar, R., Shinar, J., Glucose biosensors based on organic light-emitting devices structurally integrated with luminescent sensing element, Journal of Applied Physics, Vol. 96, No. 5, 2004, pp. 2949-2954

CHAPTER 2: ZERO FLASH ULTRASONIC MICRO EMBOSSING ON FOAMED POLYMER SUBSTRATES: A PROOF OF CONCEPT

(Accepted in the Journal of Polymer Engineering and Science)

Srikanth G. Vengasandra, Greg Harmon, David Grewell

ABSTRACT

This article reviews a novel method to produce micro-embossed features with an aspect ratio of three and negligible flash on polymer surfaces. An embossing technique that utilizes localized heating (ultrasonic energy) was used with polystyrene and polypropylene substrates. It was demonstrated that when foamed substrates were used, the amount of flash produced was negligible compared to non-foamed substrates, which has been a significant unresolved problem with embossing using localized heating. The depth of micro-embossed features as a function of heating times and amplitudes of ultrasonic embossing is detailed in this paper, along with a characterization of complex embossed geometries. It was seen that embossing depth was generally proportional to heating time and amplitude until the maximum feature depth was achieved. While this paper deals with embossing of micro-features for lab-on-a-CD applications, it is envisioned that it is also suitable for lab-on-a-chip applications.

INTRODUCTION

Micro-electro-mechanical-systems (MEMS) are common in many industries. Examples can be found from anti-locking breaking systems [1] in the automotive industry to diagnostic instrumentation [2-4] for the medical industry. For example, MEMS technology is used to identify unknown substances or to determine key DNA codes from a single drop of fluid. Historically, MEMS devices have been fabricated with/on silicon substrates leveraging off of the technology from the micro-electronic industry. In addition, there has been the development and implantation of more complex devices referred to as "labs-on-a-chip" that can perform assays as complex as DNA analyses. However, recently the use of polymer-based substrates has been investigated. These devices offer low manufacturing cost, which in turn offers disposability in many cases. While potentially having many advantages, these products have one limitation: they need dedicated instrumentation for full functionality. Work by others has demonstrated platforming these devices on standard computer CD's so that any personal computer with the proper software can read its diagnostic information [5,6]. These devices are referred to as lab-on-a-CD and can perform a wide range of functions, including mixing and fluid flow control. In addition to having the benefit of being functionalized by any PC, a lab-on-a-CD also has an added possible feature that the motion (spinning) can be used to open valves and promote mixing [7].

However, the manufacturing of "lab-on-a-CD", is relatively challenging. For example, currently injection molding is the preferred method of fabricating such devices; however, there are limitations related to aspect ratios, which are critical for many assay functionalities.

In addition, with injection molding there are high injection pressures that can damage the delicate features of the mold, as well as cause disengagement issues of the mold from the part. Researchers in this area have been developing manufacturing alternative techniques that allow depth-to-width aspect ratios ranging from 1:2 to 1:5. Techniques such as computer numerically controlled (CNC) machining, photolithography and LIGA-like processes have also been studied to manufacture features with high aspect ratios [7]. Current research has shown that embossing techniques that utilized localized heating of micro-channels has some benefits, including relatively low forces and pressures, relatively fast cycle times and relatively low capital costs. For example, as detailed in the following text, ultrasonic embossing can emboss substrates in a few seconds, with forces as low as kg (depending on the embossing size) and the capital cost of a typical system is less than $25,000 (USD) [8-10]. The development of such low-cost micro-fabrication techniques, suitable for high-volume production, will prove to be the key for commercialization of polymer micro-system technology.

However, localized heating coupled with embossing produces undesired flash, which must be removed with costly secondary operations such as machining or encapsulation [4,10]. In more detail, the flash is displaced material that usually accumulates at the surface of substrate near the embossed feature. This accumulation results in a local upheaval of the surface making it difficult to bond to that surface. It is possible to heat the entire surface of the substrate and reform the flash to a flat surface, but this is not desirable because it increases the heat input, cycle time, requires the entire substrate to be heated and results in weld lines

on the surface. Thus, zero-flash embossing is not possible with conventional methods using localized heating.

In this work, a manufacturing process has been demonstrated and developed to allow depth-to-width aspect ratios of approximately 3:1 to be embossed using localized heating without the generation of flash. In more detail, microcellular foamed substrates were embossed through a localized heating technique, namely ultrasonic heating; however, other heat sources such as lasers can be used. The concept of using microcellular foamed substrates was chosen because it allows absorption of the flash during embossing. During the absorbing phase of the embossing process, a compressional model of the cells can be used. For example, assuming a micro-cellular density of ρ_1 and a fully consolidated density of ρ_2 (no foaming remaining), the ratio of the embossed volume (V_1) to the consolidated volume (V_2) can be used to estimate the amount of material that must be absorbed, see Figure 18 and Eq, 1.

$$\frac{\rho_1}{\rho_2} = \frac{V_2}{V_1 + V_2} \tag{1}$$

Thus, heat flow and squeeze flow is critical in achieving the proper ratio of V_1/V_2 so that smooth surfaces are produced at the end of the embossing process. This dimensionless ratio allows the prediction of the volume that is required to absorb the flash produced from a given embossed feature based on foaming level. This can be used to estimate critical dimensions such as substrate minimum thickness or minimum distances between embossed features.

It should be noted that, as the cells are compressed, pressure will develop within cells that do not rupture which may result in residual stresses. In addition, ruptured cells may result in local surface roughness. Some of these effects are discussed in the "Results" section of this paper.

Because most virgin polymer surfaces are hydrophobic, the surface must be modified to promote wetting, capillary action and proper fluidic motion. This can be achieved through oxidation or chemical deposition of hydrophilic layers [11]. In more detail, ozone treatment can alter the surface property to make a surface hydrophilic. By ozone treatment, functional groups, such as carbonyl, carboxyl, C=C, peroxide and hydroxyl (OH) are formed, depending on the polymer sample, under the exposure of ozone [12,13]. Researchers have designed special chambers (burst chambers) and demonstrated their ability to stop flow and act as valves [14,15]. These valves prevent fluid flow until an outside force, such as centripetal force induced by an angular velocity, causes the valve to open. It has been proposed and demonstrated that such forces can be achieved in a standard CD player allowing the control, timing and sequencing of mixing of various chemistries.

EXPERIMENTAL

The overall approach of this research was: 1) proof of concept of zero flash embossing, 2) process and feature characterization of zero flash embossing and 3) product demonstration. In order to achieve each of these goals, experiments were conducted following the procedures detailed in the following sections.

EQUIPMENTS AND TOOLING

A 2000 Series (20 kHz, 2200 W) ultrasonic welding system (Branson Ultrasonics (Danbury, CT)), was used for embossing. A flat plate aluminum fixture with recessed features captured the samples which were secured in place with clamps.

Two separate embossing features were studied: 1) a so called dog-bone sample and 2) a complex design for application characterization. For the purpose of process characterization, the simple dog-bone geometry feature was fabricated on an aluminum horn by Branson Ultrasonics and used as an embossing tool. The details of the pattern are shown in 19.

In later trials, a more complex geometry was studied. This feature demonstrated that a wide range of feature volumes, depths and widths could be embossed without flash generation on a uniformly foamed substrate. For example, as seen in Figure 20, the feature width varied from 100 µm to 10,000 µm. The other motivation for this design was to develop a proof of concept for detection of proteins conductive to the Anthrax virus. This horn was fabricated from titanium and was also manufactured by Branson Ultrasonics.

MATERIALS

For the proof of concept experimentation, embossing was completed with four different types of materials: regular (standard) materials types of polystyrene (PS), and polypropylene (PP), microcellular (mucell) foamed types of polystyrene (microcellular PS) and microcellular PP. Standard PS samples were cut from 3.2 mm extruded sheets. In this case, the level of

foaming was 0% and was considered as the control group. Extruded foamed sheets of PS, PP and standard PS were all obtained from Trexel Corporation (MA) with a foaming level of approximately 15%, while standard PP was obtained from Washington Penn Plastics Co., Inc (PA). The PS microcellular foam had cell diameters typically ranging from 5 to 25 μm, which is approximately ten times smaller than the cell sizes found in conventional PS foam [16]. The microcellular PP foamed material had cell diameters ranging from 25 μm to approximately 200 μm. It is important to note that the size of the bubbles and the level of foaming is determined by the solubility of the foaming gas and processing conditions during the extrusion/injection molding process. Thus, the bubble size and foaming level is usually material dependent. A summary of the thermal, density and water contact angles of the various materials is detailed in Table 4. The thermal properties were measured with differential scanning calorimetery (DSC), the density was measured by volume and mass measurements and the contact angles was measured using distilled water and measuring the contact wetting angle.

EMBOSSING PROCEDURE

All four different types of materials were considered for the study. In case of PS, three different amplitudes (20 μm_{pp}, 30 μm_{pp} and 40 μm_{pp}) were based on screening experiments. These amplitudes, which are relatively low considering ultrasonic welding of PS, which typically uses 40-60 μm_{pp} of amplitude, were selected in order to reduce the risk of tool damage. While the embossing time/heating time (time the energy was applied) was varied from 0 to 10 seconds at 0.5-second intervals, the clamp force was held constant at 245N. The trigger force (force at which sonics are activated) was adjusted to match within 98% of the

weld force. This protocol was completed in order to assure a relatively constant force during the entire welding cycle and reduce experimental error.

Similarly, work with PP material involved three different amplitudes (20 μm_{pp}, 30 μm_{pp} and 40 μm_{pp}) based on screening experiments. However, the embossing time was varied from 0 to 7 s (for 20 μm_{pp}), 0 to 10 s (for 40 μm_{pp}) and 0 to 30 s (for 60 μm_{pp}), respectively for standard PP and only 0 to 7 s (for all three amplitudes) of the embossing time for microcellular foamed PP. Heating time intervals of 0.5-seconds were considered with all four different types of materials. All experiments were replicated five times.

In all cases the samples were secured with toggle clamps to an aluminum fixture and aligned with the horn by manually engaging the horn and substrate without activating the ultrasonics, Proper alignment was visually judged.

SURFACE MODIFICATION

In order to promote wetting, two different chemical coatings obtained from Goulston Technologies (Monroe, NC) were studied. Selected PP samples were pretreated either with a silicone surfactant solution system (Lurol 12134) or organic solution system (Lurol 12135). The coatings were diluted with DI (de-ionized) water at a ratio of 1:10 and the dilution was applied directly to the polymer sample (post embossing) substrates and left for approximately 15 min under clean, humid conditions. The pretreated sample surfaces were then rinsed with DI water and blown dry under air pressure.

SAMPLE CHARACTERIZATION

The quality of the embossed features was characterized with a low vacuum (variable pressure) Hitachi S-2460N Scanning Electron Microscopy (SEM) environmental system. The variations in depth of the micro-channels were estimated using an inverted optical microscope, inverted metallograph and profilometers. An optical microscopy (OM) (Olympus BX51) was used for depth measurements based on cross sectional images, an inverted metallograph (Nikon, Epiphot 200) was used based on topological focal length variations, and furthermore the depth measurements were confirmed with a laser profilometer (Model Solarius Inc. – AF 2000) and also an optical profiler (Microphotonics). For OM depth measurements, the samples were cross-sectioned using a diamond saw through the embossed feature and the depths were measured using a calibrated scale.

The surface energy of the treated and untreated substrate surfaces were measured following the ASTM D 7490-08 based on contact angle measurement techniques and Owens-Wendt-Kaelble equation, Eq 2., with water and polyethelne glycol (PEG), which has surface energies of (γ_w) 72.8 dyne/cm^2 (γ_g) 48.3 dyne/cm^2

$$\gamma_l(1+\cos(\theta)) = 2\left(\sqrt{\gamma_l^d \gamma_s^d} + \sqrt{\gamma_l^p \gamma_s^p}\right) \qquad \text{Eq. 2}$$

Where γ_l^d, γ_s^d are the dispersive components of the liquid and solids respectively and γ_l^p, γ_s^p are the polar components of liquid and solids respectively. For PEG the dispersive (γ^d_{peg}) and polar components (γ^p_{peg}) were 29.3 and 19.0 dynes/cm^2. For the water the dispersive (γ^d_{H20}) and polar components (γ^p_{H20}) were 21.8 and 51.0 dynes/cm^2.

RESULTS AND DISCUSSIONS

Proof of Concept

As seen in the SEM image, Figure 21, the embossed feature on the micro-cellular foamed sample had no flash. In more detail it regional labeled absorbed flash is the region where the foamed material has been compressed. It is interesting to note that the majority of the flash was absorbed only on one side of the feature. It is believed that this is the result of minor alignment issues. In these preliminary results, the foaming level was too high to allow for full consolidation as evident in the surface roughness. However, it is seen that there is no flash with the foamed substrate.

Figure 22 shows an SEM image of an embossed sample with regular PS, which clearly shows the generation of flash. In addition, it is seen that the amount of flash is proportional to the width of the embossed feature. For example, the flash produced from the channel is significantly less compared to the flash produced at the wider section of the reservoir. It is also seen that the interior walls of the embossed feature are relatively smooth. Because the same tool was used for both substrates, this suggests that the irregular surfaces of the micro-cellular foamed substrate (Figure 21) are the result of the morphology of the foamed substrate and it is believed that it is the caused by excessive foaming and not related to tooling.

Figure 23 shows an SEM image of an embossed PP foamed sample. It is seen that, unlike the previous results with PS, the surface at the base of the feature is smooth and the edges are also relatively smooth. This suggests that the level of foaming was nearly ideal for this material (PP) and feature size. Most importantly, it is seen that there is no flash. It is also seen that there is some surface roughness at the corner of the feature, suggesting that additional process optimization may be needed depending on the application requirements. This roughness is considered acceptable because its size is a fraction of the total size of the embossed feature. However, this roughness may prove to be an issue as the feature size decreases. The roughness seen in the corner of the features is believed to be the result of "tearing" or yielding of the resin-rich surface and may be reduced through process and material optimization. More details of this resin-rich surface are provided later in a following paragraph.

Process Characterization with PS

Figure 24 (A) and (B) show feature depth as a function of heating times for various amplitudes with standard and foamed PS substrates, respectively. As expected, depth is generally proportional to heating time; however, in most cases there is an inflection point once the depth approaches 300 µm. This is due to the fact that the tool depth is 300 µm and at this depth the tool is fully engaged into the substrate. Thus, the tool "bottomed out" and further engagement was not possible. It is important to note that the trend line is added for visualization purposes only and is not statistically significant. The standard deviation corresponds to the error bars for each data point.

It is also seen from these plots that higher amplitudes promote faster embossing. For example, as seen in Figure 24 A, with 20 µm of amplitude and with 3 s of heating, the depth is less than 50 µm, while with 40 µm of amplitude, the depth is approximately 300 µm. This is expected because heating rates are proportional to the amplitude squared. It is also seen that generally the time required to achieve the full embossing depth of 300 µm is slighlty higher for standard PS compared to foamed PS. This is expected because the foamed PS has a relatively lower density and corresponding lower thermal mass, thus requiring slightly reduced embossing time.

Process Characterization with PP

Figure 25 shows embossed depth as a function of embossing time at various amplitudes with standard (A) PP and foamed (B) samples. Again, as expected, depth is generally proportional to heating time.

In addition, it is also seen that generally the time required to achieve the full embossing depth of 300 µm is longer for standard PP compared to foamed PP. Again, this is expected because the foamed PP has a relatively lower density and corresponding lower thermal mass, thus requiring slightly smaller embossing time. It is interesting to note that standard deviation is very small for experiments. While there is no clear reason for this, it is believed to be related to crystalline structure of the PP and relatively clear melt temperature.

Verification of density model

In order to verify the density model, Eq. 1, the densities and volumes were estimated by digitizing images of the cross sectioned embossed features. In these measurements, in order to eliminate the dimension in and out of the image (Z-direction), a quasi 2-D model was assumed. This assumption is valid because in all cases the location was selected where $\frac{\partial V}{\partial z} = \frac{\partial \rho}{\partial z} = 0$ based on geometry. Thus, it was assumed that the depth was one unit deep and during the area measurements, arbitrary units of length were used. Selected images are seen in Figure 26 (A) and (B), where the features and bubble are highlighted, respectively. By using the "Area" feature in ACAD ®, the volumes of the bubbles and features were estimated and used for volume (V) and density (ρ) calculation, along with the known densities of the resin. It was found that V_1 and V_2 were 0.37 and 2.11 unit^3 and ρ_1 and ρ_2 were 0.67 and 0.76 g/mm^3, respectively. While the specified density of the base material should be 0.9 g/mm^3, as detailed by the supplier, it is seen that the actual density is slightly lower. It is believed that this difference is within experimental error of measurement of the volumes, as this is related to the skill of the operator. In addition, as seen in Figure 26, there are residual cells in the compacted region.

Based on the experimental study, the two dimensionless ratios ($\frac{\rho_1}{\rho_2}$) and ($\frac{V_2}{V_1 + V_2}$) were (0.78, 0.87, 1.06) and (0.56, 0.84, 0.70) for various locations as detailed in Figure 27, which are generally in good agreement. It is seen that with the larger embossing features (locations 1 and 3), the density ratio is slightly higher and that based on the images seen in Figure 27, the quality of the features appear to have higher fidelity. It is believed that this is caused by the larger amount of mass transfer and high compaction of the foamed material. Thus, it is

believed that the derived fundamental process model is in relatively good agreement with the physical process. It is also important to note that while the feature depth ranged from 125 to 822 µm, the resulting surfaces of the embossed features are similar. It is believed that this is due to the foaming technique that promoted a resin-rich surface that retained its original morphology and promoted relatively smooth surfaces. Evidence of the resin-rich surface is further seen in Figure 27, where there is a constant resin layer between the bubbles and the outer surface.

Surface characterization- PP/water Surface Energy Characterization

Ozone treatment did increase the surface energy of PP surface but proved to be time consuming [17]. Thus, as an alternative, PP samples were treated with two coating techniques: a silicone surfactant solution system and an organic solution system in order to increase the relative surface energies. These coatings increase surface activity and are useful not only to effectively increase energies on polymer surfaces [18], but also to promote flow [19]. As seen in Figure 28, a side view of untreated PP (A) and treated (B) PP, there is significantly more wetting with the treated sample.

The contact angles for both the uncoated hydrophobic PP and Lurol 12135 coated hydrophilic PP sample surfaces were measured using 'ImageJ' software and were found to be 72.7 and 32.7° with water, respectively. For PEG the contact angles for the uncoated and coated samples were 59.0 and 30.1°, respectively. The surface energies of the uncoated and coated samples were found to be 30.7 (γ_{pp}^{p}=21.8, γ_{pp}^{d}=8.9 dynes/cm^2) and 72.2 (γ_{pp}^{p}=69.7, γ_{pp}^{d}=2.5

dynes/cm^2) dynes/cm^2, respectively. Thus, it is seen that the surface energy of the treated sample was approximately 135% higher compared to the untreated sample.

Figure 28 (A) shows the wetting characteristics of an untreated sample with the application of blue food color and water. As expected, it is seen that there is little wetting and no capillary action. In contrast, images (B) through (E) show wetting and capillary flow for the treated samples at five second intervals. It is seen that despite the relative roughness at the corners of the samples as seen in Figure 29, the channels promote flow. As previously detailed and proposed by others [7], it is envisioned that a potential interface system design for such a design would be a standard CD platform [20].

CONCLUSIONS

It was proven that a foamed polymer substrate allows flash-free micro embossed features and reduces the required heating times by as much as 60% for foamed PP substrate compared to standard PP. The free volume of the foamed substrate absorbs the displaced material, promoting a flash-free embossed feature. It was generally seen that embossing depth was proportional to processing parameters, such as heating time and amplitude. Once the embossing tool was fully engaged, the embossing depth did not increase with additional time. Surface modification allowed the channels to act as capillaries promoting fluid flow. It has been demonstrated that ultrasonic embossing can be as fast as a few seconds. This work also verified a dimensionless ratio of volumes compared to densities based on the embossed design.

In this study it has been demonstrated that micro-embossing with localized heating is possible by using foamed polymer materials as substrates for a wide range of applications that require the functional capabilities of other commonly used substrates such as silicon and glass. In addition, chemical treatment of embossed features allowed hydrophilic surfaces to be generated on polymer substrates that promoted capillary action. Thus, this work demonstrated a novel embossing technique that, combined with the improved wetting, can be used for a variety of applications.

ACKNOWLEDGEMENTS

We are grateful to Branson Ultrasonics (Danbury, CT) for donating the ultrasonic welding equipment. We would like to thank Dr. Joseph Shinar, Dr. Stephen Holland, Dr. Zhiqun Lin and Dr. David Eisenmann for their cooperation in letting us use their ozone generating equipment, Laser Profilometer, Polarized Optical Microscope and inverted metallograph respectively. We thank Bioforce Nanosciences Inc. (Ames, IA) for letting us use their proprietary ozone generating equipment during initial studies. We also would like to acknowledge Goulston Technologies and Trexel Inc. for providing us free samples of the chemical coating material and polymer substrates, respectively.

REFERENCES

1. V. K. Varadan, V. V. Varadan, *Smart. Mater. Struct.*, **9**, 953–972 (2000).

2. W. J. Judy, *Smart Mate r. Struct.*,**10**,1115–1134, (2001).

3. A. Lee, R. B. Fair, *Proc. of the IEEE* 92, 3-5 (2004).

4. C. M. Ho, Y.C. Tai, *Annu. Rev. Fluid Mech.*, **30**, 579–612, (1998).

5. J. Steigert, M. Grumann, T. Brenner, K. Mittenbühler, T. Nann, J. Rühe, I. Moser, S. Haeberle, L. Riegger, J. Riegler, W. Bessler, R. Zengerle, J. Ducrée, *JALA*, **10**, 331-341, (2005).

6. L. Reigger, M. Grumann, J. Steigert, S. Lutz, C. P. Steinert, C. Mueller, J. Viertel, O. Prucker, J. Ruhe, R. Zengerle, J. Ducree, *Biomed. Microdevices*, **9**, 795–799, (2007).

7. L. J. Lee, M.J. Madou, K.W. Koelling, S. Daunert, S. Lai C.G. Koh, Y-J Juang, Y. Lu and L. Yu, *Biomed. Microdvcs.*, **3**, 339-351, (2001).

8. L. Chunmeng, D. Grewell, J. Lee, A. Benatar, *Poly. Eng. & Sci.*, **45**, 6, 661-666, (2005).

9. H. Becker, U. Heim, *Sens. Actuators, A.*, **83**, 130-135, (2000).

10. D. Grewell, A.Benatar , *Eng. & Sci.*, **48**, 8, 1542-1549 (2008)

11. M. J. Madou, Fundamentals of Microfabrication: The Science of Miniaturization, *2nd Ed., CRC Press, NY*, (2002).

12. K. Fujimoto, Y. Takebayashi, H. Inoue ,Y. Ikada, *J. Poly Sci, Poly. Chem.*, **31**, 1035-1043, (1993).

13. S. G. Hong, C. M. Liao, *Polym. Degrad. Stab.*, **49**, 437-447, (2000).

14. B. R. Wenner, P. M. Douglass, Y. Lu, S. Lai, Y. J. Juang, J. L. Lee, M. Madou, S. Daunert, *Intern Confer. On Enviro. Systms.*, (2000).

15. P. Jong-Myeon, *Lab Chip*, **7**, 557–564, (2007).

16. T. K. Okamoto, Microcellular Processing, Hanser Gardner Publications, (2003).

17. S. Vengasandra, D. Grewell *SPE ANTEC Proceedings, Brookfield,* 1041-1045, (2007).

18. M. Srividhya, K. Chandrasekar, B. Geetha and B. S. R. Reddy, *Polym.*, **48**, 1261–1268, (2007).

19. E. Tombacz, D. Bica, A. Hajdu, E. Illes, A. Majzik, L. Vekas, *J. Phys.: Condens. Mattr.*, **20**, 204103, (2008).

20. S. Vengasandra, D. Grewell, *SPE ANTEC Proceedings, Brookfield,* (2008).

TABLES AND FIGURES

Material	**Tg (^{0}C)**	**Tm(^{0}C)**	**Density (g/cm^3)**	**Water Contact Angle (^{0})**
PP	130	165	0.946	65.53
Foamed PP	120	160	0.804	72.65
PS	105	NA	1.05	62.57
Foamed PS	105	NA	0.892	70.42

TABLE 4. Selective properties for the materials studied

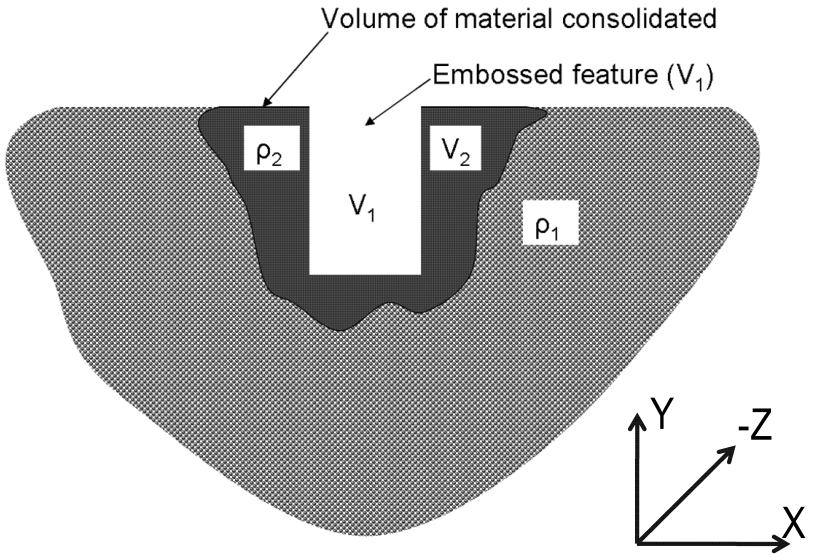

FIG. 18. Theoretical cross section of embossed micro-cellular substrate

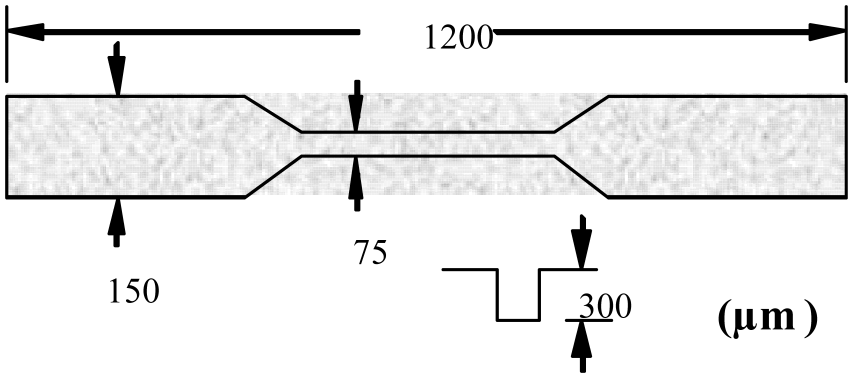

FIG. 19. Details of "dog bone" micro-feature that was considered for embossing (2 reservoirs connected by micro-channel)

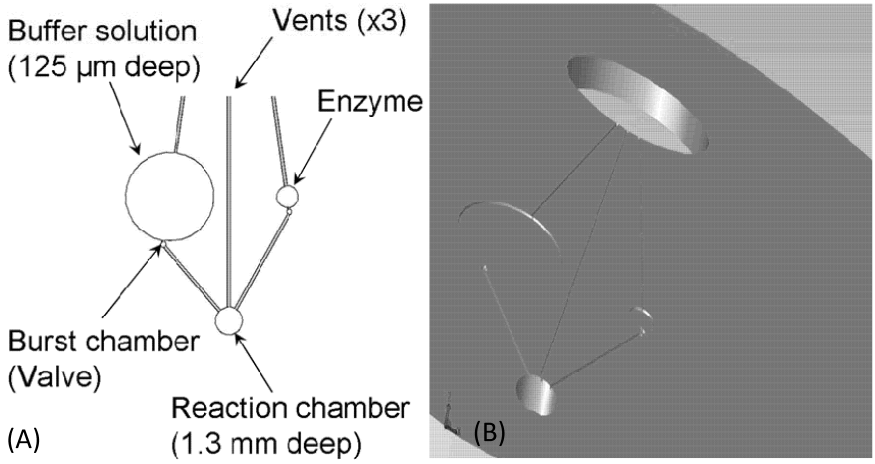

FIG. 20. (A) Details of feature for embossing on CD for anthrax detection (B) computer image of the features on the lab-on-a-CD application.

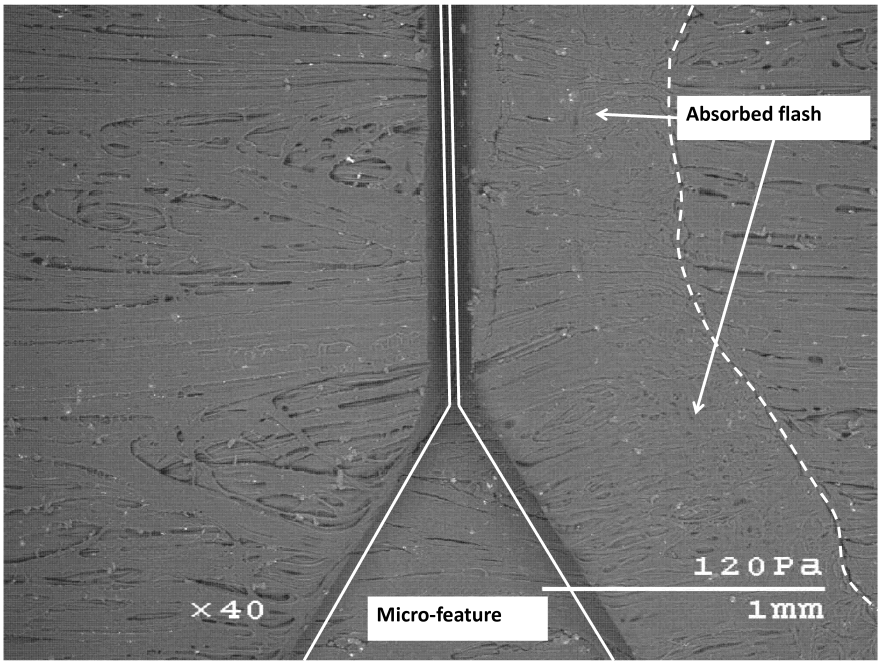

FIG. 21. SEM image of embossed feature on a foamed PS

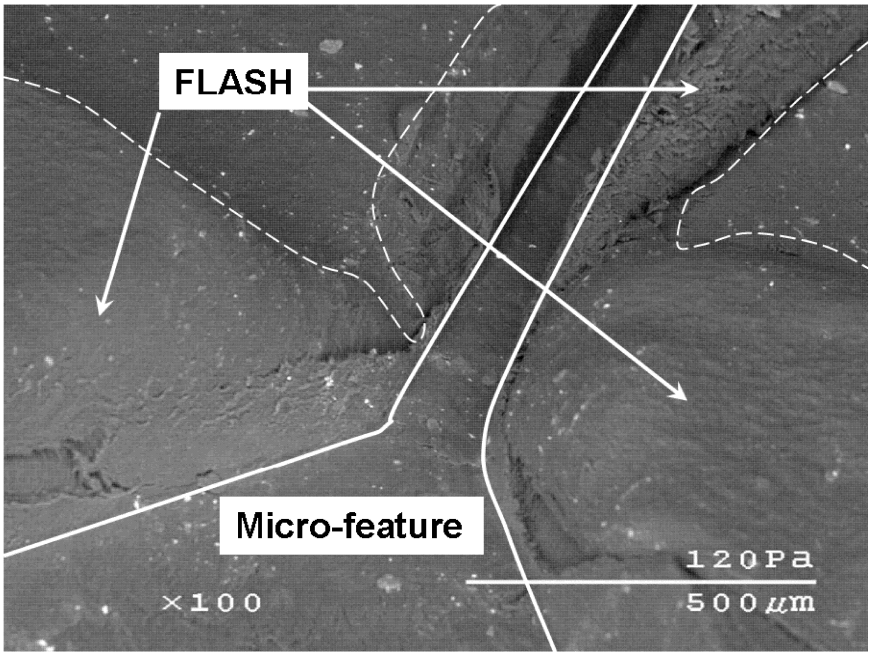

FIG. 22. SEM image of embossed micro-feature on regular PS

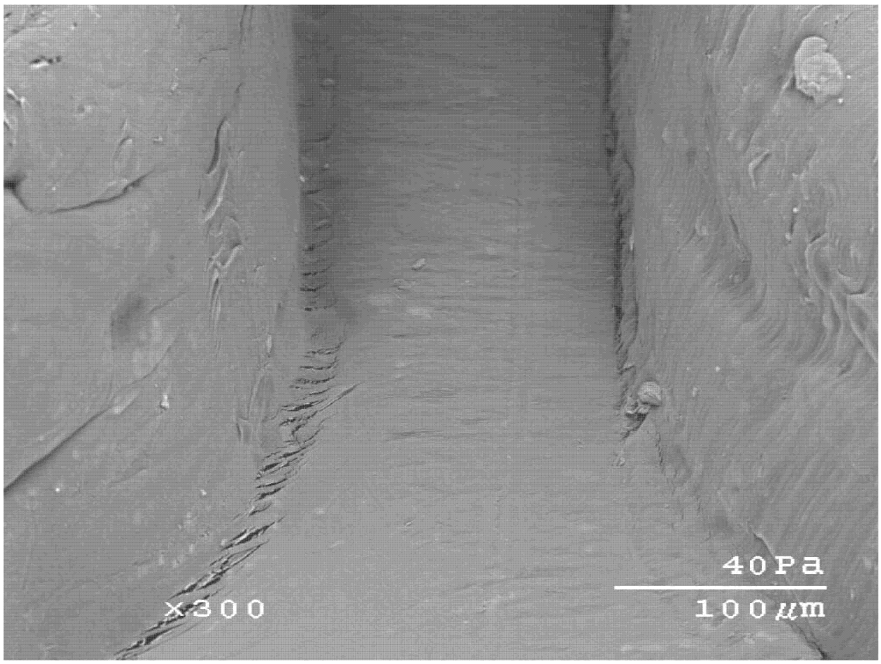

FIG. 23. SEM image (300x) of a part of a dog bone pattern on a foamed PP sample

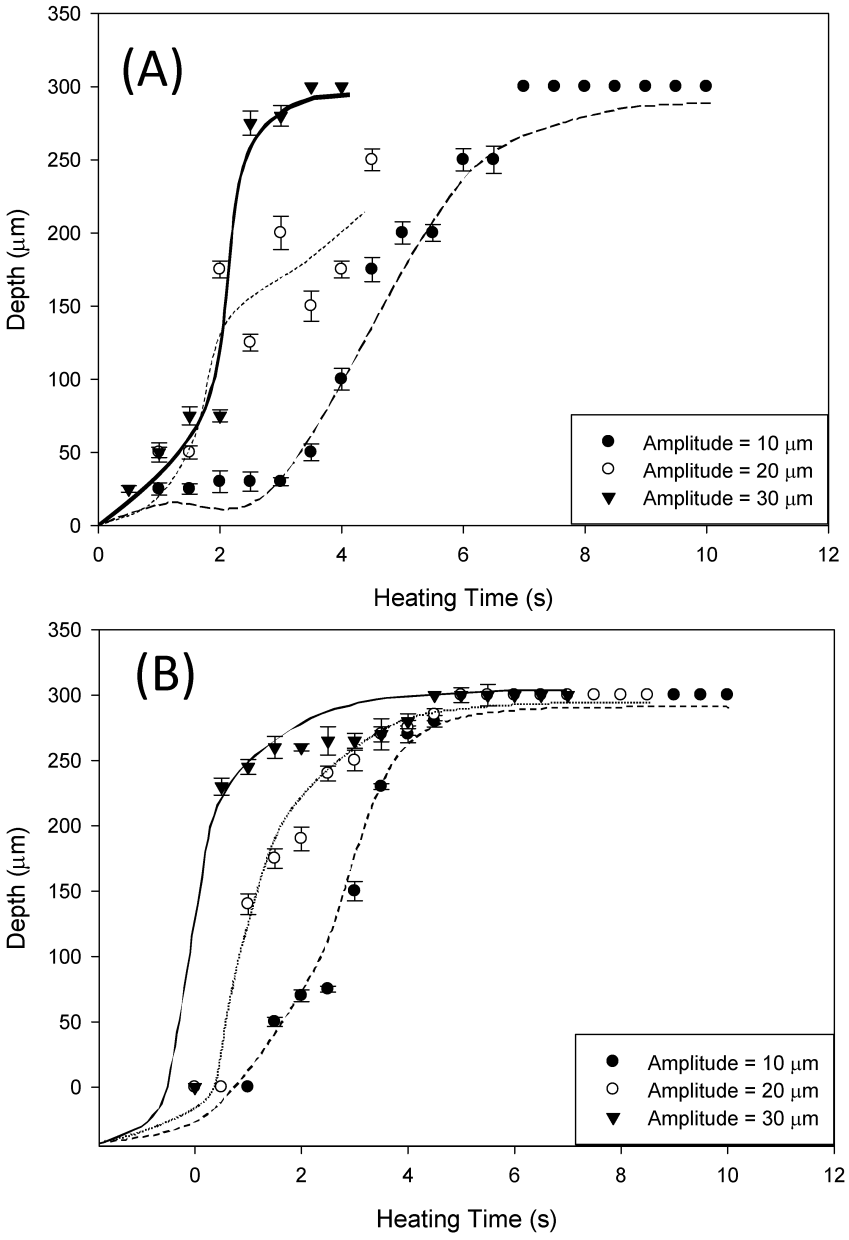

FIG. 24. Feature depth as a function of heating time at various amplitudes with (A) standard PS and (B) with foamed PS

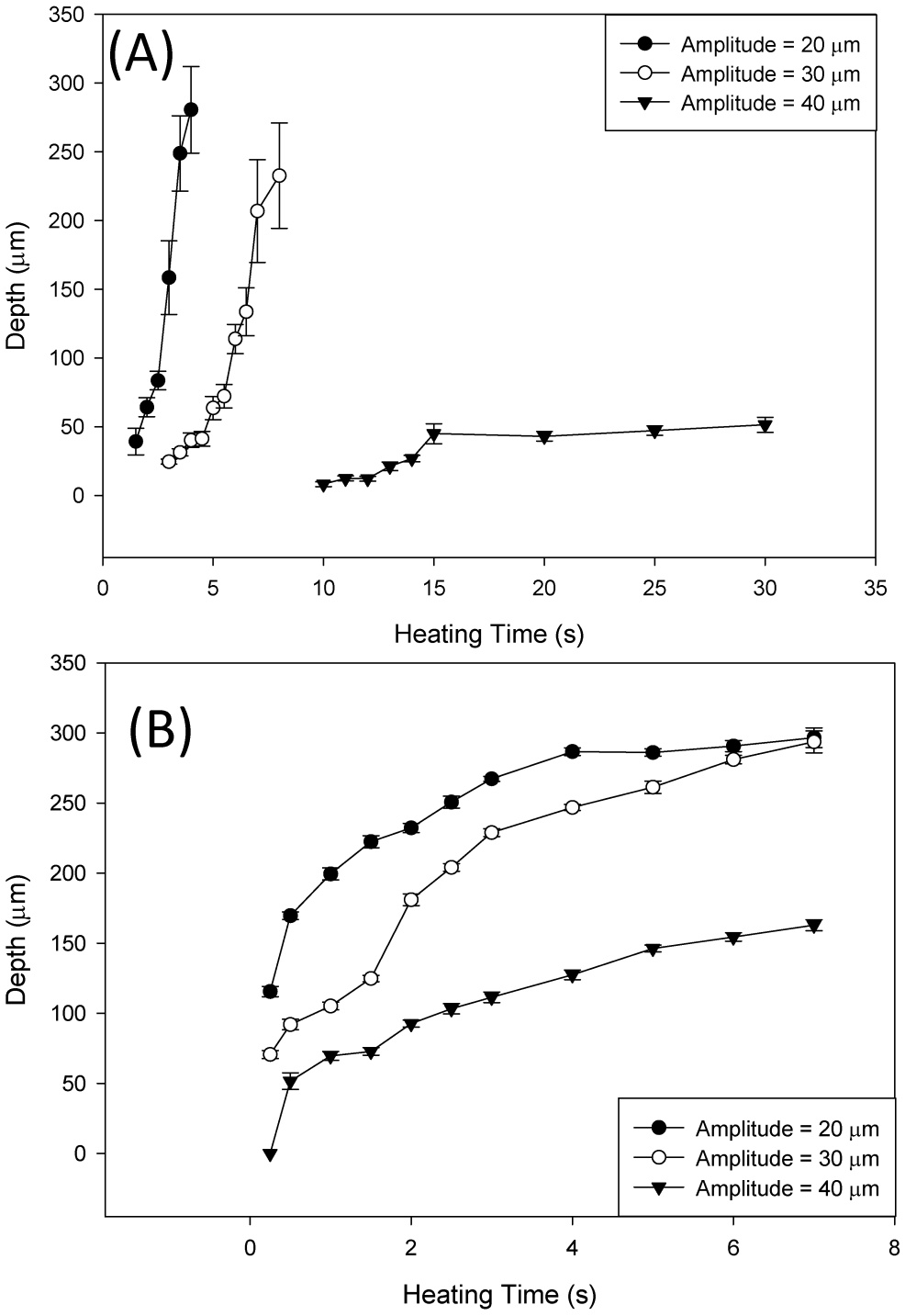

FIG. 25. A and B Embossing depth as a function of heating time at various amplitudes for standard PP and foamed PP, respectively

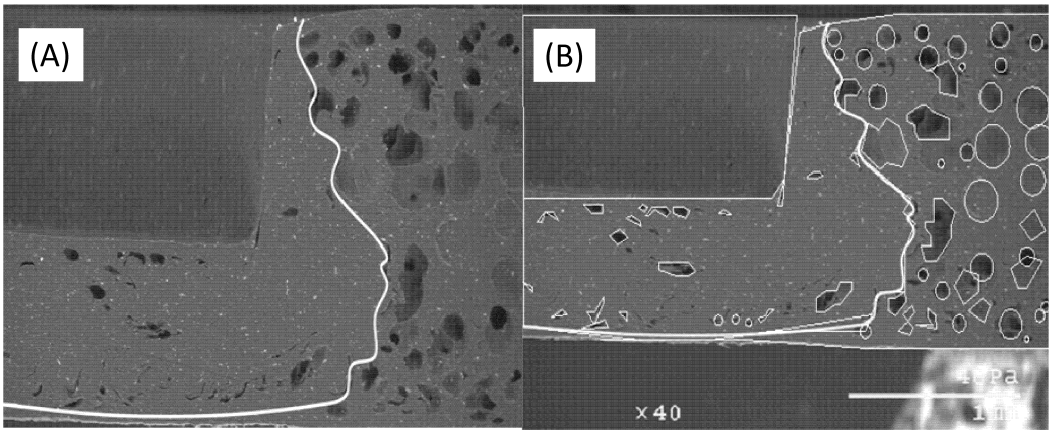

FIG. 26. SEM image of micro feature cross section, embossed on PP sample surface

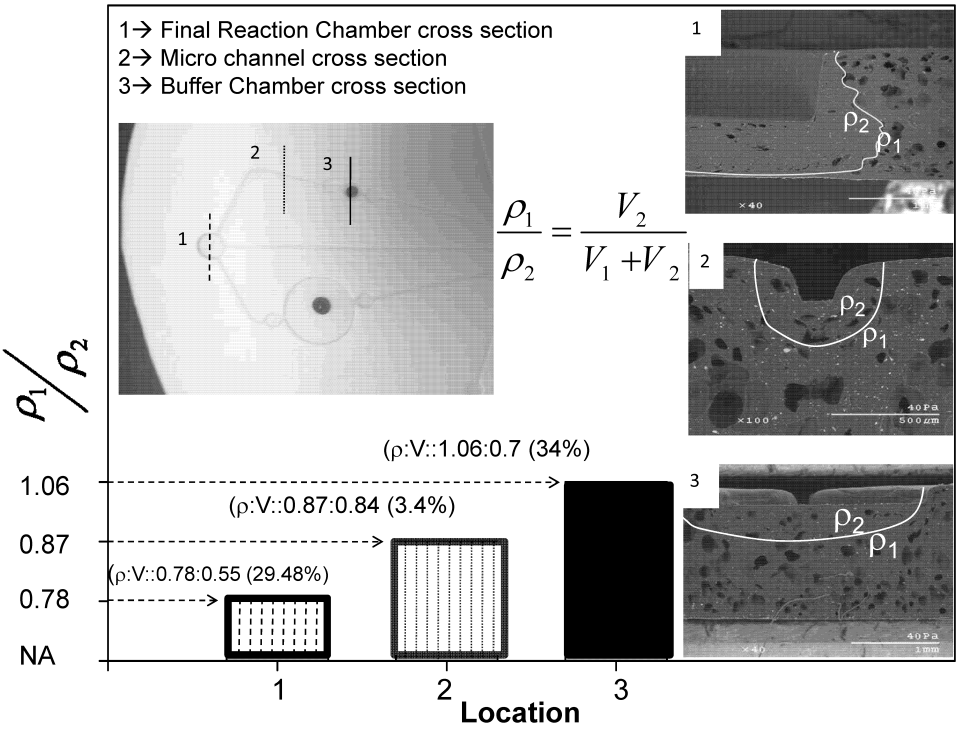

FIG. 27. ρ_1/ρ_2 values of three different cross sections on the micro feature, embossed on PP sample surface

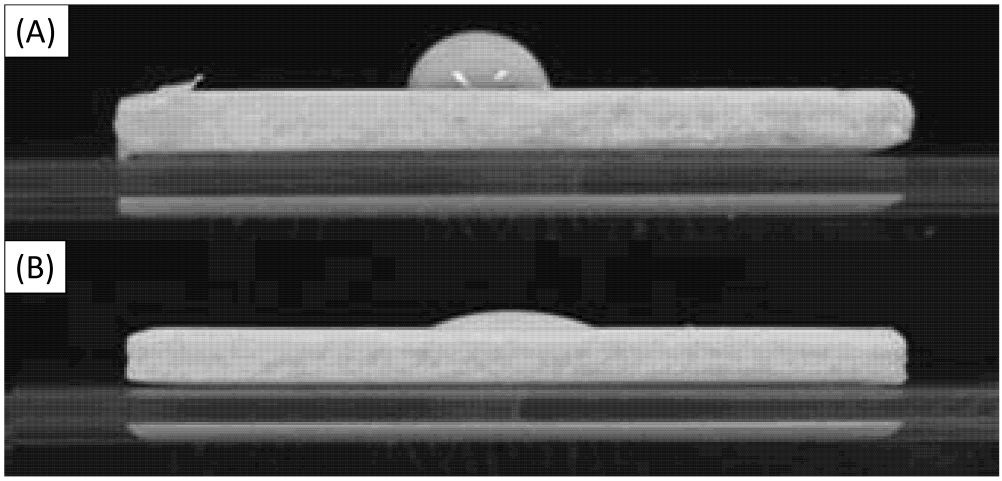

FIG. 28. Side view of a 10 µl water droplet formed on (A) standard PP and (B) chemically treated PP

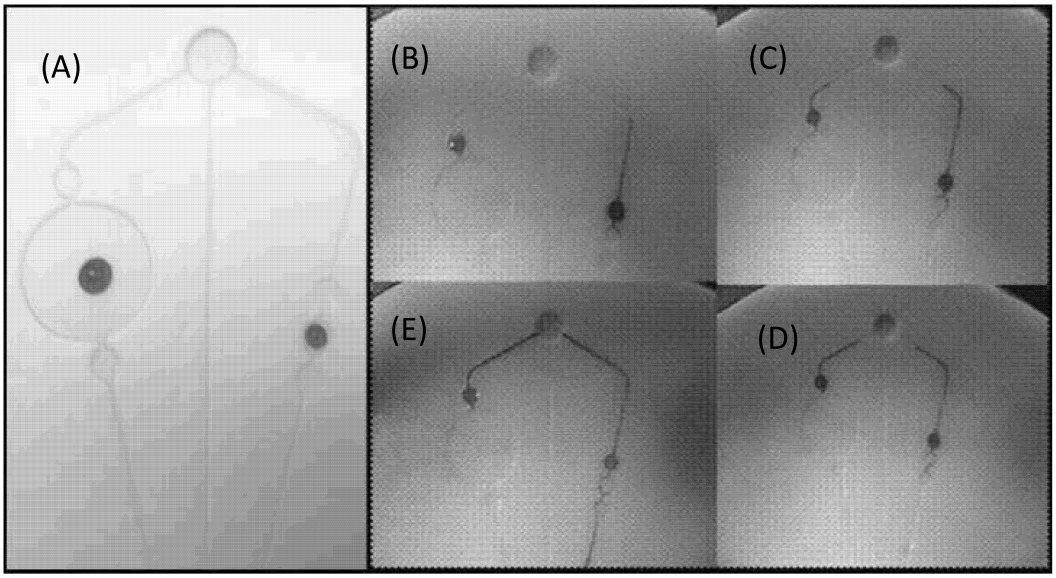

FIG. 29. Digital images captured of the capillary flow nature on the naturally hydrophobic PP surface (A) and after the surface modification (B through E).

CHAPTER 3: ULTRASONIC MICRO EMBOSSED FOAMED POLYPROPYLENE BIO-CD: A PHOTOLUMINESCENCE-BASED ESTIMATION OF GLUCOSE AND LACTATE CONCENTRATION

To be submitted-Polymer Engineering and Science

Srikanth Vengasandra, Yuankun Cai, Ruth Shinar, Joseph Shinar, David Grewell

ABSTRACT

Flash-free micro patterns were embossed on polypropylene (PP) substrates with ultrasonic heating to generate a biosensing lab-on-CD. The embossing technique relies on a micro-cellular foamed substrate to absorb the displaced material during the embossing process so that flash is not produced (zero mass transfer in near fields). The embossed features are designed to act as reservoirs, valves and reaction chambers to allow glucose and lactate levels to be measured in solution using a standard PC-CD player and thus termed 'Glucose/lactate Bio-CD'. Once embossed, the surface energy of the plastic substrate is chemically modified to make it hydrophilic by increasing the surface energy by approximately 135%. Preliminary results from the front detection of the unsealed reaction chamber using an organic light-emitting diode (OLEDs) as the excitation source resulted in good correlation between the glucose levels and the PL intensity with photoluminescence (PL) intensity-based sensing (*I* mode). In addition, glucose and lactate analyte samples were placed in separate reservoirs and directed through burst valves by rotation of the CD towards a reaction chamber in individual experiments, where both the analytes were oxidized in the

presence of oxygen and their specific oxidase enzymes. Thus, lactate and glucose concentrations were determined by measuring the dissolved oxygen content that was not consumed in the oxidation reactions. These measurements were performed in sealed cells using an oxygen-sensitive dye and monitoring its PL decay time (τ mode) following an OLED emission pulse. The results demonstrate the potential of integrating OLEDs as excitation sources in PL-based sensors with microfluidic CD-based platforms, including for simultaneous multiple analyses.

INTRODUCTION

Ultrasonic micro-embossing was used in this study as a source of localized heat. The advantages of this technique include short cycle times, ease of de-embossing and low residual stresses. It is also applicable to batch and continuous manufacturing. This paper reviews the use of ultrasonic embossing to create a Micro-Electro-Mechanical-System (MEMS) based biosensing device for measuring glucose and lactate levels (glucose/lactate bio-CD). Similar devices have previously been studied utilizing materials such as polycarbonate [1,2], polystyrene [3], polydimethylsiloxane (PDMS) [4] and PP [5,6]. This work is primarily focused on foamed PP samples and novel detection methods of various analyses.

Biomedical MEMS sensors, e.g., lab-on-CD fabricated on plastic substrates have the potential to be low cost, disposable, cross-contamination free and highly accurate. Such

sensors have additional potential benefits, including high-throughput multi-analyte detection capabilities suitable for a wide range of applications, and they are compact.

Plastics typically have relatively low surface energies making them hydrophobic. Many of the functions of microfluidic devices rely on hydrophilic properties so that the channel walls promote capillary actions. Thus, in order to fabricate a viable biomedical platform device on plastic substrates, the surface energy must be increased. This is often accomplished by chemical modifications, such as oxidization by ozone or plasma treatment.

For a standard PC-CD player to function as an assay conducting instrument, the CD must provide a detectable signal. In order to build on the plastics platform, OLEDs are proposed as an excitation source in the PL-based sensor. OLEDs are attractive because of their high brightness, ease of fabrication and integration with a sensing component, potential miniaturization, flexible design and suitability for fabrication on glass and plastic substrates. In all experiments, the PL was monitored using a photomultiplier tube (PMT). PMTs have low noise, high gain, high frequency response, and a large active area. For example, gains as high as 10^8 are possible with PMTs [7].

In this study, analytes such as glucose and lactate were monitored utilizing an oxygen-sensitive dye, e.g., Pt octaethylporphyrin (PtOEP), embedded in a thin polystyrene (PS) film. Glucose and lactate were oxidized by specific enzymes, i.e., glucose oxidase (GOx) and lactate oxidase (LOx), respectively, in the presence of oxygen. Oxygen is consumed during the oxidation reactions. Thus, by monitoring the final oxygen level in the sealed reaction

chamber, the initial analyte concentration can be determined [7]. The consumption of oxygen results in an increase in the PL intensity (*I*) and the PL decay time (τ) of the PtOEP. The enzymes can be embedded in a thin film; alternatively, they can be dissolved in solution.

This work considers two methods of estimating the glucose concentration: 1) by the analysis of the reaction products or 2) by measuring *I* or τ of the oxygen-sensitive dye co-embedded with GOx in a thin film or dissolved in solution. In the preliminary study, the glucose concentration was determined by measuring *I*. It is envisioned that a more compact sensor can also be obtained by integrating, a thin film-based photodetector (PD) in addition to the thin OLED excitation source and sensing film. Such PDs based on amorphous or nanocrystalline Si based designs are currently under development [8-11]. However, their slow speed does not allow for monitoring oxygen in the τ mode. Organic PDs are also suitable for such integration and possibly, for measuring τ of suitable luminophores.

Biotechnological application development, mainly in the area of biosensing and analyte detection using the lab-on-CD approach, has been studied by various groups for over a decade [1-4]. This paper presents novelties in two distinct areas, namely, the uniqueness in the type of material chosen for the lab-on-CD substrate and in its detection methodology utilizing an OLED sensing platform. Foamed PP material has proven to be favorable towards creating flash-free microfeatures with ultrasonic microembossing technology [14, 15], whereas previously, unfoamed Cyclic Olefin Copolymer (COC), polycarbonate (PC), and PDMS materials were predominantly chosen as lab-on-CD substrates.

In addition, for this study OLEDs are used as the excitation source. OLEDs were chosen due to their advantageous attributes: they are thin, suitable for compact, portable devices and versatile in size and shape.

EXPERIMENTAL

MATERIALS

Microcellular (mucell) foamed and extruded sheets of polypropylene (PP) were chosen as the bio-CD substrate and were obtained from Trexel Corporation (MA). The foaming level specified by Trexel ranged from 15% to 20%. The optical microscopy image of the through thickness of the foamed PP is shown in Figure. 30. As seen, the diameter of the voids varied between 75 to 150 µm. The PP sheets had a thickness of approximately 1.5 mm and were cut into the size of standard CDs with common shears. The PP – CDs were then used for ultrasonic micro-embossing.

The reagents used for the PL-based bio-CD experiment were the oxygen-sensitive dyes tris(4,7-diphenyl-1,10-phenanthroline) Ru chloride (Rudpp), (purchased from Sigma-Aldrich), at a concentration of 18.2 mg/ml, and Pt octaethyporphyrin (PtOEP), (obtained from H. W. Sands), at a concentration of 1mg/mL. Glucose oxidase, GOx, from *Aspergillus niger,* (purchased from Sigma-Aldrich) was used at a final concentration of 319.67 units/mL, and lactate oxidase, LOx, from *Pichia pastoris* (purchased from Sigma-Aldrich) was used at a final concentration of 93 units/mL. Glucose and L-lactate were purchased from Sigma-Aldrich. All reagents were dissolved in a phosphate buffered saline (PBS) solution. The

illumination or excitation source was a 4,4'-bis(2,2'-diphenylvinyl)-1,1'-biphenyl (DPVBi)-based OLED for intensity (*I* mode) monitoring of glucose as the absorption spectrum of Rudpp falls within the blue emission spectrum of DPVBi, and trisquinolinolate Al (Alq_3) -based OLED for the decay time (τ mode) analysis of both glucose and lactate concentrations [8] as the absorption spectrum of PtOEP falls within the green emission spectrum of Alq_3. PtOEP was embedded in a film of polystyrene, PS, (molecular weight 45000) obtained from Sigma-Aldrich.

Two screening experiments were conducted to determine the detection limit of the experimental procedures in the *I* mode;

- Experiments with varying fluid volumes and constant glucose concentration
- Experiments with varying glucose concentrations and constant fluid volume. Each of these experiments is detailed in the following section.

PL-INTENSITY STUDY

Equal volumes of each of the three reagents (GOx, Glucose and Rudpp) were mixed for total final volumes of 15, 12, 9 and 6 μl. The final glucose concentration was ~33 mM. The experiment was repeated three times for each of the volumes in a sealed environment.

In other experiments, four different concentrations of glucose (33, 17, 8 and 0.5 mM) were studied with a total reagent mixture volume of 15 μl. Two different control experiments were also designed to confirm the accuracy of the results from the reaction between glucose and

GOx. In one, a mixture of buffered GOx and Rudpp dye was used, and in the other, only the buffer was introduced and characterized for signal strength.

PL-DECAY TIME STUDY

In this study 200 µL of analyte samples (Glucose and Lactate) at seven different concentrations were introduced into the final reaction chamber and the resulting concentrations were 0.043, 0.087, 0.174, 0.217, 0.261, 0.35 and 0.435mM, and 30 µL of the respective enzyme samples (GOx or LOx) were introduced both into the buffer chamber and the reagent chamber. The enzyme solution was guided into the final reaction chamber following the CD rotation at approximately 1000 rpm. Based on previous studies [7, 12, 13], the final resulting enzyme concentrations were 80 units/mL of GOx and 95 units/mL of LOx. Preventing the background OLED-EL signal from reaching the PMT, during both studies, was accomplished by using a long pass filter that allowed only the PL signal from the sensing film (at 645 nm) to pass through.

EQUIPMENT

Micro-embossing was completed with a Branson 2000 Series, 20 kHz ultrasonic system. A titanium horn fabricated by Branson Ultrasonics with the feature detailed in Figure. 31 was used. The figure 31 (A) shows the titanium horn, and (B) details the functional components of the proposed Bio- CD for glucose and lactate monitoring with a photograph of the face of the horn manufactured using electrical discharge machining (EDM) technique.

The PL signal reflected back from the bio-CD was captured and measured with a PD that was typically a Hamamatsu R6060 PMT.

LAB ON CD SAMPLE AND OLED PREPARATION AND MEASUREMENT

Surface modification

To increase the surface energy of the foamed PP samples, two different chemical coatings were studied: a surfactant based and an organic-based system. Each of the two chemical coatings was individually studied and both produced the desired results. However, the results presented in this paper are from the surfactant based coatings (Lurol 12134). The coating was obtained from Goulston Technologies, Inc (Monroe, NC) and was diluted with deionized (DI) water at a ratio of 1:10; the dilution was applied directly on to the foamed PP bio-CD substrate and was allowed to cure for 15 minutes under clean, humid conditions. The treated surfaces were then rinsed with DI water and blown dry under compressed N_2 gas. Contact angles for the pretreated and treated PP sample surfaces were measured and compared for surface energy calculations using the Owens-Wendt-Kaelble equation, Eq. 1, as specified in ASTM D 7490-08, Polyethylene glycol (PEG) was used as a reference liquid.

$$\gamma_l(1+\cos(\theta)) = 2\left(\sqrt{\gamma_l^d \gamma_s^d} + \sqrt{\gamma_l^p \gamma_s^p}\right) \qquad \text{Eq. 1}$$

Where γ_l^d, γ_s^d are the dispersive components of the liquid and solids respectively and γ_l^p, γ_s^p are the polar components of liquid and solids respectively. For PEG the dispersive (γ^d_{peg}) and polar components (γ^p_{peg}) were 29.3 and 19.0 dynes/cm^2. For the water the dispersive (γ^d_{H20}) and polar components (γ^p_{H20}) were 21.8 and 51.0 dynes/cm^2 [15].

To enable “back detection” monitoring of the PL, where the PMT detects the PL through the gap between the OLED pixels, the bottom of the reaction chamber needed to be transparent. Thus the bottom surface of the CD reaction chamber was cut and sealed with a sensing film that was deposited on a thin cover glass. Figure 32 (A) shows the horn used to create the modified reaction chamber (with 10 mm dia.) and Figure 32 (B) shows the actual image of one of the four sensing segments on the bio-CD with the modified reaction chamber. While not optimized here, it should be possible to use a similar embossing technique with conditions that would leave the foamed PP so thin, that it would be sufficiently transparent to allow back detection. In this fashion, the base of the reaction chamber would not be removed and the embossed feature would be functional after embossing.

OLED fabrication

The OLEDs were prepared as encapsulated matrix arrays of 2x2 mm^2 square pixels resulting from mutually perpendicular stripes of etched ~100 nm thick indium tin oxide (ITO; the anode) and ~100 nm Al (the cathode). The organic layers sandwiched between the electrodes were deposited by thermal vacuum evaporation, as described by Cai et al and Shinar et al [7, 8]. The OLEDs were operated in a pulsed mode with a forward bias of ~20 V and a pulse width of 100 μs with a repetition rate of 50 Hz.

Embossing and PL Intensity (*I*) Measurement for Glucose Detection

Embossing of micro-features on the PP bio-CD substrate was completed using ultrasonic embossing with an amplitude of 40 μm (100%) and a heating time of 0.5 s. These conditions were based on previous studies [6].

Several μL of the three buffered reagents, glucose, GOx, and the Rudpp dye, were introduced sequentially into the final reaction chamber of the bio-CD. The reagent mixture was loaded into the open reservoirs of the PP bio-CD and then covered with a thin layer of cured PDMS (Sylgard® Elastomer 184, Dow Corning). The OLED – PMT setup was enclosed in a custom built dark chamber and was controlled by a Labview program and standard analog to digital board. The PMT was secured at an angle such that the final reaction chamber was directly below it. The OLED was attached to the PMT casing; the CD-PMT distance was roughly ~2 mm throughout this study.

Based on the screening experiments, a reaction time of 60 s was allowed before energizing the OLED. The data was digitized, averaged over 400 pulses, and analyzed using the Labview program.

PL Decay Time (τ) Measurement Procedure for Glucose and Lactate Monitoring

To evaluate the flow, mixing, operation of the valves, and response time, the analytes were sealed and the flow was characterized visually by capturing images consecutively at 2 second time intervals. In the initial studies, the analytes (enzymes) and the enzymes (analytes) were placed in the reaction chamber and reservoirs respectively. Upon rotation at ~1000 rpm the

valves burst and the buffered enzyme solutions and analyte were mixed. The reaction was performed in sealed conditions to prevent replenishment of dissolved oxygen (DO), to allow for the use of a modified Stern-Volmer relation [7]. The tested analyte concentration ranged between 0-0.3 mM, for both glucose and lactate, and the final volume contained in the reaction chamber was 230 μL (i.e., full capacity). Finally, the τ values were measured with only the buffer in the reaction chamber, which served as the control experiment.

RESULTS AND DISCUSSION

Surface energy manipulation

The photographic images in Figure. 4 show the nature of fluid flow from the enzyme reservoir of the PP bio-CD before and after coating the surface of the sub-component with the surfactant coating. As seen in Figure 33 (B) the surface modification effectively increased the surface energy to promote fluid flow.

Volume Study

Figure. 5 (A) shows the value of the PMT-measured signal as a function of time during the 100 μs, 50 Hz OLED pulse for different volumes, ranging from 6 to 15 μL. In these studies the combined reagents were buffered analyte (glucose), enzyme (GOx), and the solution of the oxygen-sensitive dye Rudpp and their ratios were held constant. As previously mentioned, a blue DPVBi-based OLED was used for this study as its emission band is compatible with the absorption band of Rudpp. It is seen that the signal intensity is generally proportional to the reagent mixture volume. However, it should be noted that a portion of the

response is due to the background light from the tail of the EL. The response signal passes through a long pass filter which, in turn, blocks emission below 610 nm. Thus, the response curves are the summations of the PL from the dye and the remnant EL tail. Differences in the response curves correlate to differences in the PL intensity as the EL contribution would be similar for the various volumes, assuming negligible attenuation.

In order to confirm the validity of the assumption tha t attenuation was negligible, the signal intensity as a function of the volume of a buffered (Rudpp) solution was measured in the absence of any enzyme or analyte. The experimental set-up was comparable to the volume study as described above (sample between the OLED and detector). As seen in Figure 34 (B), a plot of intensity through the sample as a function of sample thickness (volume), the attenuation coefficient is -0.2567/mm. This behavior is due to strong light absorption by the dye, which exceeds the signal intensity due to the increase in the PL with increasing volume. However, compared to the intensity of the luminance produced by increasing volume, this attenuation is relatively insignificant. In more, Figure 34 (C), show luminance intensity as a function of depth with the OLED and detector on the same side of the sample with the bottom reflector. It is important to note that intensity measure includes the effects of attenuation with increasing depth as well as increasing luminance intensity. It is seen, as expected the intensity increases exponentially with depth. In this case the intensity coefficient is 0.3744/mm, which is greater than the magnitude of attenuation coefficient. Thus, the assumption that attenuation is insignificant is appropriate. Figure 34 (D) shows three signals, and their average, from the lowest volume of the reagent mixture. The results show negligible variations under the same experimental conditions even without the use of

an optical filter. However, in some cases slight differences have been observed and this could be attributed to the fact that there is a possibility of EL differences due to alignment variations of the final reaction chamber with respect to the OLED. This error was minimized by conducting three consecutive trials at each of the volumes considered. Because 3 µL was the smallest difference in volume considered in this study it is assumed that this detection mechanism has a volume resolution of at least 3 µL at the lowest concentration range tested. In addition, this experimental design limited the final reaction volume to 15 µL. Integration of the values in these data gives the total intensity (PL + EL tail) over time when the OLED pulse is energized. Finally, the normalized area under each of the curves increases with the total volumes of the reagent mixtures, as shown in the calibration plot in Figure 34 (E).

Concentration Study

Figure. 35 (A) shows the measured intensity for different glucose concentrations. As expected, the most intense signal occurs with the highest glucose concentration of 33 mM. A negligible signal was measured in the case of the control experiments where no glucose was present. As previously mentioned, this signal is primarily due to the EL background. Following subtraction of the background signal, these results show a generally linear relationship, between the integrated signal intensity and the glucose concentrations as shown in Figure 35 (B), indicating that the proposed monitoring technique is valid.

PL Decay Time (τ) Study

To maximize the detection sensitivity the PL decay time (τ) method was used instead of the PL intensity (*I*) mode [14], where the reduced detection sensitivity was due to the EL tail reaching the PD. The τ mode of analyte monitoring is insensitive to the EL background as the analyte is monitored during the off time of a pulsed OLED.

As shown by Cai et al. [7], calibration lines obtained from experiments performed in sealed containers follow a modified Stern-Volmer equation:

$$I_0/I = \tau_0/\tau = 1 + K_{SV} \times \{[DO]_{initial} - [analyte]_{initial}\} \quad \text{Eq. 2}$$

Where I_0 and τ_0 are the unquenched PL intensity and decay time, respectively, and K_{SV} is a film- and temperature-dependent constant.

Figures 7 and 8 show the modified model Stern-Volmer results obtained for glucose and lactate, respectively. The reagents were mixed by opening the burst valves following rotation of the CD. The measured values of τ at ambient temperature for both glucose and lactate varied from ~30 to ~90 μs for solutions containing 0 and ≥0.25 mM analyte concentrations, respectively.

In the case of glucose:

$$\text{Glucose} + O_2 \xrightarrow{\text{GOx}} H_2O_2 + \text{Gluconic Acid} \quad \text{Eq. 3}$$

In the case of lactate:

$$\text{Lactate} + O_2 \xrightarrow{\text{LOx}} H_2O_2 + \text{Pyruvic Acid} \qquad \text{Eq. 4}$$

PL decay time measurements were completed with trials of five different concentrations of glucose and lactate. As can be seen from Figures 36 (A) and 37 (A), τ increased with the increasing analyte concentrations. As mentioned, this is the result of the decreasing residual [DO] in the reaction chamber with increasing analyte concentrations that consumed the DO. Figures 36 (B) and 37 (B) show the linear plots of $1/\tau$ vs analyte concentration with their respective correlation coefficients (R^2). The results further demonstrate the validity of the OLED-Bio-CD approach when using the modified Stern-Volmer model (Eq. 2) for measurements in sealed containers.

CONCLUSIONS

A novel embossing technique has been developed and demonstrated in this study. Use of foamed substrates, demonstrates that complex features could be embossed with ultrasonics without the production of flash. The features have the ability to act as reservoirs, channels, and reaction chambers.

Additionally, it has been demonstrated that the surface and interior surfaces of the micro-features could be modified to make them hydrophilic. The low surface energy of PP material was modified successfully and the energy was increased by 134% using a chemical coating.

It was also seen that OLEDs could be used in conjunction with the micro-embossed lab-on-CD device for the purpose of excitation of the biosensing film. Preliminary results on a PL-based glucose sensor demonstrate a correlation between the PL intensity and the glucose concentrations. The data also suggest that because the volumes (beyond 90 µL) affected the PL intensity measurements of the glucose concentrations, the fidelity of the embossed micro-features and metering of the samples during testing is critical to accurately determine the concentration. However, since a smaller range of volumes was considered, attenuation did not impact the measured PL intensity. Results obtained using the PL-decay time mode , which eliminated issues related to background light, also demonstrate the validity of the OLED_Bio-CD approach for sensitive analyte monitoring. Future integration with thin-film based photodetectors, to replace the PMT, should lead to compact sensors for simultaneous detection of multiple analytes.

FUTURE WORK

The incorporation of a Si photodiode, or better, a thin film PD (whether based on amorphous or nanocrystalline Si, or organic materials) to replace the PMT is expected to lead to a more compact, field-deployable device. It should also be possible to detect and measure simultaneously, the unknown concentration of four different analytes by utilizing the four separated segments together with four compatible PDs on the same CD. In the future, four such PDs will be designed to form a ‘novel quad pre-amp OLED disk sensor’ such that simultaneous monitoring of multiple analytes can be achieved on the same lab-on-CD.

Preliminary results that have already been obtained for the detection of unknown glucose concentrations present in real-world samples, such as corn slurries obtained from an ethanol plant, are promising and will be published in a forthcoming paper.

ACKNOWLEDGEMENTS

We are grateful to Branson Ultrasonics (Danbury, CT) for the donation of the ultrasonic embossing equipment and tooling. We acknowledge Goulston Technolgies, Inc. for providing free samples of their chemical coating material for our use. Ames Laboratory is operated by Iowa State University for the United States Department of Energy (USDOE).

REFERENCES

1. L. J. Lee, M.J. Madou, K.W. Koelling, S. Daunert, S. Lai C.G. Koh, Y-J Juang, Y. Lu and L. Yu, *Biomed. Microdevices.,* **3**, 339-351, (2001).
2. L. Reigger, M. Grumann, J. Steigert, S. Lutz, C. P. Steinert, C. Mueller, J. Viertel, O. Prucker, J. Ruhe, R. Zengerle, J. Ducree, *Biomed. Microdevices,* **9**, 795–799, (2007).
3. D. C. Duffy, H. L. Gillis, J. Lin, N. F. Sheppard, G. J. Kellogg, *Anal. Chem.*, **71** (20), 4669 – 4678, (1999).
4. J. Kim, S. Jang, J.V. Zoval, N.Da Silva, M. Madou, *Proc. SPIE Int. Soc. Opt. Eng.* **5455**, 331-340 (2004).
5. G. Harmon, D. Grewell *SPE ANTEC Proceedings, Brookfield*, 1051-1055, (2007).
6. S. Vengasandra and D. Grewell *SPE ANTEC Proceedings, Brookfield*, 1041-1045, (2007).
7. Y. Cai, R. Shinar, Z. Zhou, J. Shinar, *Sens. Actuators*, B 134, 2, 727-735, 2008.

8. R. Shinar, D. Ghosh, B. Choudhury, M. Noack, V.L. Dalal, J. Shinar, *J. Non-Cryst. Solids*, **352** (9-20), 1995-1998 (2006).

9. D. Ghosh, R.Shinar, V. L. Dalal, Z. Zhou, J. Shinar, *Mater. Res. Soc. Symp. Proc.* **989,** 989-A12-01, (2007).

10. D. Ghosh, R. Shinar, Y. Cai, Z. Zhou, V. L. Dalal, J. Shinar, *Proc. SPIE Int. Soc. Opt. Eng*., **6659**, 66590E-1, (2007).

11. D. Ghosh, R. Shinar, V.L. Dalal, Z. Zhou, J. Shinar, *J. Non-Cryst. Solids*, **354** (19-25), 2606-2609 (2008).

12. B. Choudhary, R. Shinar, and J. Shinar, *J. Appl. Phys.* **96**(5), 2949-2954 (2004).

13. K. O. Cheon and J. Shinar, Appl. Phys. Lett. **83**, 2073-2075 (2003).

14. S. Vengasandra, Y. Cai, R. Shinar, J. Shinar, D. Grewell, *SPE ANTEC Proceedings, Brookfield*, (2008).

15. S. G. Vengasandra, G. Harmon and D. Grewell, *Polym. Eng. Sci*. (In Press).

FIGURES

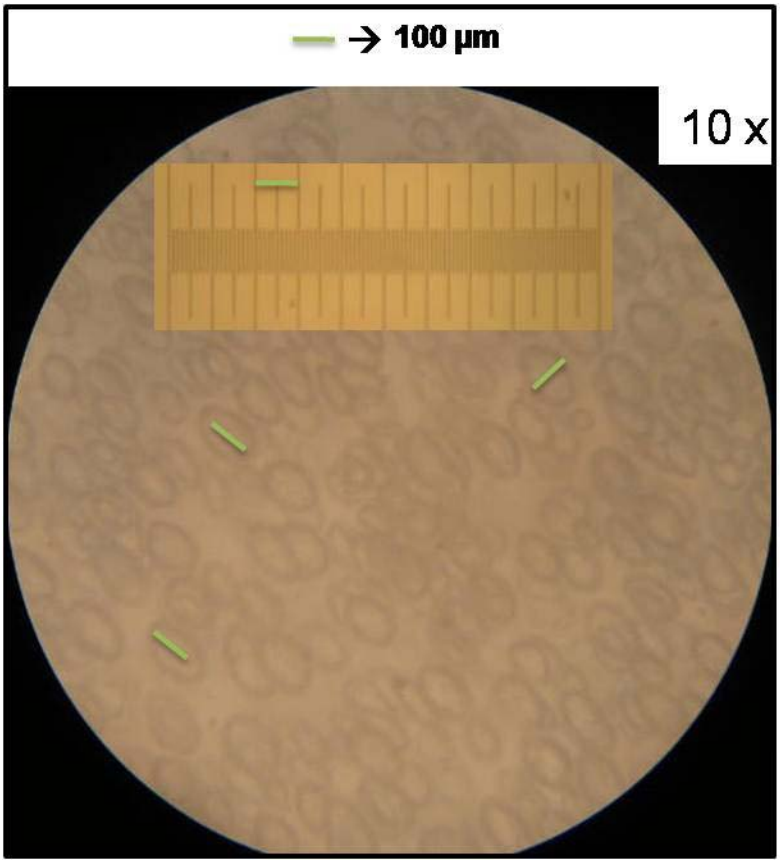

Figure 30. Optical microscopy image of the surface of foamed PP material.

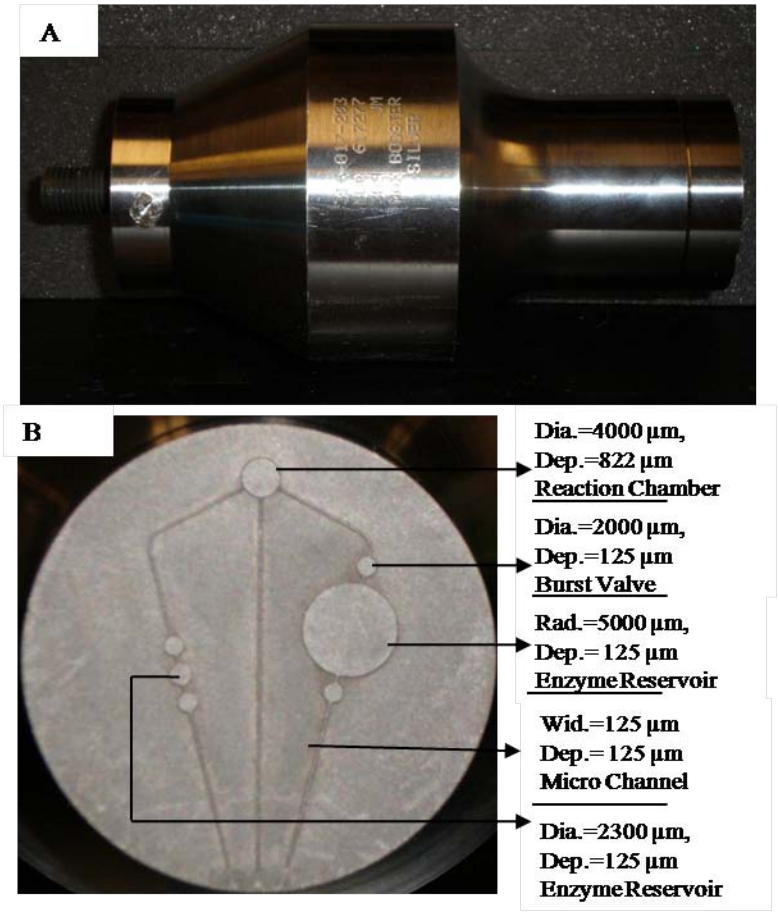

Figure 31. Details of the structure and functions on the proposed Bio- CD for monitoring glucose and lactate, (A) the titanium horn used for microembossing and (B) a photograph of the face of the horn showing the structural and dimensional details.

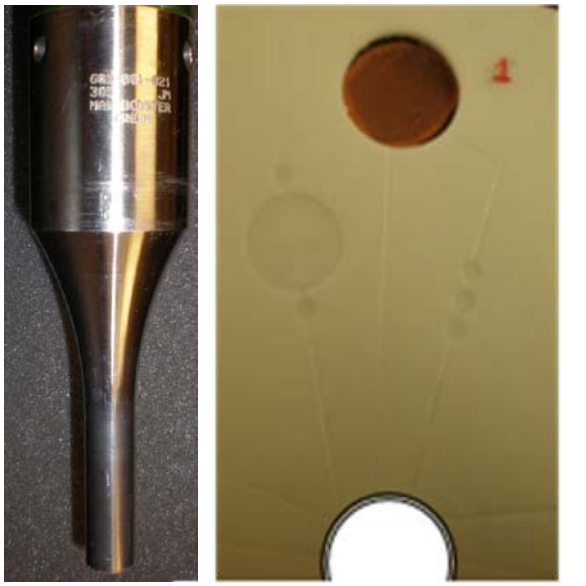

Figure 32 (A). The ultrasonic horn used for manufacturing the modified reaction chamber and (B). Image of one of the four sensing segments on the bio-CD showing the modified reaction chamber.

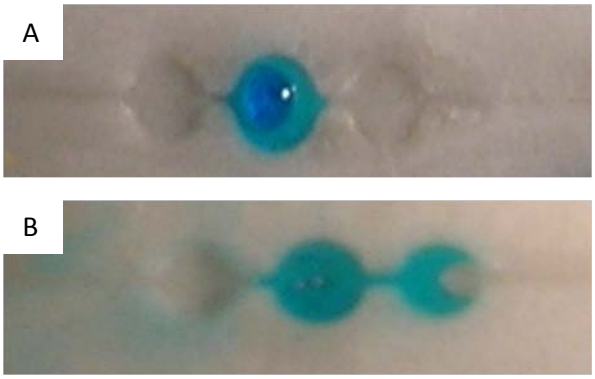

Figure 33. Photographic images of fluid flow from enzyme reservoir before (A) and after (B) the surface coating

(A)

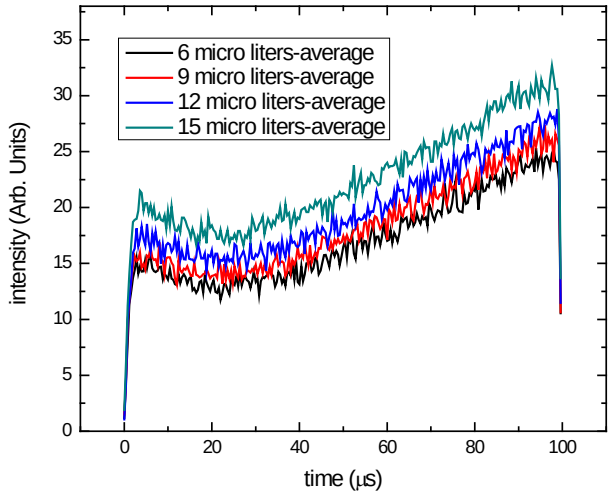
6 micro liters-average
9 micro liters-average
12 micro liters-average
15 micro liters-average
intensity (Arb. Units)
time (μs)
0
5
10
15
20
25
30
35
0
20
40
60
80
100

(B)

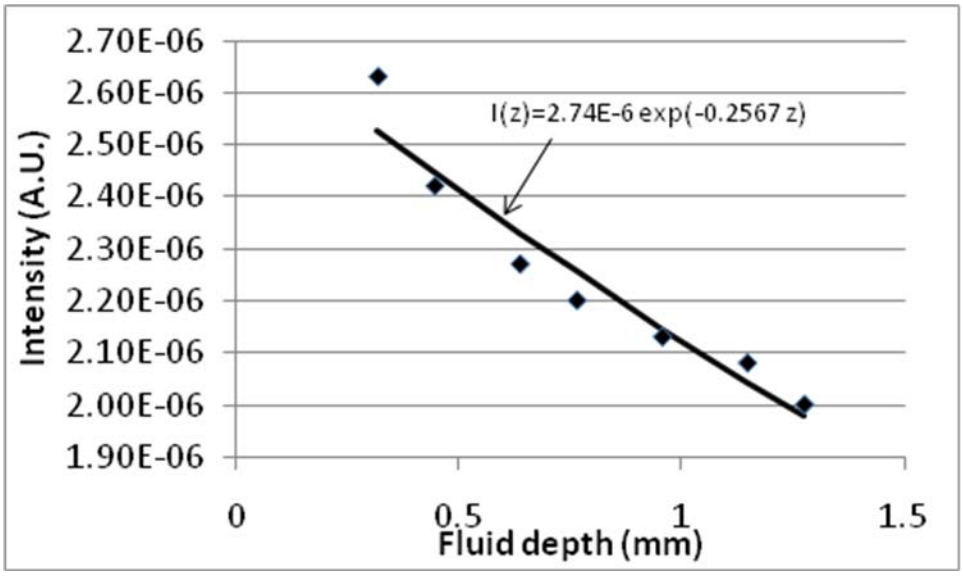
I(z)=2.74E-6 exp(-0.2567 z)
Intensity (A.U.)
Fluid depth (mm)
2.70E-06
2.60E-06
2.50E-06
2.40E-06
2.30E-06
2.20E-06
2.10E-06
2.00E-06
1.90E-06
0
0.5
1
1.5

(C)

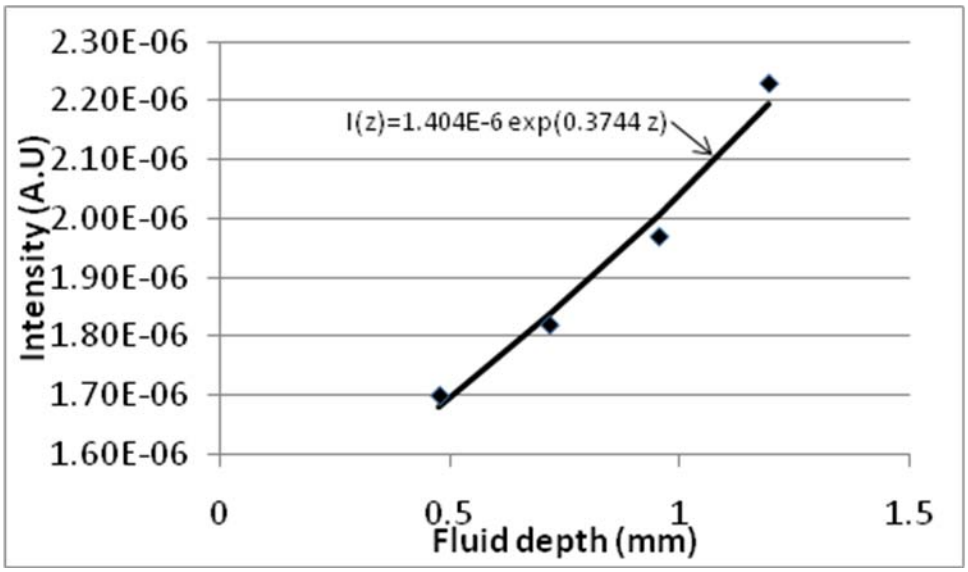
2.30E-06
2.20E-06
2.10E-06
2.00E-06
1.90E-06
1.80E-06
1.70E-06
1.60E-06
Intensity (A.U)
I(z)=1.404E-6 exp(0.3744 z)
0
0.5
1
1.5
Fluid depth (mm)

(D)

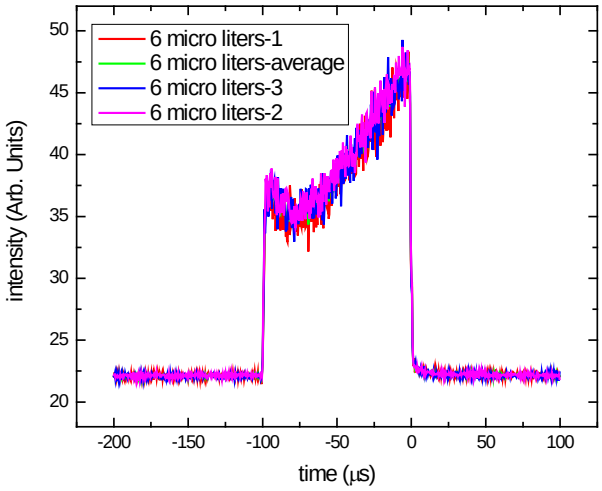
6 micro liters-1
6 micro liters-average
6 micro liters-3
6 micro liters-2
intensity (Arb. Units)
50
45
40
35
30
25
20
-200
-150
-100
-50
0
50
100
time (μs)

(E)

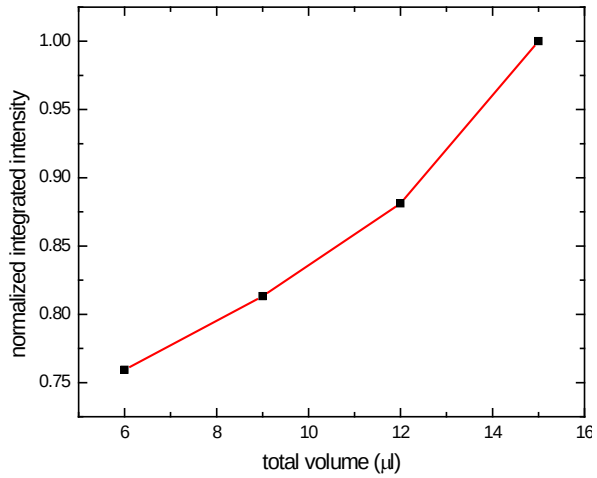

Figure 34 (A). the signal intensity as a function of time for different total reagent volumes during the 100 µs OLED pulse width. (B) measured light intensity versus reagent sample thickness when the sample was between the OLEDs and the PD (C) measured luminance intensity versus reagent sample thickness when the OLEDs and the PD was on the sample side of the sample (D). The signal intensity as a function of time in three measurements, and their average, for a total reagent volume of 6 µL and (E). The normalized integrated intensity versus the reagent volume.

(A)

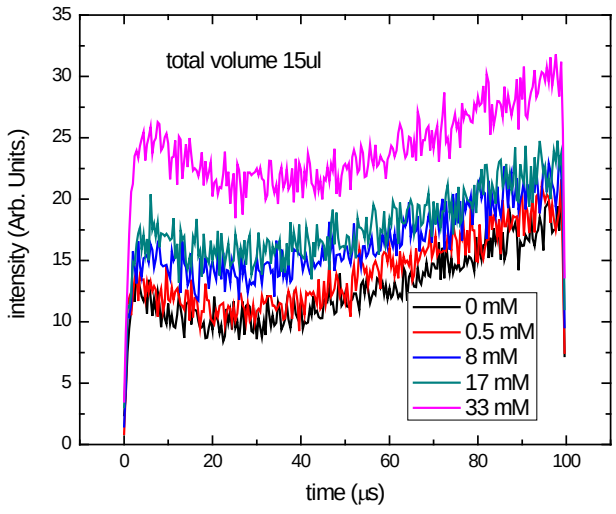

(B)

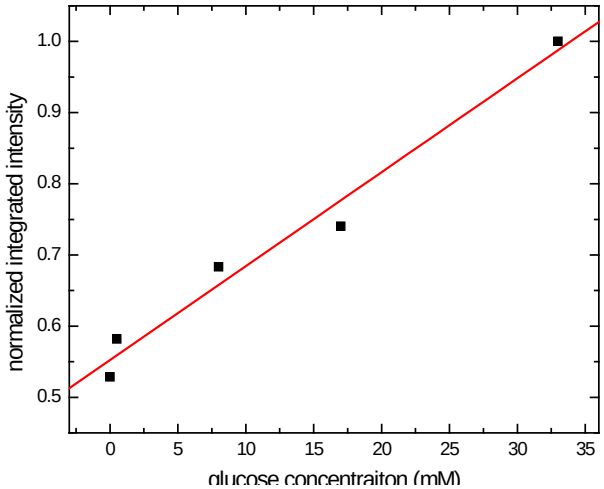

Figure 35 (A). The signal response curves for different glucose concentrations and (B). The normalized integrated intensity versus glucose concentration for the data shown in (A).

(A)

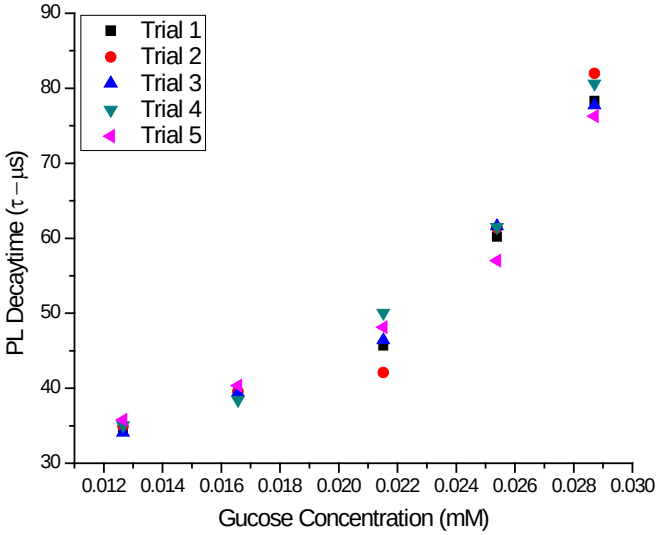

(B)

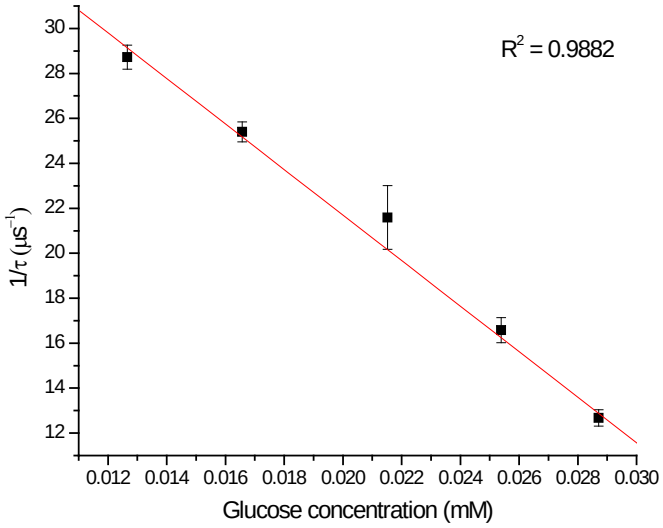

Figure 36 (A). The PL-decay times as a function of glucose concentrations, (B) The modified Stern-Volmer calibration line for glucose in a sealed cell at 23°C.

(A)

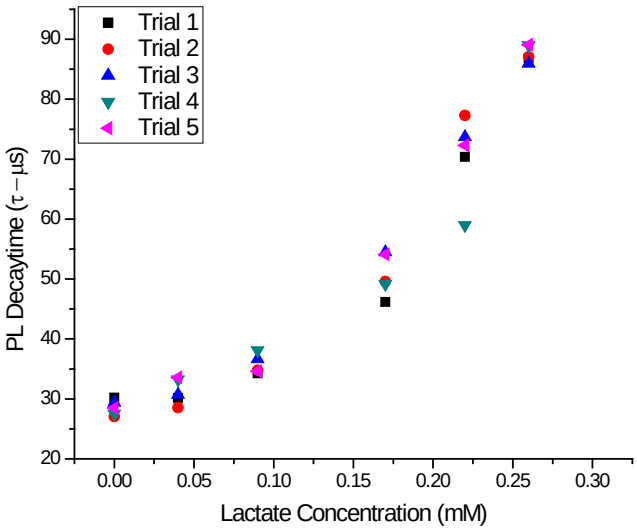

(B)

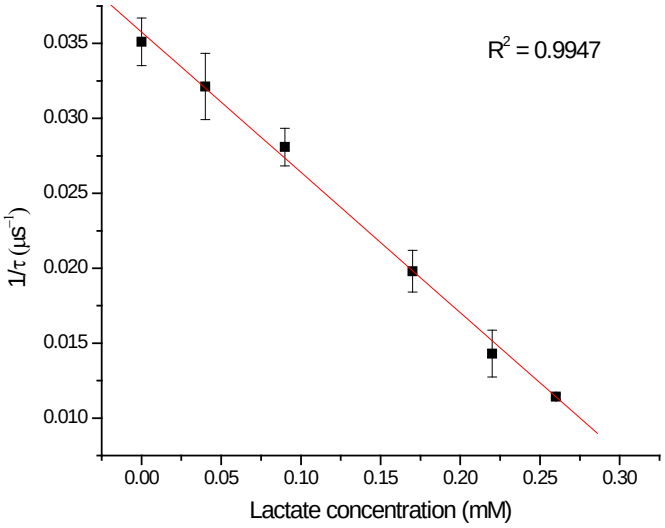

Figure 37 (A). PL-decay times versus lactate concentrations with 5 trials for each concentration, and (B) the modified Stern-Volmer calibration line for lactate in a sealed cell at 23^{o}C.

CHAPTER 4: OLED-POLYPROPYLENE BIO-CD FOR COMBINATORIAL SENSOR STUDY

To be submitted-Biomedical Microdevices

Srikanth Vengasandra, Yuankun Cai, Joseph Shinar, Ruth Shinar, David Grewell

ABSTRACT

The goal of this work was to develop microfluidic platforms for sensing applications for a biosensing lab-on-CD application. Flash-free micro patterns were embossed on polypropylene (PP) surfaces with ultrasonic heating. The embossed features were designed to function as reservoirs, valves, and reaction chambers to allow, in combination with a compact sensing platform, the characterization of various analyte levels using a standard PC-CD player. A photoluminescence (PL)/Organic light emitting diodes (OLED)-based combinatorial detection system was designed and fabricated to measure the concentrations of glucose, lactate and ethanol. In addition the glucose concentration was measured in a corn slurry sample which naturally contains numerous containments. Analyte concentrations were determined by measuring the dissolved oxygen level, which was correlated to the PL decay time of an oxygen-sensitive dye. The analyte was oxidized with a specific oxidase enzyme, which resulted in consumption of the dissolved oxygen. It was found that the system correlated very well with known concentrations. The results demonstrate the potential of integrating OLEDs as excitation sources in PL-based sensors with microfluidic CD-based platform.

Keywords: Organic light-emitting diode, OLED, lab-on-CD, bio-CD, photodetector, PD, glucose sensor, lactate sensor, ethanol sensor, ultrasonic microembossing

INTRODUCTION

Biomedical microelectromechanical system (MEMS)-based sensing platforms fabricated on plastic substrates have the potential of being low cost, disposable, cross-contamination free, high throughput and be able to characterize a range of analytes. The advantages of lab-on-CD- based biosensing platform include its simplicity and compact size.

This paper describes the use of ultrasonic micro-embossing to produce microfluidic channels, valves, reservoirs, and reaction chambers in a polypropylene (PP) PC compact disc (CD) [10]. A range of researchers have demonstrated microfluidic CD with materials such as polycarbonate [1], polystyrene (PS) [2], polydimethylsiloxane (PDMS) [3], and PP [4].

As shown in this work, a CD can be integrated with a photoluminescence (PL)-based OLEDs (Organic Light Emitting Diodes) sensing platform to generate a compact device for monitoring e.g., lactate, glucose and ethanol in a combinatorial fashion. Because plastics are hydrophobic and microfluidic devices rely on hydrophilic properties to promote capillary actions and allow proper fluid flow the surface energy are typically increased by chemical treatment and oxidization by ozone or plasma.

In this work, various analytes were characterized with oxygen-sensitive dye embedded in a thin film that was deposited in the base of the reaction chamber on the CD. Glucose, lactate

and ethanol were oxidized by specific enzymes, i.e., glucose oxidase (GOx), lactate oxidase (LOx) and alcohol oxidase (AOx), respectively. With the assumption that the initial oxygen level is 0.26 mM (8.6 ppm) at room temperature if oxygen is consumed during this reaction and by controlling the volume of the oxygen, the final oxygen ($[DO]_{final}$) level plus the initial analyte concentration ($[analyte]_0$) will be equal to the initial dissolved oxygen ($[DO]_0$) level in a sealed atmosphere with the presumption that the initial analyte concentration is ≤ 0.26 mM at ambient conditions [5]. Based on the assumption it is possible to derive a relation (Eq. 1.) between the various concentrations.

$$[DO]_{final} = [DO]_0 - [analyte]_0. \quad \text{Eq. 1}$$

The enzymes can be embedded in a thin film placed at the bottom of the reaction chamber or dissolved in solution. The consumption of oxygen in the oxidation reactions results in an increase in the PL intensity (I) and the PL decay time (τ) of the oxygen-sensitive dye. The PL was measured using either a photomultiplier tube (PMT) or a 'quad preamp OLED disk sensor' with four Si (silicon) photodiodes making the bio-CD sensor compact and field-deployable. It is envisioned a more compact sensor can also be designed by integrating the OLED and the sensing film on a thin film-based photodetector (PD). Such PDs based on amorphous or nanocrystalline Si are currently under development [6-9], however, their slow response prevent measuring oxygen concentration in the τ mode.

EXPERIMENTAL

Materials

Microcellular foamed sheets of polypropylene (PP) were chosen as the bio-CD substrate and were obtained from Trexel Corporation (MA). The foaming level specified by Trexel was between 15% and 20%.

The reagents used for the PL based bio-CD experiment were the oxygen-sensitive Pt octaethyporphyrin (PtOEP), obtained from H. W. Sands, at a 1mg/mL. 200 proof ethyl alcohol (EtOH) (purchased from Sigma-Aldrich), Ethanol Oxidase (EOx) (purchased from Sigma-Aldrich). All the analytes and enzymes were dissolved in a phosphate buffered saline (PBS) solution. PtOEP based sensing dye film was made by ultrasonicating (standard laboratory cleaning system) a mixture of PtOEP (1mg), polystyrene (PS) (molecular weight 45000 g/mol) (40mg) and titanium (1mg) in 1mL of Toulene for about 3 hours and drop casting it on a regular Corning 18 mm Sq. cover glass.

In order to confirm the results obtained from the lab-on-CD method of determining unknown glucose concentrations in corn slurry samples, alternative standard reference method (dinitrosalicylic acid, DNS), was used for comparison measurement which is detailed in the following text.

Ten (10) mL of corn slurry stock sample, obtained from Lincolnway Energy (Nevada, IA), was collected in 50ml polypropylene centrifuge tubes and mixed with 25mL of 0.1M sodium acetate buffers pH 4.3 and 20µL enzymes containing both alpha-amylases and gluco-amylases (STARGEN^{TM} 001, Genencor, a division of Danisco US, Inc., Rochester, NY). The sample mixture was then introduced into a vortex mixer, then liquefied and saccharified

in shaking incubators at 32°C for 0, 2, 4, and 6 h. Further, as the samples were harvested, enzymatic hydrolysis was stopped by adding 5ml of 4M HCl-Tris buffer (pH 7.0) and boiled for 10 min. The samples were then cooled in ice bath and centrifuged at 2,500 rpm for 15 min. The supernatant was then analyzed for glucose concentration using a modified dinitrosalicylic acid (DNS) method [7]. Dinitrosalicylic acid (DNS) reagent was prepared by mixing 0.25 g of 3,5dinitrosalicylic acid and 75 g sodium potassium tartrate with 50 mL of 2 M NaOH and completing the volume to 250ml with distilled water. One milliliter (1mL) of DNS reagent was added to a 100µL of supernatant samples then mixed vigorously in 1.5mL micro-centrifuge tubes. The samples were heated in a boiling water bath (75-80˚C) for 10 min then cooled in an ice bath. Absorbance of the sample was measured at a wavelength of 570nm using a spectrophotometer (ThermoSpectronic Genesys 2—model W1APP11, Rochester, NY). Glucose concentrations were determined using a pre-calibrated standard curve obtained using absorbance measurements for standard solutions of D-glucose reacted with DNS reagent prepared as detailed above [8].

Tools and Equipment

Micro-embossing was completed with a Branson 2000 Series, 20 kHz ultrasonic welding system (Danbury, CT). Two types of horns were used to manufacture the desired product for application characterization. A titanium horn fabricated by Branson Ultrasonics with the feature detailed in Figure 38 was used. The figure shows the sub-components of the proposed Bio- CD for PL monitoring of glucose, lactate and ethanol concentration.

The reflected PL signal from the bio-CD was measured using two different sensors: 1) a photodetector (PD) that was typically a Hamamatsu R6060 photomultiplier tube (PMT) was used in case of measuring ethanol concentrations and 2), a 'quad pre-amp disk sensor' (Figure 39 A) was used for simultaneous detection of three different analyte concentrations.

Bio-CD fabrication conditions

The foamed PP sheets had a thickness of approximately 1.5 mm and were cut into the size of standard CDs (12 cm – dia.) with common shears. Subsequently the PP – CDs micro-embossing with ultrasonics. Based on previous work [10] the horn shown in Figure. 40 (A). was used at an 100% amplitude setting (40 μm_{pp}) and a constant force of 245 N. A heating/welding time of 0.5 s and a holding time of 5 s was also considered. Once the pattern was embossed (burst valves, microchannels and reagent chambers), a 10 mm flat faced horn was used to further emboss the final reaction chamber (RC) as shown so that the base of the final chamber could be removed and replaced with a transparent glass sheet (~ 500 um thick). This approach was used because of experimental equipment limitations and it is envisioned that in mass production, this would be completed with a single horn/step.

Bio-CD material characterization, surface modification and sealing

To characterize the distribution and size of the pores found in the foamed PP substrate, a cut sample was characterized using a low vacuum (variable pressure) Hitachi S-2460N Scanning Electron Microscopy (SEM) environmental system.

In order to promote wetting, a surfactant solution system in the form of a chemical coating was adequate to promote hydrophilicity [10].

This study also evaluated several sealing techniques on the embossed microfeatures. The techniques included: plasma treated thin (approximately 500 μm) and thick (approximately 3mm) layers of PDMS, scotch tape and a silicone rubber with an adhesive side.

OLED fabrication

The excitation of the PL was a green light emitting layer of 1% volume C545T doped (10-(2-benzothiazolyl)-1,1,7,7-tetramethyl-2,3,6,7-tetrahydro-1H,5H,11H-[1]benzopyrano [6,7,8-ij]-quinolizin-11-one) in tris (8-hydroxyquinoline) Al (Alq_3) based OLED. The OLEDs were fabricated as an encapsulated matrix array of 2x2 mm^2 square pixels resulting from mutually perpendicular stripes of etched ~150 nm thick indium tin oxide (ITO; the anode) and ~100 nm Al (the cathode). The organic layers sandwiched between the electrodes were deposited by thermal vacuum evaporation, as described previously [7, 8]. The OLEDs were operated in a pulsed mode with a forward bias of ~20 V and a pulse width of 100 μs with a repetition rate of 50 Hz.

Estimation of Glucose concentration in corn slurry samples using the OLED-PP-Bio-CD

Corn slurry sample containing various levels of glucose were characterized with the DNS method then diluted with DI water so that the final glucose concentration was within the sensitive range of the OLED-PP bio-CD, which was 0 to ~0.26 mM at room temperature because analyte molecules reacts with oxygen molecules at 1:1 ratio and DO content is only about 0.26 mM (or 8.6 ppm). Two hundred (200) μL of the corn slurry analyte with beta-D glucose concentration was introduced into the final reaction chamber. Thirty (30) μL of GOx enzyme at an initial concentration of 2500 units/mL was then introduced into the buffer chamber and the enzyme chamber of the bio-CD. Before rotation, the bio-CD was sealed using the silicone rubber. Following the rotation, the bio-CD was immediately placed above the OLED pixels and the PD window of the PMT. The OLED was then energized and the resulting PL signal from the dye was measured with a Labview data acquisition system. PL decay time was further estimated using OriginPro software. An estimated time interval of about 60 s was consistently given between bio-CD spinning and engaging the OLED. The final glucose concentration was determined by comparing the decay time value with the calibration curve obtained for standard beta-D glucose. The PL decay time was measured five times for each sample and after each measurement the bio-CD was washed with distilled water and blown dry under compressed N_2 gas.

PL decay time determination of ethanol concentration

In the experiments that determined the ethanol concentration based on PL decay time of ethanol, 200 µL of known concentrations of ethanol was loaded into the final reaction chamber and 30 µL of alcohol oxidase (AOx) enzyme at a concentration of 1500 units/mL was loaded into the enzyme chambers of the bio-CD. The PL decay time was measured five times for each concentration of ethanol. Because of the relatively long reaction time between AOx and ethanol, the time interval was set to 180 s between the bio-CD spinning and powering of the data acquisition system for PL decay time determination.

Simultaneous PL decay time determination of multiple analytes

a. The PL decay times of ethanol, glucose and lactate, each at a final concentration of ~ 0.0875 mM and ~ 0.13 mM, and
b. The PL decay times of three different concentrations of all three analytes mixed together - were simultaneously detected using the 'quad pre-amp disk sensor' that in turn composed of four Si PDs as shown in Figure 39 (A). The Bio-CD rotation speed was between 500 – 1000 rpm in all the experiments.

RESULTS AND DISCUSSION

Foamed PP material analysis

Figure 40 shows a SEM image of the foamed PP sample taken at its wedge. It can be seen that although the pores or voids are relatively evenly distributed, their size varied from tens of microns to approximately 200 µm.

Surface modification of the microembossed features on the Bio-CD

A 30 µL of a blue colored food dye was diluted in distilled water and introduced with a micropipette into the reagent chambers to study the nature of flow before and after coating the surface with the surfactant (Lurol 12134) solution. As can be observed from Figure 41 (A), a well defined droplet was formed on the uncoated surface indicating that the standard PP surface was highly hydrophobic to prevent any fluid flow while, the flow was easily enabled on the surfactant coated surface of the same PP sample substrate. As can be seen in Figure 41 (B), the surfactant coated PP surface created a hydrophilic surface and thus promoted the fluid flow through the microchannels.

Sealing of the microembossed features on the Bio-CD

Several techniques for sealing the embossed features were evaluated. Plasma treated PDMS films pressed against the CD's initially sealed the features however leaked during the spinning process. Scotch® tape was not effective because of its small thickness that prevented it from buckling over the larger sample. This effectively reduced the final volume of the chamber. However, the silicone rubber with an adhesive backing proved effective in sealing the microembossed features, even during the spinning process. As seen in Figure 42 (A) and (B), the SEM images show the cross section of a silicone rubber sealed microchannel and the burst valve, respectively.

Verification of glucose measurements with DNS

Six different corn slurry samples, each corresponding to zero to five hours of saccharification times at 1 h intervals, were characterized using a DNS methodology for sugar concentration and their corresponding values were 11.23, 33.66, 38.58, 49.03, 55.15 and 73.22 g/L respectively.

Based on the CD results of the various hydrolysis times (0-5h) of the corn slurry, the glucose concentrations were 2.6, 15.56, 26.46, 35.28, 25.94, 52.92 g/L. Figure 43 shows the correlation between the DNS measurements and the measurements of the CD sensor. It is seen that there is a good correlation between the two techniques. This suggests that despite the fact that corn slurry has a wide range of containments (proteins, oils, etc) the CD method is able to accurately measure glucose levels.

PL decay time measurement of ethanol concentration

Figure 44 (B) shows the modified Stern-Volmer [11] plot for the results obtained for ethanol using the Bio-CD sensor that required a green emitting C545T doped (1%) in Alq_3-based OLED whose emission spectrum falls within the range of the absorption spectrum of the PtOEP dye, and a PMT. The measured values of τ for ethanol varied from approximately 30 to approximately 90 μs for solutions at equilibrium with air (i.e at zero ethanol concentration) at ambient temperature and solutions containing at least 0.25 mM of ethanol, respectively.

The samples with the longer τ values (90 µs) correspond to a solution devoid of oxygen, which was consumed by the oxidation reaction.

Decay time measurements as a function of ethanol concentrations is seen in Figure 44 (A). It is seen that the inverse of the decay time is directly proportional to the analyte concentration (ethanol) as expected as less oxygen remained in the analyte concentration verifying that relatively less O_2 remained in the reaction chamber to quench the PL with increasing analyte (ethanol) concentrations. Figure 44 (B) shows the same data represented in terms of Stern-Volmer relationship (Eq. 1), which explains the underlying physics in the relation between the PL decay time (τ) and PL intensity (I) with respect to the available oxygen concentration.

Simultaneous multi-analyte concentration sensing via PL decay time measurement

To validate the results from the multi-analyte sensing, each dye film was calibrated with respective analytes. Figures 45 (A), (B) and (C) show the calibration obtained with lactate, glucose and ethanol respectively. Two different final concentrations of ~ 0.0875 mM and ~ 0.13 mM were considered for lactate, ethanol and glucose. It is seen that the decay time values measured from multi-analyte sensing for each analyte is in good agreement with the calibrated value.

To further validate the capabilities of the lab-on-CD based multi-analyte sensing, ethanol, glucose and lactate, each at a final concentration of 0.043mM, 0.056mM and 0.13mM respectively, were combined together in equal proportions in separate reaction chambers of

the PP lab-on-CD. Following CD rotation, at approximately 500 rpm, the decay-time values were measured at approximately 180 s after the three enzymes namely: ethanol oxidase, glucose oxidase and lactate oxidase were introduced by the corresponding micro channels into each of the reaction chambers. Figure 46 shows the comparison of the measured decay-time values of multi-analyte mixture with the respective enzyme against the corresponding calibration value which, it was determined under similar experimental conditions.

CONCLUSIONS

Foamed PP bio-CD has proven to be a good sensor in detecting different PL decay times of several ethanol concentrations as well as in detecting unknown glucose concentrations in a corn slurry when used in conjunction with OLEDs. The bio-CD also proved to be versatile in its effectiveness in being able to simultaneously detect PL decay times of multiple analytes such as glucose, lactate and ethanol in a single step. It was seen that the bio-CD was able to measure several chemistries, namely glucose, lactic acid and ethanol in pure solutions as well as corn slurries where numerous contaminants are present. These results were confirmed using standard methods.

Incorporation of OLEDs as a source for EL makes the design relatively flexible in terms of simplicity, compactness and field deployability.

FUTURE WORK

To further enable the product towards further compactness, design flexibility and power efficiency, organic photovoltaic (OPVs) can be proposed to be used to power the OLEDs.

This will add further novelty to the bio-CD product while helping it derive applications for other biotechnological challenges.

AKNOWLEDGEMENTS

We are grateful to Branson Ultrasonics (Danbury, CT) for donating us the ultrasonic embossing equipment and tooling. We thank Dr. Melissa Montalbo for performing DNS measurements of glucose in corn slurry samples. We would also like to thank Ames Laboratory for their co-operation. Ames Laboratory is operated by Iowa State University for the United States Department of Energy (USDOE).

REFERENCES

1. L. J. Lee, M.J. Madou, K.W. Koelling, S. Daunert, S. Lai C.G. Koh, Y-J Juang, Y. Lu and L. Yu, *Biomed. Microdevices.,* **3**, 339-351, (2001).

2. G. Harmon, D. Grewell *SPE ANTEC Proceedings, Brookfield,* 1051-1055, (2007).

3. J. Kim, S. Jang, J.V. Zoval, N.Da Silva, M. Madou, *Proc. SPIE Int. Soc. Opt. Eng.* **5455**, 331-340 (2004).

4. S. Vengasandra and D. Grewell *SPE ANTEC Proceedings, Brookfield,* 1041-1045, (2007).

5. Y. Cai, R. Shinar, Z. Zhou, J. Shinar, *Sens. Actuators*, B 134, 2, 727-735, 2008.

6. R. Shinar, D. Ghosh, B. Choudhury, M. Noack, V.L. Dalal, J. Shinar, *J. Non-Cryst. Solids*, **352** (9-20), 1995-1998 (2006).

7. G. L. Miller, *Anal. Chem.*, 31, 426 – 428 (1954).

8. S. K. Khanal, M. Montalbo, J. V. Leeuwen, G. Srinivasan, D. Grewell, *Biotechnol. Bioeng.*, **98** (5), 978 – 985 (2007).

9. D. Ghosh, R. Shinar, V.L. Dalal, Z. Zhou, J. Shinar, *J. Non-Cryst. Solids*, **354** (19-25), 2606-2609 (2008).

10. S. G. Vengasandra, G. Harman, D. Grewell, *Polym. Eng. Sci.* (in press).

11. J. Shinar and R. Shinar., *J. Phys. D: Appl. Phys.* 41 (2008) 133001.

FIGURES

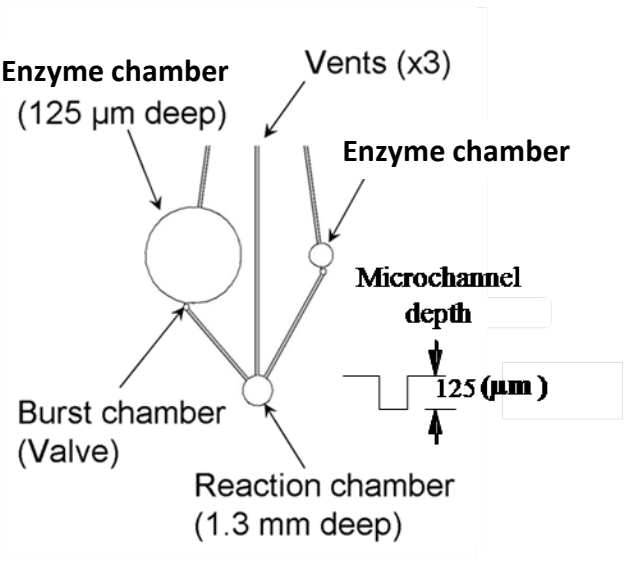

Figure 38. Shows the schematic of the critical components of the foamed PP bio-CD and its dimensions.

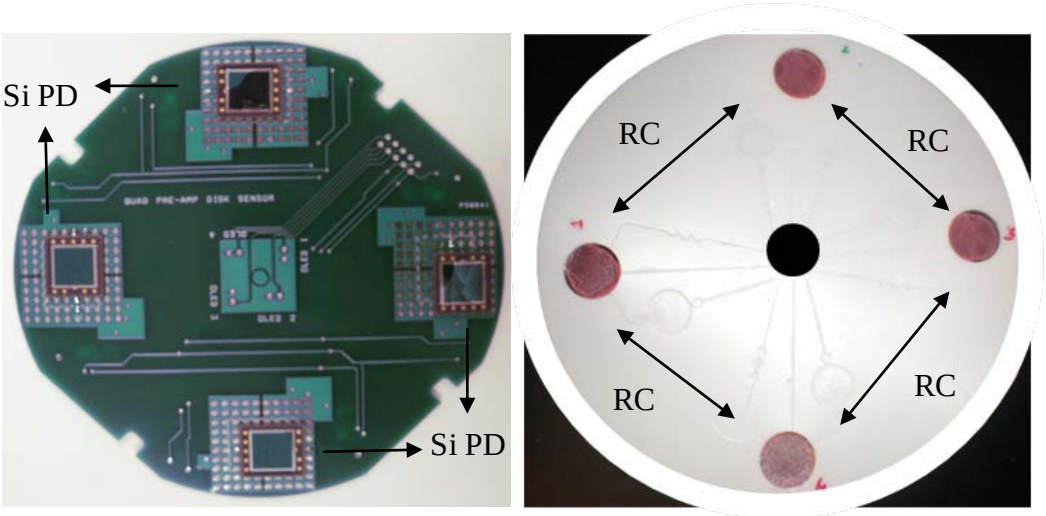

(A) (B)

Figure 39 (A). Image of the 'quad preamp OLED disk sensor' for simultaneous PL sensing and (B). Image of the foamed PP bio-CD with PtOEP dye films serving as the bottom of the reaction chamber.

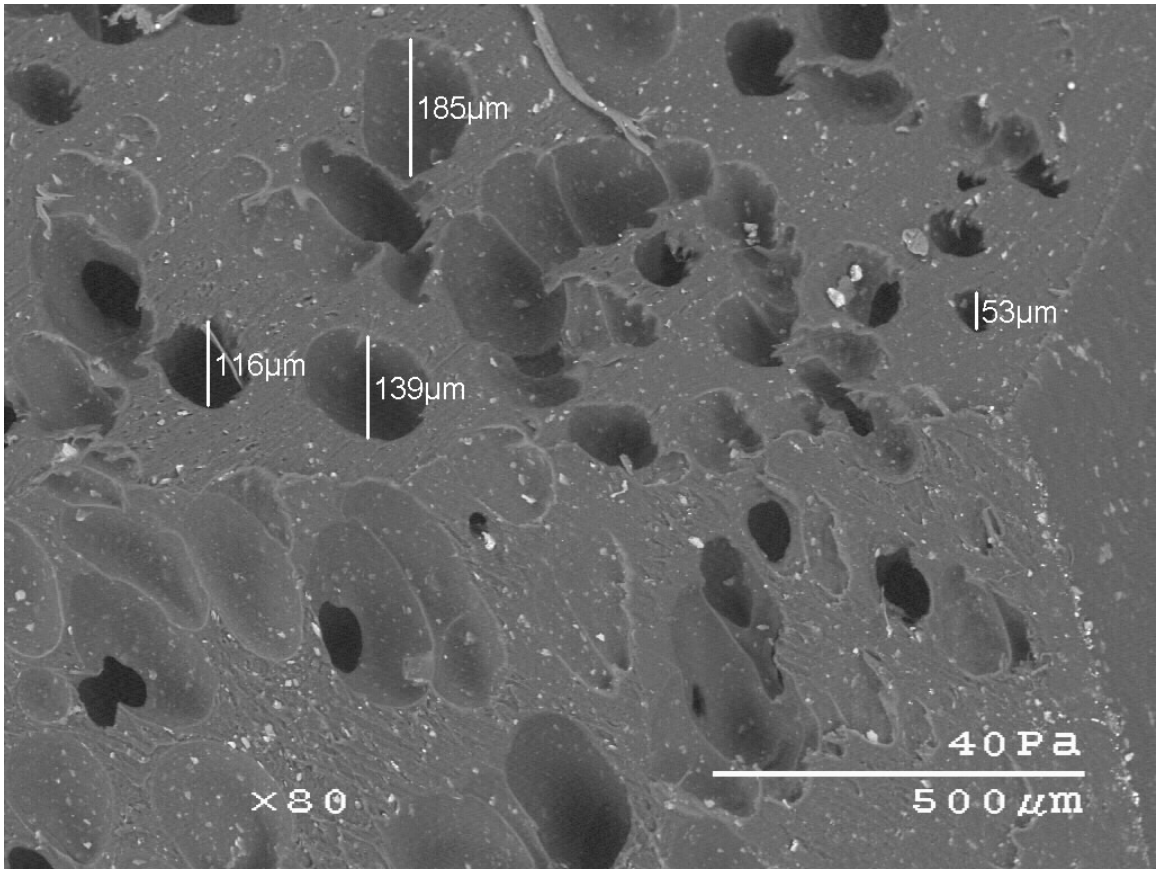

Figure 40. SEM image obtained at the wedge of the mucell foamed PP material.

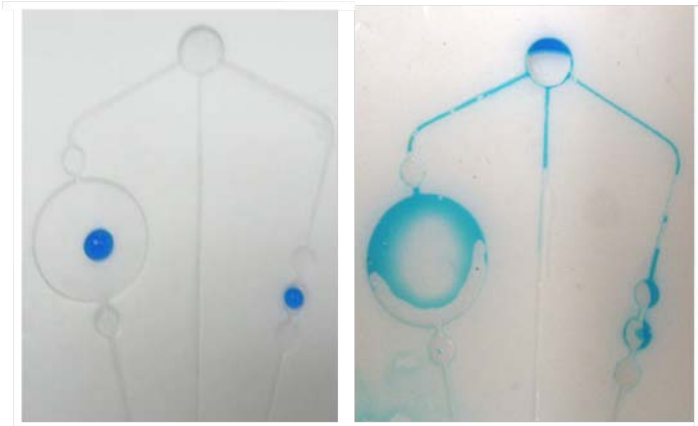

(A) (B)

Figure. 41 (A) Uncoated foamed PP substrate and (B). fluid flow on the surfactant coated PP substrate

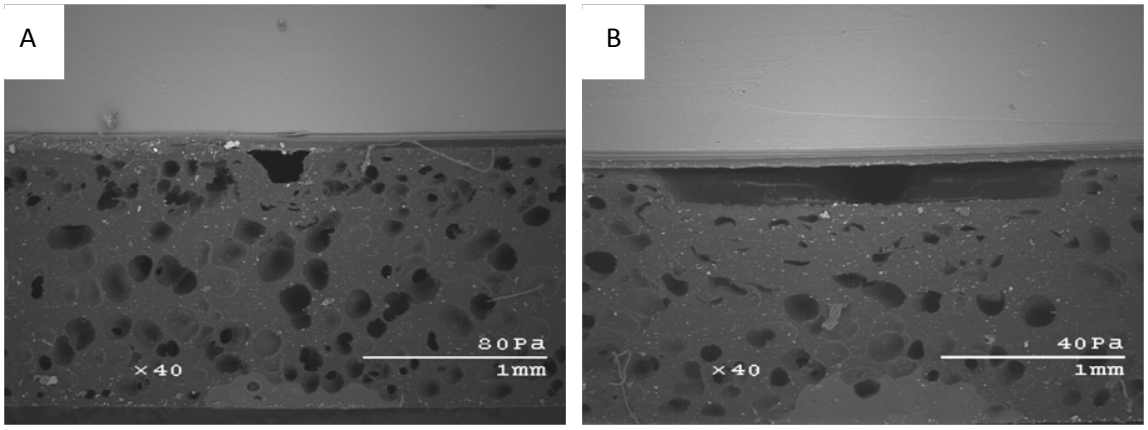

Figure 42. SEM images of the cross section of the microchannel (A) and a burst valve (B)

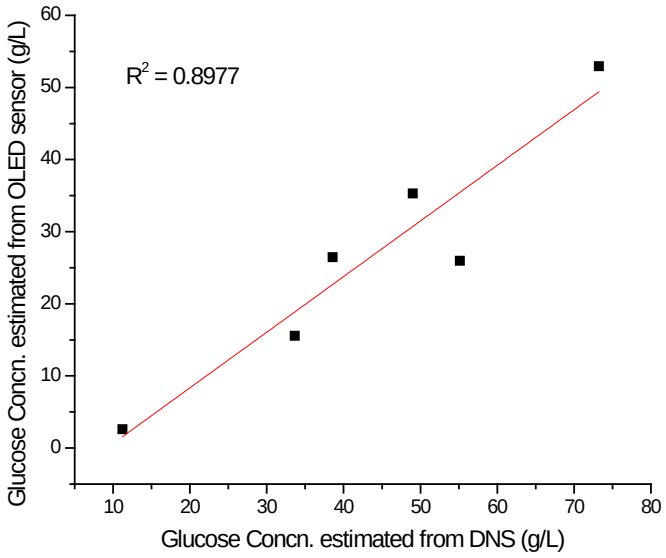

Figure 43. Correlation of OLED-Bio-CD versus DNS method for glucose concentration measurement.

(A)

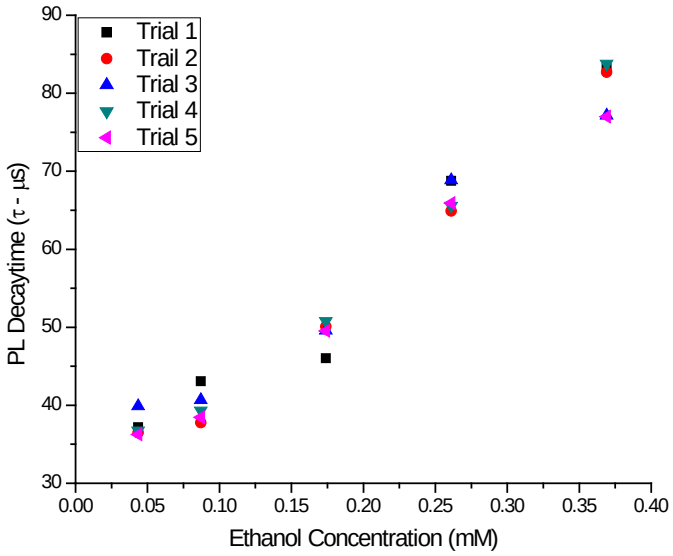

(B)

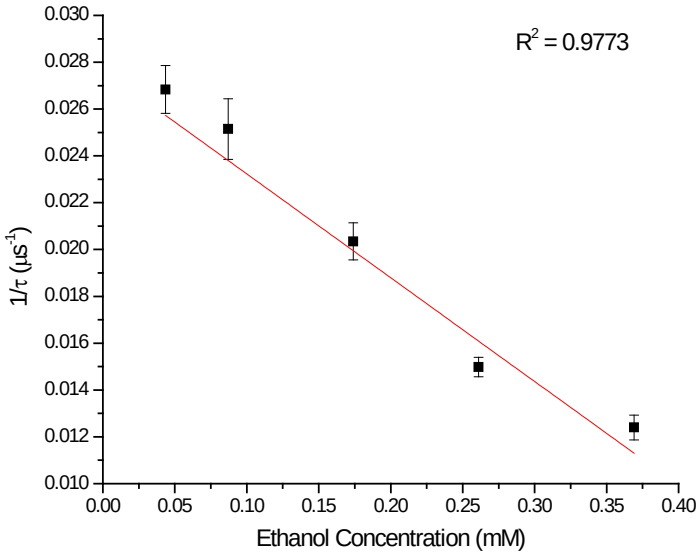

Figure 44 (A). Plot of observed PL-decay times versus different ethanol concentrations. (B) Modified Stern-Volmer calibration line for ethanol in a sealed cell at 23^{o}C.

(A)

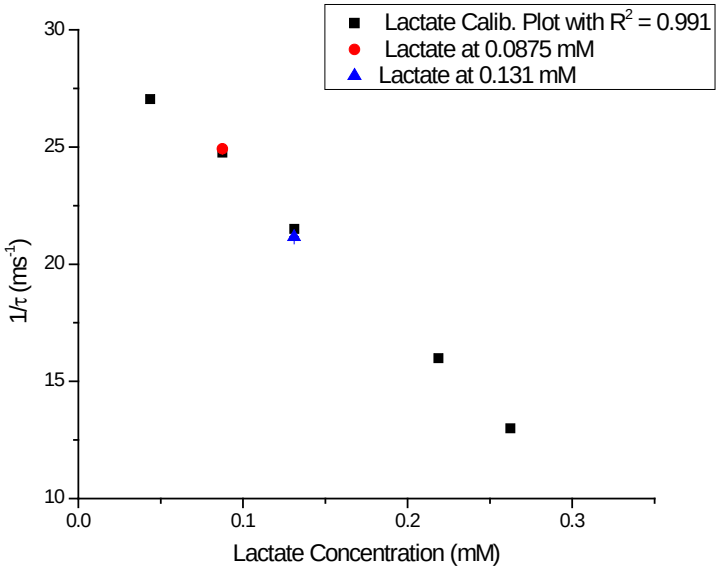
Lactate Calib. Plot with R2 = 0.991
Lactate at 0.0875 mM
Lactate at 0.131 mM
1/τ (ms-1)
Lactate Concentration (mM)
30
25
20
15
10
0.0
0.1
0.2
0.3

(B)

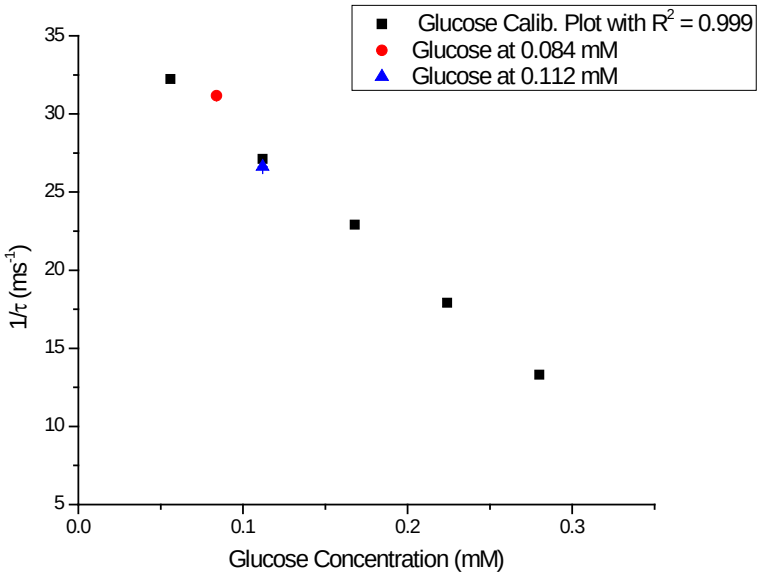
Glucose Calib. Plot with R2 = 0.999
Glucose at 0.084 mM
Glucose at 0.112 mM
1/τ (ms-1)
Glucose Concentration (mM)
35
30
25
20
15
10
5
0.0
0.1
0.2
0.3

(C)

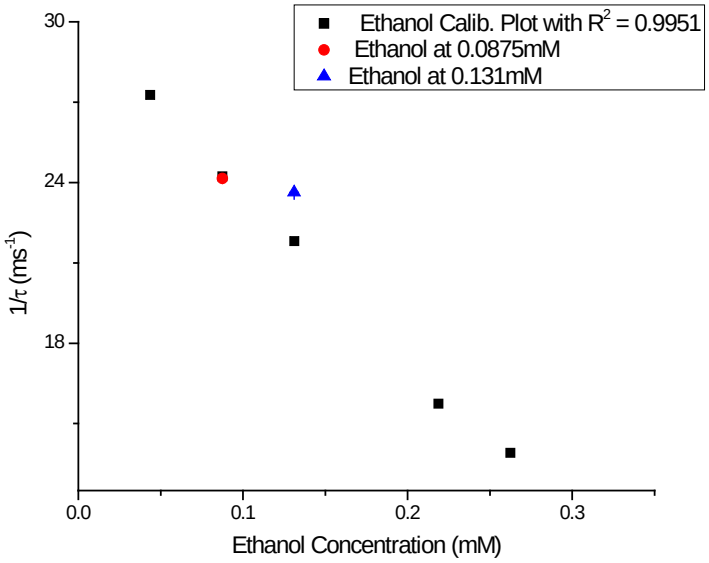

Figure 45 (A), (B) and (C). Calibration plots for lactate, glucose and ethanol respectively. The plots also show the nature of respective multianalyte sensing at two different concentrations.

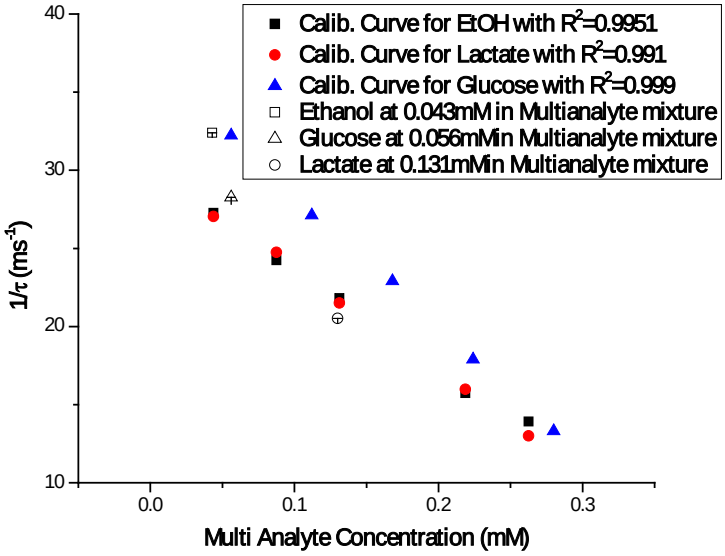

Figure 46. Plot showing the nature of multianalyte mixture sensing at different concentrations against the respective calibration curves.

CHAPTER 5: GENERAL CONCLUSIONS

Based on the results from this work it is concluded that high power ultrasonic microembossing technology (HPUMT) is an efficient polymer microfabrication technology to produce precise, flash free microfeatures on microcellular foamed polymer substrates. It was proven that the use of microcellular foamed substrates allow absorption of the flash during embossing. A compressional model of the process based on the assumption that the micro-cellular density is ρ_1 and a fully consolidated density of resin ρ_2 (no foaming remaining), a non-dimensional ratio (Eq. 1) of the embossed volume (V_1) to the consolidated volume (V_2) was experimentally verified.

$$\frac{\rho_1}{\rho_2} = \frac{V_2}{V_1 + V_2} \tag{1}$$

This model allows the prediction of the volume that is required to absorb the flash produced from a given embossed feature based on the foaming level (% reduction of the material density) as it can be used to estimate critical dimensions such as substrate minimum thickness or minimum distances between embossed features.

In addition, results from the design of experiment that characterized parameters of the HUMPT such as embossing heating time (s) and embossing amplitude (µm), at a constant holding force (N), in characterizing the depth (in µm) showed that the optimum amplitude was 30 µm with a weld time of 2 s and a weld force of 245 N. With these conditions the cycle time was minimized and the features were fully embossed to a maximum depth of 300 µm.

The issue of hydrophobicity of most virgin polymer surfaces was resolved by surface functionalization to promote wetting, capillary action and proper fluidic motion. Because the conventional techniques such as ozone and plasma treatment proved to be ineffective in promoting the hydrophilicity of the foamed PP surface, an organic surfactant coating was studied that proved to be effective in increasing the surface energies of both the PS and PP material surfaces irrespective of its foaming level.

The second phase of this research work enabled OLEDs to be incorporated in conjunction with the micro-embossed PP lab-on-CD (bio-CD) device for the purpose of different biosensing applications. Preliminary results on a PL-based glucose concentration sensing application demonstrated a good correlation between the PL intensity and the different glucose concentrations. Further experimentation verified that the effect of attenuation was insignificant in the measurement of the luminance intensity produced by increasing volumes of the reagent solution.

Results obtained using the PL-life time value determination of glucose, ethanol and lactate analytes further demonstrated the validity of the OLED_Bio-CD approach for monitoring of analyte concentrations.

It was also determined that the bio-CD was effective in detecting concentrations of ethanol samples in a pure solution as well of detecting unknown glucose concentrations in a corn slurry. This is important to note because the corn slurry contained a wide range of

containments which did not adversely affect the functionality of the bio-CD. With the design and development of a ‘4 PD Quad pre-amp disk sensor’ the bio-CD also proved to be versatile in being able to simultaneously detect, the PL decay times of multiple analytes such as glucose, lactate and ethanol in a single step. The results of estimating unknown glucose concentration in a corn slurry sample was confirmed using a standardized dinitrosalycylic acid test method (DNS).

In summary, it is shown that the developed polymer microfabrication technology, namely HPUMT, can be utilized to produce complex, flash-free features on microcellular polymer substrates with various feature depths and geometries. Utilization of organic light emitting diodes (OLEDs) as an excitation source to the biosensing dye element enabled the biosensing functionality of the Bio-CD. The standard curves of photoluminescence (PL) decay times (τ) of glucose, lactate and ethanol samples can be used to estimate unknown concentrations.

APPENDIX 1

Project: Business Plan developed for Entrepreneurship and New Business Creation (MGMT 566) class in Spring 2007

An Innovation Plan from

ACE BIOMEDICAL SOLUTIONS, INCORPORATED

presented as a class project for

Management 566 – Entrepreneurship and New Venture Creation

Dr. Howard Van Auken

ISU - MBA PROGRAM

by

Sam Ghose - sghose@iastate.edu
Jorge Martinez - jarzate@iastate.edu
Tim Norris - tim_norris@adp.com
Claudia Prado - cmprado@iastate.edu
Srikanth Vengasandra – kanth@iastate.edu

Spring - 2007

TABLE OF CONTENTS

EXHIBITS

BUSINESS DESCRIPTION

FIRM DESCRIPTION

ACE Biomedical Solutions Inc. is a company intending to start-off primarily as a medical diagnostic tool development company. The company's main focus lies in the areas of researching and developing proprietary medical diagnostic technologies and patenting the same. Commercializing and marketing of forward looking, convenient biomedical solutions would be the ultimate goal of the company. The company's proprietary technology is currently in the area of lab-on-CD. The advanced bio-CD applications towards diagnosis will all be developed on a common patent pending polymer material.

BACKGROUND OF THE OWNER

Srikanth Vengasandra is the founder and President of ACE Biomedical Solutions Inc. He will also be the Chief Executive Officer and Chief Technology Officer of the company. Several other professionals are also identified as key associates to recognize their involvement and contributions since the inception of the company. The biographies of all the members follow:

- *Srikanth Vengasandra* – Founder, President, Chief Executive Officer, Chief Technology Officer

Ph.D – Industrial Technology, Iowa State University, 2009
MS – Chemical Engineering, Illinois Institute of Technology (IIT), Chicago, 2002
BS – Chemical Engineering, Bangalore University, India, 1999

Mr.Vengasandra has three full years of work experience gained that were directly related to research and applications development in two different start-up companies involved in bio/nanotechnology areas. During his tenure as a Research Scientist he co-authored and published a dozen publications, all in international peer reviewed journals. With the patent pending BioCD application; international acceptance as a nanotechnology scientist; strong technical and educational background and a good understanding of the working of start-up companies makes him worthy of this leadership role.

- *Tim Norris* – Vice President of Sales & Marketing

MBA – Marketing, Iowa State University, 2007
BA – Marketing, Iowa State University, 1998

Mr. Norris has over seven years of experience in national and international consulting, sales, and marketing functions within two Fortune 500 companies. His excellent inter- and intrapersonal communication skills and creative drive position him to lead a exciting and developing company.

- *Sam Ghose* – Vice President of Finance and Strategy

MBA – Finance, Iowa State University, 2007

Mr. Ghose joins Ace Biomedical as a veteran of the Genomics industry, having worked on cutting edge projects within one of the world's top Genome centers. As part of the NIH funded International Hapmap Project, he collaborated with cutting edge companies like Affymetrix and startup Parallele Bioscience. Parallele was subsequently acquired by Affymetrix for over $120 Million, one of many indicators of the success of Sam's collaborations.

- *Jorge Arzate Martinez* – Chief Operating Officer

Mr. Martinez has a BS degree in Marketing by the University of Colima, Mexico City. He is currently an MBA student specialized in the communication technologies. He is fluent in Spanish and English. He is greatly influenced by the medical industry.

- *Claudia* Marcela Prado – Vice President of Manufacturing

Ms. Prado has a BS degree in Economics by the University of Colima, in Mexico. She is currently an MBA student specialized in community development. She is fluent in Spanish and English. She had work in the medical industry.

ORGANIZATIONAL FORM

■ Srikanth Vengasandra will be in charge of the total management of the company. He will also be responsible, as a CTO, to guide the R&D division.

■ Timothy Norris will handle commercializing and marketing aspects of the company and will serve as the Vice President (VP) of Sales and Marketing.

■ Sam Ghose will handle the strategic growth plans and capitalization and will serve as the Vice President (VP) of Finance and Strategy.

■ Jorge Martinez will handle operations through managing day-to-day activities and also implementing and achieving strategic plans. Jorge will serve as the Chief Operating Officer (COO).

- Claudia Prado will be responsible for initial manufacturing, sourcing and distribution. She will hence serve as a Vice President (VP) of Manufacturing.
- All these professionals will be directly reporting to the CEO.
- Additional personnel will be hired to assist each of the above executives in their respective areas.

BUSINESS GOALS

1. To gain recognition as a quality R&D company in the area of providing innovative, cost effective and simple medical diagnostic solutions.
2. To achieve 10% market penetration in the area of innovative disease diagnosis market by the year 2009.
3. To raise $1 million in private seed capital in the first half of 2008.
4. To win low interest loans and grants from state and federal governments totaling $2 million in 2007.
5. To license its technology for at least $1 million by 2009.
6. To continue enhancing the value of the company through strong partnerships and collaborations.

MILESTONES

A. Raise Start-up capital.

B. Gain recognition as an innovative biomedical solution provider via selling the idea of lab-on-CD for Glucose detection.

C. Write scientific papers explaining the technology that would enable detection of several major pathogens and publish the same in international, high impact factor journals.

D. Develop new marketing strategies to either sell/license the technology or the products through established distributors worldwide.

E. Build strong partnerships and customer relationships.

OPERATING PLAN

STAGE OF DEVELOPMENT

- Product manufacturing: The extruded Polypropylene sheets are cut to the shape of a regular compact disks (CD). The micro-channel patterns are then ultrasonically embossed on the polymer substrate. The patterned CD surface is now capable of guiding the biochemical fluid flow towards selective intermixing and hence also will facilitate further reactions. The CDs are then packed in packages of ten CDs/pack.
- Problem identification:
  - Cutting of extruded sheets into a perfect CD shape needs to be automated.
  - Lack of funds to purchase enough embossing equipments.
  - Noise level operation of the equipment is high.
  - Lack of BS-2 (Bio Safety Level 2) type of laboratories that would help to securely handle hazardous biochemicals.
- Compliance with Law: All technicians and lab assistants will be made certain to strictly adhere to safety regulations and other laws of the organization.
- Suppliers: Trexel, based in Pennsylvania will be the primary supplier of the special polymer material. However, contacts with two other manufacturers have already been established as an alternative in case Trexel fails to support us adequately. Branson will however be our primary supplier of the specialized embossing equipments. This is in recognition of their faith through continued financial support towards the progressive development of our product.
- Quality Control measures: Concerned employees will all be trained in six sigma and lean manufacturing processes to help make better manufacturing and production changes in the products to enhance quality.

PRODUCTION PROCESS

- General: Day-to-day activities will include rigorous research in terms developing further innovative biomedical solutions, applications and technical writing; manufacturing; sale and marketing and shipping. The business will be operational only 8 hours per day. The business will not be open during weekends however the business will be functional on all seasons.
- The physical plant: Current facility is a small 1000sqft lab facility at Iowa State University's Food Science building. Initial start-up funds raised will however be used towards leasing or renting a larger facility at ISU research park.
- Equipments: The only equipment that is currently within our access is ultrasonic plastic welding machine. This is the most expensive of all the equipments that might be needed to make the bio-CD product. It also a very important enabler towards obtaining

precise micro-patterns on the CD substrate. The other equipments needed for research and application development are easily accessible with the help of our collaborators at the Ames Lab, which is an US-DOE facility.

- Assets: The patent pending bio-CD product material and its strong proprietary technology and intellectual property are the only concrete assets of ACE Biomedicals Solutions Inc. besides owning several ultrasonic welding equipments.
- Special Requirements: The Company does not have any special requirements other than a Bio Safety level 2 type of facility, the funding for which has already been secured.
- Materials: Specialized polymer materials that are primarily needed to make the products will be bought from Trexel. Financially very feasible deal has been negotiated and signed by both parties in terms of purchasing this material from Trexel.
- Cost: ACE Biomedical Solution's first product namely the 'Glucose detection CD kit' will be sold in packs of 10 CDs for $250. The cost is expected to vary with respect to the type of application and is also believed to start at the base cost of $250 per pack.

EXIT STRATEGY

- ACE Biomedical Solutions Inc. would be open to acquisitions through carefully developed negotiations with interested businesses.
- ACE Biomedical Solutions Inc. would also like to choose going public with an IPO as an alternative exit strategy.

MARKET ANALYSIS

INDUSTRY INFORMATION

- Biotechnolgy Industry:

- Spent an average of eight years and $1.2 billion to get a new treatment to the market, about 24 percent more than it cost makers of traditional drugs to develop a medicine. *Source: Tufts Center for the Study of Drug Development at Tufts University.*

- The biocompatible materials market is estimated to reach nearly $11.9 billion by 2008.1 Biomaterials are used in every medical device meant for body contact, from orthopedic implants and bone grafts to coronary stents and soluble sutures. *Source: Biocompatible Materials for the Human Body, 2003.*

- Drug Delivery Industry:

- The global market for drug-device combinations is expected to increase at an average annual growth rate of 13.6% and reach $11.5B in 2010, compared with $5.4B in 2004. *Source: Business Communications Co. Inc.*

- The US pharmaceutical packaging market is set to grow at a compound annual rate of 3.3% between 2004 and 2011. A major portion (16.8%) of this revenue is set to come from the fastest growing prefilled syringes sector. *Source: Frost & Sullivan, US Pharmaceutical Packaging Market Report 2005.*

- General Health Care:

- 125 million Americans have one or more chronic conditions (e.g. congestive heart failure, diabetes.) Chronic diseases account for 75% of all health care expenditures. *Source: Burrill & Company, 2006.*

- Medical Devices Industry:

- The market for coatings and surface-treatment processes used on medical devices will reach more than $5.31 billion by 2010. The 12.4% annual growth rate will be fueled by explosive growth in high-value combination products. *Source: Medical Device Coatings Report, BCC Research, April 2006.*

- The medical devices and equipment industry employs more than 411,400 workers, accounting for nearly one third of all US bioscience jobs. *Source: Medical Product Outsourcing 2006.*

- Pharmaceutical Industry:

- Big Pharma companies forecast about 60% of revenue growth to come from biologic products. The forecast revenue growth rate to 2010 for biologics is 13%, compared to 0.9% for small molecule products. *Source: Datamonitor.*

- The U.S. market for pharmaceutical packaging will grow by nearly a third between 2004 and 2011, from $2.6 billion to just under $3.4 billion. At the same time, pharmaceutical packaging will play an increasingly important role in effective drug delivery. *Source: Frost & Sullivan*

TARGET MARKET

- Worldwide Nanotechnology Market - $1 Trillion (10 – 15 yrs). [National Nanotechnology Institute, 2002].
- Life Science Pharmaceutical Market - $180 Billion (10 – 15 yrs). [Punk, Ziegel & company, 2002].
- Diagnostics 7 BioChip Market - $46 Billion (2012). [MedMarket Diligence, 2003].
- Protein Chips - $723 Million (2006). [BioInsights, 2000].

COMPETITIVE ADVANTAGE

Customers:

- Commercial National diagnostic labs.
- Federal research and diagnostic labs.
- Federal and local governments.
- Hospitals and clinics.
- Pharmaceutical R & D companies.

COMPETITIVE STRATEGY:

Four companies identified as competition

	ACE Bio-CD	***Abaxis***	***Gyros AB***	***Alliance Protein Laboratories***
Location	Ames, IA	Union City, CA	Uppasala, Sweden	Thousand Oaks, CA

Detection Method	CD based	Sensor chip and CD based	Sensor chip and CD (circular dichroism) spectroscopy	CD based
Product/Service	Diagnoses	Diagnoses	Diagnoses	Protein Characterization
Strengths	Simple, flexible effective, cost effective	proven	proven	proven
Weaknesses	Lack of public relations	expensive	expensive	expensive

RISK ASSESSMENT

- FDA and other regulatory bodies.
- Larger companies that sell bulky equipment will not delay product entry to put us out of business.
- Courting larger companies like Affymetrix.
- Assume adequate start-up funds.

MARKETING PLAN

IMAGE

When people and medical professionals in particular think of the ACE Bio-CD (ACE), the words accurate, fast, and confidential should be the first ones that come to mind. Our product will be taking over an already proven technology that patients have come to trust. In order for medical professionals to offer our product we have to give them a good argument to present to their patients. In essence, we must prove that ACE is:

- Accurate – ACE must be a far superior diagnostic tool and technique than those used now. It's accuracy must be measurably different in order for medical professionals to entrust their patients diagnostic needs to it. If our product is more reliable and accurate it will be good ROI for medical professionals financially and will increase their patient satisfaction scores.
- Fast – ACE needs to really hammer into medical professionals the amount of saved time between collecting, running and analyzing test samples. At this time we estimate that ACE will be able to provide test results from the average clinic in just 24 hours or less compared to the national average of 90 hours currently. This will increase patient satisfaction and decrease the stress patients feel while waiting for results. It will also allow medical professionals to act quicker to combat certain diseases.
- Confidential – ACE's unique value proposition is that fewer eyes will see each test. Currently, each test is seen by the technician who runs the test, the peer reviewer who checks the test, the doctor who ordered the test, his/her personal nurse, and in some cases a secondary nurse who calls the patient with the results. Using the ACE product, doctors could perform the tests themselves or train their personal nurses to do the testing. This would cut the number of people who see what each patient is being tested for as well as the results of said tests from 5 people to 2 or just possibly 1 person.

In today's time and age of HIPAA, Sarbanes-Oxley, and other privacy concerns, medical providers who switch to the ACE product will be able to proactively create value for their patients.

PRICING

ACE will price our product at a premium in the market. ACE should be viewed in the patients mind as the cutting-edge, industry leading provider of diagnostic tools. Patients should ask for our product by name, and they should be willing to absorb higher costs in order to have our products used in their clinics and labs.

PROMOTIONS

We will be advertising and marketing our product through medical and bio-technology professionals across the country. We will use a combination of articles, advertisements, and provide testimonies in medical magazines and journals, and also attend expositions and conferences across the country to get our message about our product and its attributes to our core audience.

Magazines and journals to be considered:

Acadiana Medical News	*ADDitude*	*Alternative Medicine*	*Arthritis Today*
Body and Soul	*Consumer Reports on Health*	*Discover*	*Family Doctor*
Health Management Technology	*Natural Health*	*Psychology Today*	*Scientific American*
Totalhealth	*AgBioForum*	*Annals of Biomedical Engineering*	*ASBMB's Journal of Biological Chemistry*
Bioline Journals	*BioChemNet*	*BioOptics Online*	*Biotechnology Today*
Cell Press	*Chemistry & Industry*	*Chemistry Today*	*COMPLEXITY INTERNATIONAL*
Conservation Ecology	*International Antiviral News*	*Journal of Molecular Biology*	*Journal of Molecular Diversity*
Journal of the National Cancer Institute	*Nature Biotechnology*	*Nucleic Acids Research*	*Oak Ridge National Laboratory Review*
Protein Science	*Science*	*Science Notes*	*The Scientist*

Expositions and conventions being considered can be found as **Exhibit 1.**

FINANCIAL PLAN

FINANCIAL STATEMENTS

Financial statements have been provided as part of **Exhibit 1**.

EXHIBIT 1

ACE BIOMEDICAL SOLUTIONS INC. – BALANCE SHEET

BALANCE SHEET		
As of Dec 31,2008 day before business opens		
Assets		
Current assets		
	Cash	$2,000,000.00
	Accounts receivable	$0.00
	Inventory	$0.00
Fixed assets		
	Equipment	$100,000.00
	Total assets	$2,100,000.00
Liabilities		
	Total liabilities	$0.00
Net worth		
	Total net worth	$2,100,000.00

EXHIBIT 1

ACE BIOMEDICAL SOLUTIONS INC. – INCOME STATEMENT

INCOME STATEMENT AS OF YEAR END 2008			
Sales		$	%
	Beginning inventory	0.00	0
	Materials purchased	76,850.00	0
	Ending inventory	76,850.00	0
Cost of goods sold			
	Purchases(merchandise)	76,850.00	0
	Gross wages(excludes withdrawals)	1,030,000.00	0
	Payroll expenses(taxes, etc.)	216,000.00	0
	Outside services	1,000.00	0
	Supplies(office and operating)	5,300.00	0
	Repairs and maintenance	1,200.00	0
	Car, delivery, and travel	8,000.04	0
	Accounting and legal	88,500.00	0
	Rent	39,999.96	0
	Telephone	1,500.00	0
	Utilities	1,500.00	0
	Subtotal	1,469,850.00	0
Total operating and fixed expenses		1,469,850.00	0
	Operating profit	-1,469,850.00	0

EXHIBIT 2 - Biotechnology conventions and expositions

2007 Bio-IT World Conference and Expo http://www.bio-itworldexpo.com/

22nd Annual DIA CLINICAL DATA MANAGEMENT Symposium and Exhibition Integration Across the Clinical Trial Continuum United States - 18 Mar 2007 to 20 Mar 2007

Clinical Data Management United States - 19 Mar 2007 to 21 Mar 2007

Hands-On Biomanufacturing Training Seminar United States - 26 Mar 2007 to 28 Mar 2007

Second Annual Medical Device Regulatory, Reimbursement and Compliance Congress at Harvard United States - 28 Mar 2007 to 30 Mar 2007

Fourth Health Information Technology Summit United States - 28 Mar 2007 to 30 Mar 2007

22nd Annual DIA CLINICAL DATA MANAGEMENT Symposium and Exhibition Integration Across the Clinical Trial Continuum United States - 18 Mar 2007 to 20 Mar 2007

Hands-On Biomanufacturing Training Seminar United States - 26 Mar 2007 to 28 Mar 2007

Second Annual Medical Device Regulatory, Reimbursement and Compliance Congress at Harvard United States - 28 Mar 2007 to 30 Mar 2007

Introduction to Good Clinical Practices and Auditing Training Course United States - 30 Apr 2007 to 02 May 2007

Fundamentals of Clinical Research Monitoring Training Course United States - 30 Apr 2007 to 02 May 2007

Advanced Valuation of Pharmaceutical Strategic Alliances United States - 03 May 2007 to 04 May 2007

Good Clinical Practices for the Clinical Research Professional Training Course United States - 21 May 2007 to 21 May 2007

Second National Medicaid Congress United States - 13 Jun 2007 to 15 Jun 2007

Project Management: Planning, Executing and Controlling Projects in Pharmaceutical and Biotechnology United States - 13 Aug 2007 to 14 Aug 2007

Sixth Quality Colloquium at Harvard United States - 19 Aug 2007 to 21 Aug 2007

Overview of Drug Development Training Course United States - 20 Aug 2007 to 20 Aug 2007

Third FDA Regulatory and Compliance Symposium at Harvard United States - 22 Aug 2007 to 24 Aug 2007

Pediatric Clinical Research: Where Are We and Where Do We Go From Here? United States - 17 Sep 2007 to 18 Sep 2007

Clinical Statistics for Nonstatisticians United States - 24 Sep 2007 to 25 Sep 2007

Second National Consumer-Driven Healthcare Summit United States - 26 Sep 2007 to 28 Sep 2007

APPENDIX 2

VITA

VITA

CHRONOLOGY

March 9th, 1977……...Born, Bangalore, India

1999…….B.S., Chemical Engineering
M S Ramaiah Institute of Technology, Bangalore, India

2002……....M.S., Chemical Engineering
Illinois Institute of Technology, Chicago, IL

2003…….Research Scientist, Bioforce Nanosciences
Ames, IA

2005……Research Scientist, Anderson Materials Evaluation
Columbia, MD

2006 to 2009...…….PhD, Industrial Technology
Iowa State University, Ames, IA

2006 to 2009...……Research Associate, Ames Laboratory
USDOE, Ames, IA

May '09 to Aug '09…….....Intern, Integrated Sensor Technologies, Inc.
Ames, IA

AUTHORED PUBLICATIONS

1. **"Zero Flash Ultrasonic Micro Embossing on Foamed Polymer Substrates A Proof of Concept."**
Polymer Engineering and Science (In Press).

2. **"Microfabricated Biomolecular Ink Cartridges - Surface Patterning Tools (SPTs) for the Printing of Multiplexed Biomolecular Arrays."**
Sensors & Actuators B 113, 1034 – 1041 (2006).

3. **"Microfluidic Ultramicroscale Deposition and Patterning of Quantum Dots."**
Nanotechnology, 16, 2052 – 2055 (2005).

4. **"Microfabricated Quill-Type Surface Patterning Tools for the Creation of Biological Micro/Nano Arrays."**
Biomedical Micro devices, 6:2, 117 – 123, (2004).

5. **"NanoArrays."** *Microsc Microanal* 10 (Supply 2), (2004).

6. **"Virichip: A Solid Phase Assay for Detection and Identification of Viruses by AFM."**
Nanotechnology, 15, 383 – 389 (2004).

7. **"Label-free Protein and Pathogen Detection Using the Atomic Force Microscope."**
Journal of Biomolecular Screening, 9:6, 491-497(7) (2004).

8. **"Virichip™ Enhances RT-PCR in Biological Fluids and Environmental Samples."**
Analytical Biochemistry, 330, 350 – 352 (2004).

9. **"Analysis of Solid-Phase Immobilized Antibodies by Atomic Force Microscopy."**
J. Biochem. Biophys. Methods, (2004).

10. **"Characterization of Testudine Melanomacrophage Linear, Membrane Extension Processes – Cablepodia - by Phase and Atomic Force Microscopy."**
In Vitro Cellular & Developmental Biology, 41, 225 – 231 (2005).

11. **"Studies on Protein-Receptor Interaction Using the Atomic Force Microscope."**
Langmuir, 19(26), 10940 – 10946 (2003).

12. **"Probing the Nature of Cholera Toxin B Oligomer by the Atomic Force Microscopy."**
Chemistry Letters, 11, 1170 (2001).

AUTHORED CONFERENCE PRESENTATIONS AND POSTERS

- "Zero Flash Micro-Embossing." The Polymer Processing Society 24th Annual Meeting 2008, Salerno-Italy.

- "OLED-Polypropylene bio-CD sensor." SPIE 2008, San Diego-CA.

- "Polypropylene Bio-CD: A Novel Photoluminescence Based Estimation of Glucose Concentration with Ultrasonic Technology as an Enabler." Antec 2008, Milwaukee-WI.

- "Microfabrication on Polymer Substrates for Lab-on-a-CD Applications." Antec 2007. Cincinnati-OH.

- "Ultraminiaturized protein nanoarrays for novel applications." CHI PepTalk, 2005.

- "Nanoarrays as an ultraminiaturized platform for novel screening applications." Lab Automation, 2005.

- "Nanoarrays as an ultraminiaturized platform for novel screening applications." Biophysical Society, 2005.

- "Nanoarrays as an ultraminiaturized platform for novel screening applications." Experimental Biology, 2005.

- "The ViriChip: A Solid-Phase Affinity Substrate for Rapid, Virus Particle Detection and Identification." ASM Biodefense meeting, Baltimore, 2004.

- "Label Free Protein and Pathogen Detection and Characterization." Society for Biomolecular screening, The Next Wave of HTS Technologies-Part I, 2003.

- "The ViriChip: A rapid, multiplexed, label-free virus particle detection and identification platform." Biodefense Issues/Solutions, Cambridge Health Institute, 2003.

- "ViriChip: solid state detection system." SARS Working Group Meeting, 2003.

- "Exploration of Biomolecular interactions by the Atomic Force Microscopy." 223rd ACS National Meeting, Symposium of Proteins at Interfaces, 2002.

- "Surface Modification of Proteins for AFM Analysis." 223rd ACS National Meeting, Symposium of Proteins at Interfaces, 2002.

HONORS/AWARDS/RECOGNITION

- ***Best Technical Paper and Presentation Award***
  - *Antec 2008 conference, Society of Plastics Engineers (SPE), Medical Plastics Special Interest Group*

- ***Scholarship Award***
  - *Institute for Food Safety and Security (IFSS) for research in Lab-on-CD Technology – Fall 2007*

- ***Marquis Who's Who in the World***
  - *Biographical sketch in prestigious American Biographical Society, 27th Edition*